ISSN 2221-6413 (Print), ISSN 2223-2559 (Online)
Coden: PJSIB5 59(1) 1-62 (2016)

Pakistan Journal of Scientific and Industrial Research

Series A: Physical Sciences

Vol. 59, No.1, January-February, 2016

(for on-line access please visit web-site http://www.pjsir.org)

Published by
Scientific Information Centre
Pakistan Council of Scientific and Industrial Research
Karachi, Pakistan

Pakistan Journal of Scientific and Industrial Research
Series A: Physical Sciences

Pakistan Journal of Scientific and Industrial Research started in 1958, has been bifurcated in 2011 into:

Series A: Physical Sciences [**ISSN 2221-6413 (Print); ISSN 2223-2559 (online)]** (appearing as issues of January-February, May-June and September-October) and
Series B: Biological Sciences [**ISSN 2221-6421 (Print); ISSN 2223-2567 (online)]** (appearing as issues of March-April, July-August and November-December).
Each Series will appear three times in a year.

This Journal is indexed/abstracted in Biological Abstracts and Biological Abstracts Reports, Chemical Abstracts, Geo Abstracts, CAB International, BioSciences Information Service, Zoological Record, BIOSIS, NISC, NSDP, Current Contents, CCAB, Rapra Polymer Database, Reviews and Meetings and their CD-ROM counterparts etc.

Subscription rates (including handling and Air Mail postage): ***Local:*** Rs. 2500 per volume, single issue Rs. 425; ***Foreign:*** US$ 450 per volume, single issue US$ 75.

Electronic format of this journal is available with: Bell & Howell Information and Learning, 300, North Zeeb Road, P.O. 1346, Ann Arbor, Michigan 48106, U.S.A; Fax.No.313-677-0108; http://www.proquest.com

Photocopies of back issues can be obtained through submission of complete reference to the Executive Editor against the payment of Rs. 25 per page per copy (by Registered Mail) and Rs. 115 per copy (by Courier Service), within Pakistan; US$ 10 per page per copy (by Registered Mail) and US$25 per page per copy (by Courier Service), for all other countries.

Printed and Published by: PCSIR Scientific Information Centre, PCSIR Laboratories Campus, Shahrah-e-Dr. Salimuzzaman Siddiqui, Karachi-75280, Pakistan.

Editorial Address

Executive Editor
Pakistan Journal of Scientific and Industrial Research, PCSIR Scientific Information Centre
PCSIR Laboratories Campus, Shahrah-e-Dr. Salimuzzaman Siddiqui, Karachi-75280, Pakistan
Tel: 92-21-34651739-40, 34651741-43; Fax: 92-21-34651738; Web: http://www.pjsir.org, E-mail: info@pjsir.org

AIMS & SCOPE

Pakistan Journal of Scientific and Industrial Research (PJSIR) was started in 1958 to disseminate research results based on utilization of locally available raw materials leading to production of goods to cater to the national requirements and to promote S&T in the country. Over the past 58 years, the journal conveys high quality original research results in both basic and applied research in Pakistan. A great number of major achievements in Pakistan were first disseminated to the outside world through PJSIR.

It is a peer reviewed journal and published in both print and electronic form. Original research articles, review articles and short communications from varied key scientific disciplines are accepted however, papers of Pure Mathematics, Computer Sciences, Engineering and Medical Sciences are not entertained.

From 54th Volume in 2011, it has been bifurcated into Series A: Physical Sciences & Series B: Biological Sciences. Each series appears three times in a year as follows:

Physical Sciences in January-February, May-June and September-October issues. It includes research related to Natural Sciences, Organic Chemistry, Inorganic Chemistry, Industrial Chemistry, Physical Chemistry, Environmental Sciences, Geology, Physics, Polymer Sciences and Technology.

Biological Sciences in March-April, July-August and November-December issues. Papers included in this series are from Agriculture, Agronomy, Botany, Biochemistry, Biotechnology, Food Sciences, Genetic Engineering, Pharmaceutical Sciences, Microbiology, Marine Sciences, Soil Sciences, Tissue Culture, Zoology and Technology.

Due to many global issues, we are encouraging contributions from scientists and researchers from all across the globe with the sole purpose of serving scientific community worldwide on the whole and particularly for our region and third world countries.

Pakistan Journal of Scientific and Industrial Research
Series A: Physical Sciences
Vol. 59, No.1, January-February, 2016

Contents

Short Communications

Pak. j. sci. ind. res. Ser. A: phys. sci. 2016 **59** (1) 1-10

Preparation, Characterisation and Photocatalytic Activity of La-doped ZnO Nanopowders Synthesised using Auto-combustion

Mukhtar Ahmad[ab*], Eijaz Ahmed[a], Muhammad Ikram[a], Zhanglian Hong[b], Abdul Hafeez[c], Khalid Nadeem Riaz[d], Fezza Zafar[a], Niaz Ahmed Niaz[a] and Waqar Ahmed[ef]

[a]Department of Physics, Bahauddin Zakariya University, Multan 60800, Pakistan

[b]State Key Laboratory of Silicon Materials, Department of Materials Science & Engineering, Zhejiang University, Hangzhou 310027, China

[c]Science and Technology Division, University of Education, Lahore, Pakistan

[d]Department of Physics, University of Gujrat, Gujrat 50700, Pakistan

[e]Institute of Nanotechnology and Bioengineering, University of Central Lancashire, School of Medicine, Preston PR1 2HE, United Kingdom

[f]Dentistry and School of Pharmacy, Preston PR1 2HE, United Kingdom

(received August 18, 2014; revised August 9, 2015; accepted August 18, 2015)

Abstract. Nanocrystalline nanoparticles of pristine ZnO and La-doped ZnO have been synthesised using a combustion method using various concentrations of lanthanum dopant followed by calcination for 3 h at 700 °C. The crystalline structure, chemical composition and optical characteristics have been characterised using X-ray diffraction (XRD), scanning electron spectroscopy (SEM) attached with energy dispersive X-ray (EDX) spectroscopy, Brunauer Emmett Teller (BET), UV-vis. spectroscopy and photoluminescence (PL) spectroscopy. Absorption spectra showed that the absorbance increased with La-doping and the blue shift observed was due to an increase in the band gap from 3.24 to 3.27 eV. The photocatalytic activities of the samples prepared were evaluated using the photocatalytic degradation of methyl orange (MO) under irradiation by sunlight. The textile mill effluents containing organic matter were also irradiated with sunlight inducing photocatalysis and the chemical oxygen demand (COD) of the treated effluent were investigated. The results showed that the ZnO photocatalyst doped with 1.0 at.% lanthanum exhibited four times enhancement in the photocatalytic activity compared to pure ZnO.

Keywords: ZnO, combustion, XRD, photocatalysis, methyl orange, La-doped ZnO

Introduction

Fabrication and characterisation of semiconducting nanostructured materials have received considerable attention over the last few years due to increasing influence on our everyday life (Suwanboon and Amornpitoksuk, 2011; Wang and Herron, 1991). Zinc oxide (ZnO) has attracted interest due to its photocatalytic ability useful for the degradation of environmental pollutants and is attractive alternative to TiO_2 as a photoactive catalyst (Kaneva *et al.,* 2011; Anandan *et al.,* 2007). ZnO has exhibited superior performance with lower cost compared to TiO_2 in degrading organic dyes in acidic and basic media. It has a hexagonal wurtzite structure with an *n*-type conductivity (Reddy *et al.,* 2011; Chen *et al.,* 1998). The structural, optical, electrical and physical properties of ZnO nanoparticles and the effects of doping on these properties have been studied earlier by several researchers (Ahmad *et al.,* 2013; Shinde *et al.,* 2006; Ismail *et al.,* 2001). Dramatic changes in the electrical and optical properties of ZnO and unique properties due to doping have been observed by Bouderbala *et al.* (2008). Due to its useful properties, ZnO has been used in photocatalytic applications (Xiao *et al.,* 2015; Zhou *et al.,* 2009). ZnO is an ideal catalyst in photocatalysis since it is nontoxic with holes of strong oxidising power and being inexpensive (Peng *et al.,* 2007). When ZnO nanoparticle is illuminated with a light of appropriate wavelength, the valence band potential is positive enough to generate hydroxyl radicals at the surface, and the conduction band potential is negative enough to reduce molecular O_2. The hydroxyl radical is a powerful oxidising agent and can attack organic pollutants present at or near the surface of the ZnO to degrade it. However, the photocatalytic efficiency at the present stage is still very low, which is mainly caused by the fast recombination of photogenerated electron-hole pairs during photocatalysis. Thus, further improving the photocatalytic efficiency is still a major challenge in the research field of photocatalysis until

*Author for correspondence; E-mail: mzkhm73@gmail.com

now. Therefore, for enhancing photocatalytic activity of ZnO, doping of metal or nonmetal ions is a useful technique (Abed *et al.,* 2015; Elangoran *et al.,* 2015). Metal doping induces localized states between the valence band and the conduction band. These mid-gap states could trap temporarily the photogenerated electron-hole pairs, thus suppress the recombination of charge carriers (Wan *et al.,* 2015; Zhao *et al.,* 2015). Recent research has been focused on the doping of ZnO by lanthanide ions with 4f electron configuration. Lanthanide ions can form complexes with various Lewis bases including organic acids, amines, aldehydes, alcohols, and thiols by the interaction of the functional groups with their f-orbital (Ahmad *et al.,* 2015). Thus, doping lanthanide ions into a ZnO matrix could provide a means to concentrate organic pollutants on the semiconductor surface and therefore, can improve the separation efficiency of photo-induced electron-hole pairs of ZnO to enhance the photoreactivity (Ahmad *et al.,* 2015; Ciciliati *et al.,* 2015).

In this study, pure ZnO and La-doped ZnO using the auto-combustion technique has been synthesised producing highly pure nanocrystalline powders with large surface area at relatively low temperatures (Hwang and Wu, 2004). Variations in the properties of ZnO powders were studied as a function of the lanthanum dopant concentrations.

Materials and Methods

Synthesis of undoped and La-doped ZnO nano-powders. Pure and La-doped ZnO nanopowders were synthesised using the combustion technique. Zinc nitrate ($Zn(NO_3)_2.6H_2O$) and glycine (NH_2CH_2COOH) were used as starting reagents. The zinc nitrate served as a source of zinc and as an oxidising agent whereas glycine acted as a fuel (Ahmad *et al.,* 2013).

Precursor formation. For pure ZnO, homogeneous mixture of glycine and zinc nitrate was obtained by mixing them together in the optimised molar ratio (Ahmad *et al.,* 2012a) through magnetic stirring. This resulted in the formation of transparent slurry by absorbing moisture from air due to the hygroscopic nature of zinc nitrate. The slurry was then dehydrated at 130 °C to obtain precursor using a hot plate.

Auto-ignition. The precursor was heated at 200 °C to cause precursor ignition. During combustion the evolution of gases occurred with generation of heat. Heat treatment at 700 °C was done for 3 h resulting in the liberation of gases and formation of dry, crystalline white ZnO powders. For the preparation of La-doped ZnO samples, lanthanum nitrate [$La(NO_3)_3.6H_2O$] was added to the initial mixture of zinc nitrate and glycine. Rest of the process was similar to that used for pure ZnO. The following chemical reaction occurs during the synthesis of La-doped ZnO samples:

$$Zn(NO_3)_2.6H_2O + La(NO_3)_3.6H_2O \xrightarrow{\text{Glycine}} Zn_{1-x}L_xO + \text{Gases } (CO_2 + N_2 + H_2O \text{ vapours})$$

Characterisation. Powder X-ray diffraction (XRD) patterns of as-synthesised ZnO and La-doped ZnO samples were recorded using a Rigaku Dmax-IIIA X-ray diffractometer with Ni filtered Cu Kα radiation source. The surface morphology, particle size and compositional analysis of photocatalysts were examined using a scanning electron microscope (Hitachi S-4800) with EDX and transmission electron microscope (JEOL JEM 1200EX) and X-ray photoelectron spectroscopy (XPS, VG ESCALAB MARK II) with a monochromatic Mg Kα X-ray source. Specific surface areas of samples were determined using Brunauer Emmett Teller (BET) surface area analyzer (NOVA 2200e Quantachrome, USA) using nitrogen as a purge gas. UV-vis diffuse reflectance spectra (DRS) were measured in the range of 380-460 nm using a Hitachi U-4100 UV-vis pectrometer. PL emission spectra were recorded using Hitachi F-4500 fluorescence spectrophotometer. The sample excitation was made at 325 nm at room temperature.

Measurement of photocatalytic activity. Photocatalytic activities of ZnO and La-doped ZnO nanopowders were estimated by monitoring the degradation of methyl orange (MO) as a model compound in a self-assembled apparatus under natural sunlight radiation source. In this study, photocatalytic activities under natural sunlight were investigated. The peak at 464 nm was used to monitor the photocatalytic degradation of MO. For the photocatalytic experiment, 50 mg photocatalysts were suspended in MO aqueous solution (50 mL) with a concentration of 20 mg/L in a beaker. The suspension was magnetically stirred for 30 min to reach the adsorption/desorption equilibration without light exposure. This was followed by a photocatalytic reaction started by the exposure of the desired light. The temperature of the suspension was kept at about 20 °C by an external cooling jacket with recycled water. After a setup exposure time, 5 mL suspension was sampled, centrifuged and the supernatant was taken out for uv-

vis absorption spectrum measurement. The intensity of the main absorption peak of the MO dye was referred to as the measure of the residual dye concentration.

Analytical method. Total organic carbon (TOC) content was measured after the degradation of model dye in the presence of the photocatalysts under sunlight irradiation (Mukherjee, 2011). After photodegradation, the total organic carbon content of model dye was observed to decrease with time. The decrease of carbon content indicates the degradation of the organic dye into nontoxic decomposed compounds. Moreover, the mineralisation of substrate was measured by chemical oxygen demand (COD) reduction method. Chemical oxygen demand of textile effluent was estimated before and after the photocatalytic treatment with a standard dichromate method, using COD digester. Arsenic effluent was diluted to facilitate light penetration through solution and the initial COD of diluted effluent was 412 mg/L. The amount of catalysts was 50 mg/25 mL and an average intensity of sunlight was 1.20×10^5 lux during the photocatalytic measurements. The percentage photodegradation efficiency (η) was calculated from the following expression:

$$\eta = \left[\frac{\text{CODi} - \text{CODf}}{\text{CODi}}\right] \text{x}100$$

Where:
CODi = before treatment
CODf = after treatment
All the experiments were performed under the same experimental conditions such as sunlight irradiation (between 9 am and 3 pm), constant temperature, pH and photocatalyst load etc.

Results and Discussion

XRD analysis. Figure 1 shows powder X-ray diffraction patterns of pure ZnO and La-doped ZnO as a function of lanthanum dopant concentrations. The physical characteristics such as crystallite size and unit cell parameters are presented in Table 1. The strong and sharp peaks existing in the XRD spectra show the presence of wurtzite structure of ZnO. The strong peaks are located at an angle (2θ) of 31.7°, 34.4° and 36.2° correspond to (1 0 0), (0 0 2) and (1 0 1) along with the other peaks which are found at the angles of 47.5°, 56.6°, 62.9°, 66.4°, 67.9°, 69.2°, 72.7° and 77.0° correspond to (1 0 2), (1 1 0), (1 0 3), (2 0 0), (11 2), (2 0 1), (0 0 4) and (2 0 2) planes, which all are found

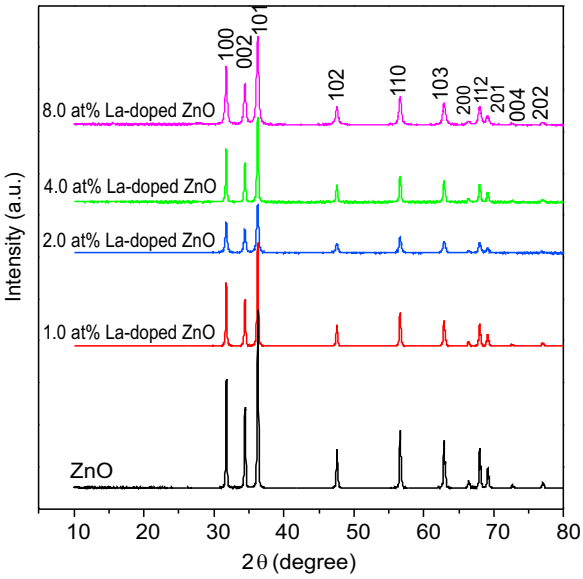

Fig. 1. X-ray diffraction patterns of pure ZnO and La-doped ZnO sample

Table 1. Crystallite size and unit cell parameters of pure ZnO and La-doped ZnO sample.

Photocatalysts	Crystallite size (nm)	Lattice parameters 'a' (Å)	'c' (Å)
Pure ZnO	27	3.254	5.208
1.0 at.% La-doped ZnO	24	3.258	5.203
2.0 at.% La-doped ZnO	22	3.262	5.199
4.0 at.% La-doped ZnO	23	3.263	5.195
8.0 at.% La-doped ZnO	19	3.265	5.186

in correspondence to those given in JCPDS 05-0664 and previous studies (Ghouri *et al.,* 2014; Ahmad *et al.* 2013). The diffraction patterns of La-doped ZnO were similar to the undoped ZnO showing that lanthanum doping in ZnO did not affect its crystal structure.This also indicates that La^{3+} is uniformly dispersed on ZnO nanoparticles in the form of small La_2O_3 cluster (Anandan *et al.,* 2007). The observed peaks for La-doped ZnO, however, are wider with the width increasing with increasing La-content. La-doping caused a random variation in diffraction peak intensities. Intensity decreased up to 2.0 at% La-content and then increased. The change in the intensity and width of the observed diffraction peaks as a function of La-content is attributed to the decrease in the crystallite size (Suwanboon and

Amornpitoksuk, 2011; Flickyngerova *et al.,* 2008; Anandan *et al.,* 2007), which goes on changing inversely with change in La concentration. Lattice parameters *'*a*'* and 'c*'* were estimated using the formula:

$$\left[\frac{1}{d_{hkl}}\right]^2 = \frac{4}{3}\left[\frac{h^2 + k^2 + hk}{a^2}\right] + \frac{l^2}{c^2}$$

Lattice parameters and crystallite size variation as functions of La-content were calculated. The calculated values of lattice parameters *'*a*'* and 'c*'* are 3.254 Å and 5.208 Å while for 2.0 at.% La-doped ZnO are 3.262 Å and 5.199 Å, respectively. Lattice parameters increased with increase in La-content which is obvious as ionic radius of Zn^{+2} is 0.074 nm and that of La^{+3} is 0.106 (Suwanboon and Amornpitoksuk, 2011) and lattice parameters should expand if ionic radius of the dopant is greater as compared to Zn ions (Dole *et al.,* 2011). Average crystallites sizes were estimated using the full width at half maximum (FWHM) of highly intense diffraction peak in Debye-Scherrer's formula (Culity and Stock, 2001).

$$t = \frac{0.9\lambda}{\beta \cos\theta}$$

Average crystallite size estimated for pure ZnO to be 27 nm which decreases up to 19 nm with increase in La-content. It is interesting to note that the particle size of La doped ZnO is smaller as compared with that of the pure ZnO. The decrease in the particle size of La-doped ZnO is mainly attributed to the formation of La–O–Zn on the surface of the doped samples, which hinders the growth of crystal grains (Korake *et al.,*2014; Jia *et al.,* 2009; Anandan *et al.,* 2007).

SEM, EDX and TEM. Figure 2(a-d) displays the surface morphology of pure ZnO and 2.0 at% La-doped ZnO nanopowders. SEM micrographs of pristine ZnO nanopowders exhibited clusters of tiny particles, whilst 2.0 at% La-doped ZnO nanopowders revealed flakes of ultrafine particles with voids or holes. The high porosity in the nanopowders could be attributed to the liberation of large amount of gaseous products such as H_2O vapours, CO_2 and N_2 during combustion process (Ahmad *et al.,* 2013b). TEM images in Fig. 2, show that, for undoped ZnO nanopowders, the particles are spherical and. larger and, while for 2.0 at% La-doped ZnO nanopowders, they are smaller and quasi spherical. Lanthanum doping thus changes the morphology of the

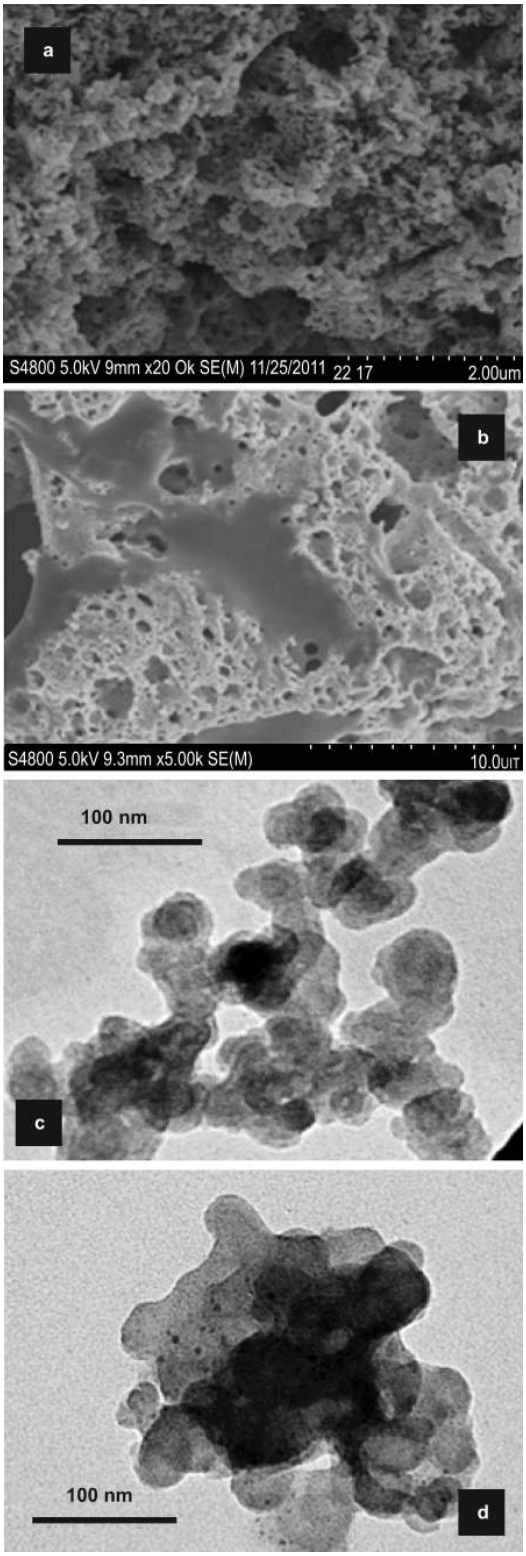

Fig. 2. (a-d) SEM micrograph of (a) pure ZnO and (b) 2.0 at% La-doped ZnO samples; TEM images of (c) pure ZnO and (d) 2.0 at% La-doped ZnO sample.

final product. TEM investigations of all of the samples revealed that the crystallites are of nanometer size. The diameter of ZnO and 2.0 at% La-doped ZnO were found to be about 33 and 24 nm, respectively agreeing with the XRD results. The chemical compositional analysis is important for monitoring the concentration of the dopant. Figure 3 shows the EDX spectra of undoped ZnO and La-doped ZnO nanoparticles. The EDX spectrum of the La-doped ZnO displays a clear lanthanum line at 4.65 keV showing La doping. No traces of other elements were found in the spectra which confirm the purity of the samples. Also Table 2 shows the atomic percentage of Zn, La and O for undoped and La-doped ZnO samples. Here the actual concentration of La is found to be 1.76 at% for 2.0 at% La-doped ZnO sample.

XPS analysis. The nature and the co-ordination of the elements present in the La-doped ZnO were investigated by X-ray photoelectron spectroscopy (XPS). The La 3d spectrum of 2.0 at% La-doped ZnO is shown in Fig. 4.

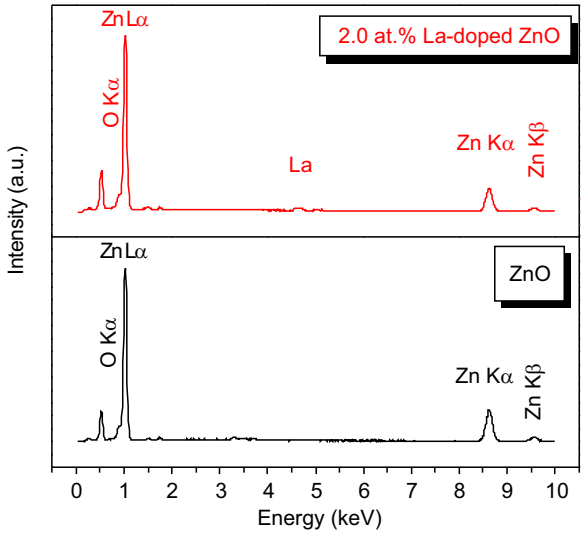

Fig. 3. EDX pattern of ZnO and 2.0 at%La-doped ZnO sample.

Table 2. Chemical composition (atomic % of ZnO and La-doped ZnO sample.

Element	Zn (at%)	O (at%)	La (at%)	Total (at%)
ZnO	50.68	49.32	-	100
2.0 at% La-doped ZnO	48.73	49.51	1.76	100

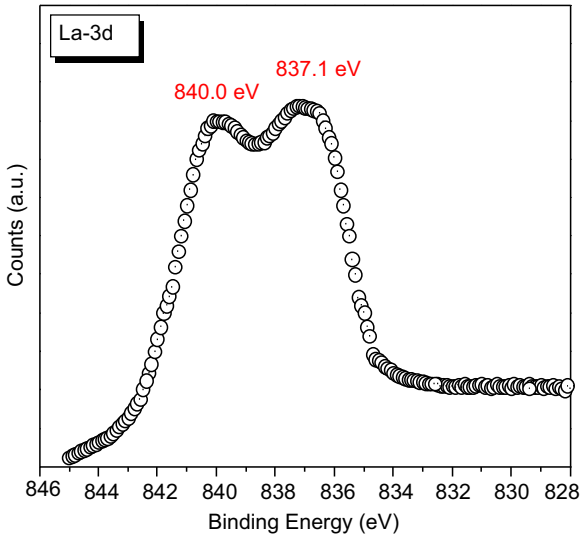

Fig. 4. XPS high resolution spectra of La-3d region for 2 at % La- ZnO sample.

The spectrum exhibits two components with the binding energy values of 837.1 eV and 840.0 eV. The highest energy contribution is assigned to the bonding between lanthanum and zinc while the lowest energy contribution is attributed to the bonding in the lanthanum oxide clusters (Anandan *et al.,* 2007). These results demonstrated that the bonding between the lanthanum and zinc has occurred and the interaction between the lanthanum oxide clusters and the ZnO surface are strongly developed.

UV-visible spectra. Optical properties of ZnO and La-doped ZnO photocatalysts with different La-content were measured by diffuse reflectance spectroscopy (DRS) at room temperature. The absorbance spectra of different samples are shown in Fig. 5. The band edge for the ZnO sample was appeared at about 387 nm while the band edges of the La-doped ZnO samples was shifted to shorter wavelength regions with higher absorption intensity after La-doping. The blue shift in wavelength is attributed to gradual increase in band gap of ZnO on La-doping. The absorbance coefficient (α) was calculated from the raw absorbance data to obtain the optical band gap (Eg). The band gap values were thus determined by the extrapolation of the linear portion of the $(\alpha h\nu)^2$ curve versus the photon energy $h\nu$ and are shown in Table 3. With increasing the La-content from 0.0 at% to 8.0 at%, the band gap energies increased in the range of 3.24-3.27 eV as shown in Fig. 6. The following explanation may be given; the band gap of ZnO is about 3.37 eV whereas that of La_2O_3 is about

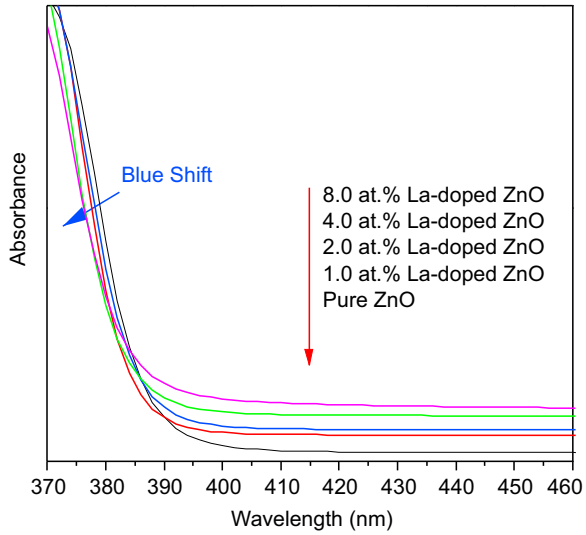

Fig. 5. Absorption spectra for pure ZnO and La-doped ZnO sample.

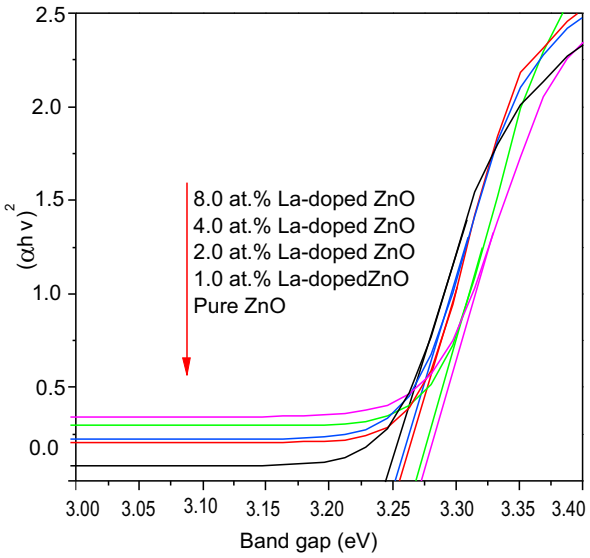

Fig. 6. Band gap energies of ZnO and La-doped ZnO sample.

Table 3. Band gap energy, BET surface area of ZnO and La-doped ZnO samples and apparent kinetic values for the degradation MO model dye under sunlight irradiation

Photocatalyst	Band gap (eV)	BET surface area (m^2/g)	For sunlight irradiation	
			r_0 (mg/L/min)	$t_{1/2}$ (min)
ZnO	3.24	33.4	0.038	217
1.0 at.% La-doped ZnO	3.25	37.3	0.162	86
2.0 at.% La-doped ZnO	3.25	39.5	0.132	104
4.0 at.% La-doped ZnO	3.26	42.3	0.106	130
8.0 at.% La-doped ZnO	3.27	45.1	0.092	149

5.5 eV (Jia *et al.,* 2009), which is much higher than that of pure ZnO. An additional energy level could be formed above the conduction band of ZnO due to the La-doping. Furthermore, this could be attributed to the quantum size effect as well as the strong interaction between the surface oxides of Zn and La. These observations strongly suggest that the La doping significantly affects the particle size and hence the absorbance properties. Moreover, these results are in good agreement with the conclusion derived from the XRD results and a similar result has also been reported in La-doped TiO_2 by Liqiang *et al.(*2004) and La-doped ZnO by Anandan *et al.* (2007).

Photoluminescence. Photoluminescence (PL) is a powerful tool to investigate optical properties of wide band gap semiconductors. A comparison of PL emission spectra intensity of prepared samples excited with 325 nm wavelengths ranging up to 600 nm is shown in Fig. 7. PL emission intensity decreased with La-concentration i.e. pure ZnO has highest emission

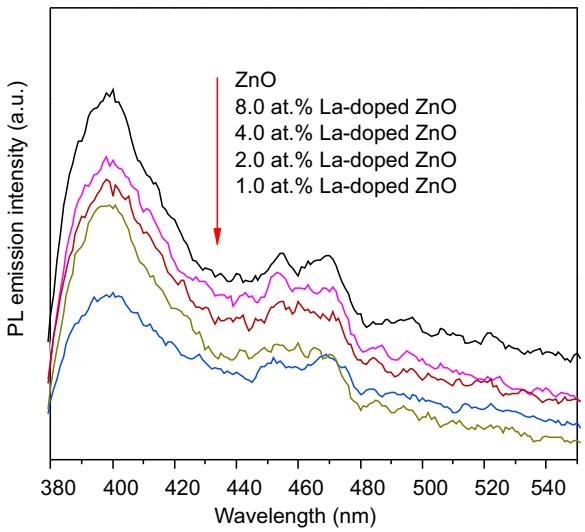

Fig. 7. PL emission spectra for pure ZnO and La-doped ZnO nanoparticles.

intensity, which can be attributed to several defects such as oxygen and zinc vacancies or oxygen and zinc interstitials (Ismail *et al.,* 2001). However, the addition of La ions tends to stop the reduction in the band gap resulting in lower PL emission intensity first and then increasing with increasing dopant La-content.

Photocatalytic activity. Pristine ZnO and doped ZnO are well known catalysts used in photocatalytic degradation of pollutants. Photocatalytic activities of the ZnO and La-doped ZnO samples were determined through a series of experiments carried out for degradation of methyl orange (MO) in aqueous suspension under natural sunlight irradiation. A blank experiment study of MO degradation without catalyst loading under the same condition was also observed. The results indicate that the mere photolysis can be ignored as the corresponding degradation is about 0.3% after irradiations for 2 h. Figure 8 shows a comparison of photocatalytic performances of pure ZnO and La-doped ZnO nanoparticles. About 9% of the MO was adsorbed for ZnO sample upon stirring for 30 min in the dark and increased for La-doped ZnO in comparison to ZnO nanopowders. The pronounced adsorption is due to increase in specific surface area, increase in porosity and defects creation within band gap by

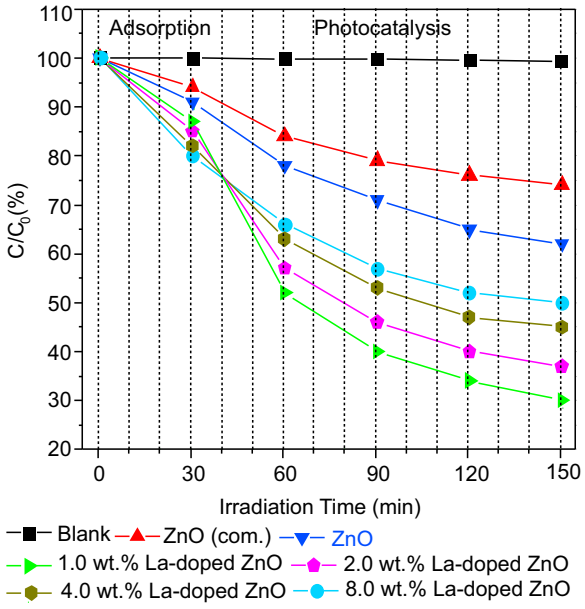

Fig. 8. Photocatalytic activity of pure ZnO, Commercial ZnO and La-doped ZnO nanopowders for MO degradation under sunlight irradiation.

lanthanum doping. Photocatalytic degradation of MO follows pseudo first-order reaction kinetics for low dye concentrations

$$\ln(C_0/C) = k_{appt}$$

where:

k_{app} = the apparent constant, used as the basic kinetic parameter for different photocatalysts; C_0 = the initial concentration of MO in aqueous solution and C = the residual concentration of MO at time t.

The initial degradation rate ($r_0=k_{app}C_0$) of 20 mg/L MO with different photocatalysts was studied and the results are presented in Table 3. The photodegradation rate of MO follows the ascending order; 1.0 at% La-doped ZnO > 2.0 at% La-doped ZnO > 4.0 at% La-doped ZnO > 8.0 at% La-doped ZnO > ZnO > commercial ZnO. The degradation rate under sunlight for 1.0 at% La-doped ZnO photocatalyst was found superior to other La-doped ZnO and ZnO samples. The specific surface areas were seen to increase gradually with the increasing lanthanum content (Table 3) enhancing the adsorption performance. The photocatalytic efficiency of La-doped ZnO mainly originates from the formation of La-O-Zn bonds on ZnO surface. Photocatalytic degradation rate of MO is observed to be lower under La-doped ZnO. Table 3 shows that the degradation rate of MO enhanced with La-content up to 1.0 at% La-content and then decreased with La-loading leading to the conclusion that 1.0 at% doping concentration is the optimum loading to ZnO that is more efficient in separating photoinduced electron-hole pairs which in turn increases photoactivity of ZnO. The high photocatalytic activity at 1.0 at% La-doped ZnO can be explained as follows: lanthanum ions in ZnO can result in the formation of a space charge layer on the surface of ZnO which acts as a barrier for recombination of photoinduced electron-hole pairs resulting in an increase in the photocatalytic activity. This increase was observed up to 1.0 at% La-doping in the present study. The decrease in photocatalytic activity of ZnO beyond 1.0 at% La-doping is justified as: The incorporation of lanthanum beyond 1.0 at% is supposed to likely result in the formation of more La-O-Zn bond on ZnO surface due to which surface charge region is negatively affected causing a decrease in its efficiency to separate the photoinduced electron-hole pairs and instead of acting as traps sites for photoinduced electron-hole pairs, it acts as recombination centre (Jia *et al.,* 2009). This results in decrease of photocatalytic activity of ZnO.

A simple mechanism to understand the enhancement of photocatalytic activity of La-doped ZnO photocatalysts is the loading of lanthanum metals on the ZnO surface, which can accelerate the transport of photogenerated electrons to the outer systems. The transfer of electrons to the deposited metal causes these to become negatively charged (Behnajady *et al.,* 2009). In the photocatalytic systems, lanthanum deposited on the ZnO surface increased the photocatalytic activity by accelerating the transfer of electrons to dissolved oxygen molecules. Superoxide anion radical was prepared as a result of oxygen reduction by transfer of trapped electrons from lanthanum metal to oxygen. Consequently, the recombination of the photo-generated carriers were effectively suppressed leading to an increase in the photo-oxidation efficiency. The photocatalyst 1.0 at% La-doped ZnO exhibited superior catalytic performance, but further increase in the concentration of lanthanum would decrease photocatalytic activity because too much doping of lanthanum is likely to serve as recombination centre than as trap sites for the charge transfer at the interface. The total organic carbon (TOC) content was measured after the degradation of methyl orange dye in the presence of the photocatalysts under sunlight irradiation. After photodegradation the total organic carbon content of MO was observed to decrease with time and the results are presented in Fig. 9. TOC_o and TOC_t are the initial concentration and the reaction concentration of MO, respectively. The experimental data are fitted using the pseudo-first-order kinetic equation.

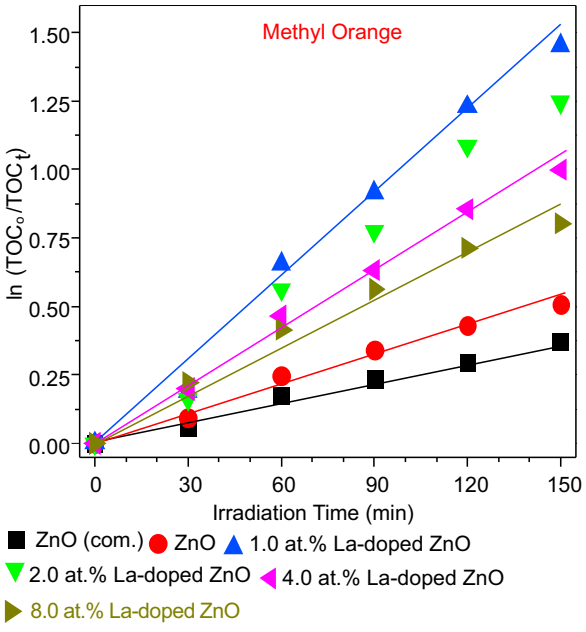

Fig. 9. The $In(TOC_o/TOC_t$ vs time curves of mineralization of methly orange.

During dye production and textile manufacturing processes an enormous amount of waste water containing dyestuffs with intensive colour and toxicity is introduced into the aquatic system. An effluent of this type has been considered for this photocatalytic degradation study using the same experimental conditions discussed in the experimental section. COD removal efficiencies of the effluent by ZnO, La-doped ZnO nanopowders

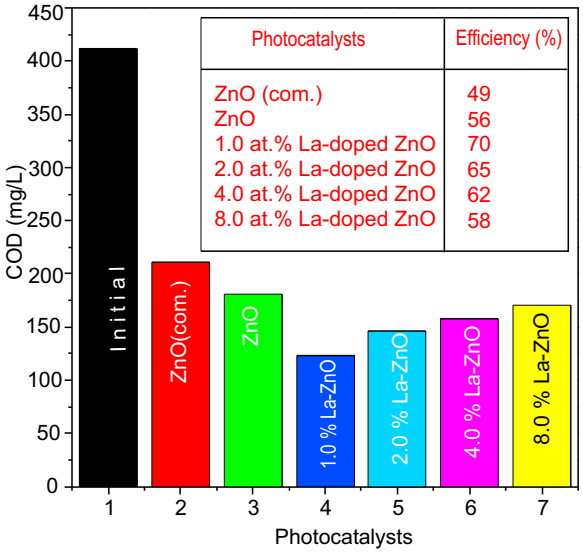

Fig. 10. COD values of the treated effluent and percentage photodegradation efficiency (η) for different photocatalysts under sunlight irradiation

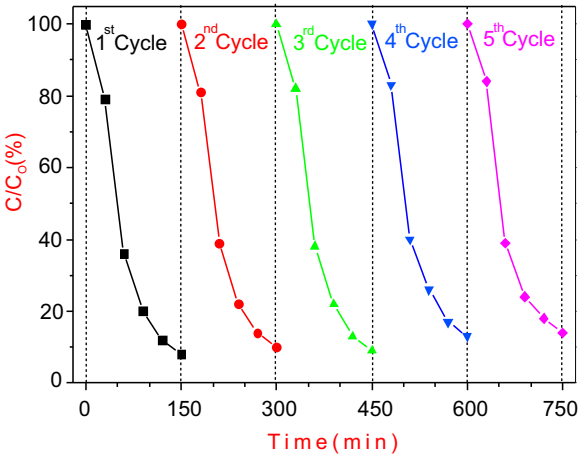

Fig. 11. Photo-stability of 1.0 at% La-doped ZnO sample.

photocatalysts under the sunlight irradiation are shown in Fig. 10. COD reduction confirms the destruction of the organic molecules in the effluents along with colour removal. The photo-stability of 1.0 at% La-doped ZnO sample as catalyst under sunlight was also studied (Fig. 11). The photocatalytic activity of the sample did not decrease significantly after five successive cycles of degradation tests, indicating that the photocatalyst was fairly stable under the conditions used in this study.

Conclusion

Pure ZnO and La-doped ZnO nanoparticles were synthesised via fast and facile conventional combustion method and characterised using a variety of characterisation techniques. From XRD patterns all synthesised samples had a hexagonal wurtzite structure showing that La-doping has no structural effect on ZnO. It was found that La^{3+} is uniformly dispersed on ZnO nanoparticles in the form of small La_2O_3 cluster. The XRD and UV-vis results revealed that the particle size of La-doped ZnO is much smaller as compared to that of pure ZnO and decreases with increasing La loading. Highly porous surface of La-doped ZnO was observed by SEM, which is critical for enhancing the adsorption and photocatalytic activity. The photocatalytic activity of La-doped ZnO for the degradation of MO was studied and the results are compared with ZnO and commercial ZnO. It was observed that the rate of degradation of MO over La-doped ZnO increases with increasing La loading up to 1.0 at% and then decreases. The TOC results demonstrated that La-doped ZnO requires shorter irradiation time for the complete mineralization of MO than pure ZnO. The relative photonic efficiencies and the photocatalytic activity of the 1.0 at% La-doped ZnO are much higher as compared to those of pure ZnO and commercial ZnO. It is concluded that, small particle size, separation of charge carriers, highly porous surface and larger specific surface area of La-doped ZnO are the major constituents for its enhanced photocatalytic activity in the present study.

Acknowledgement

Mukhtar Ahmad is thankful to Higher Education Commission (HEC) of Pakistan for providing financial assistance through Indigenous and IRSIP Scholarship Programme and the Zhejiang University of China for providing opportunity to work in its laboratories.

References

Abed, C., Bouzidi, C., Elhouichet, H., Gelloz, B., Ferid, M. 2015. Mn doping induced high structural quality of sol-gel ZnO crystals: Application in photocatalysis. *Applied Surface Science,* **349:** 855-863.

Ahmad, M., Ahmed, E., Zafar, F., Khalid, N.R., Niaz, N.A., Hafeez, A., Ikram, M., Khan, M.A., Hong, Z.L. 2015. Enhanced photocatalytic activity of Ce-doped ZnO nanopowders synthesized by combustion method. *Journal of Rare Earths*, **33:** 255-260.

Ahmad, M., Ahmed, E., Hong, Z.L., Iqbal, Z., Khalid, N.R., Abbas, T., Ahmad, I., Elhissi, A., Ahmed, W. 2013. Structural, optical and photocatalytic properties of hafnium doped zinc oxide nanophotocatalyst. *Ceramic International,* **39:** 8693-8700.

Ahmad, M., Ahmed, E., Hong, Z.L., Khalid, N.R., Zhang, Y., Ullah, M. 2013a. Preparation of highly efficient Al doped ZnO photocatalyst by combustion synthesis. *Current Applied Physics,* **13:** 697-704.

Ahmad, M., Iqbal, Z., Hong, Z., Yang, J., Zhang, Y., Khalid, N.R., Ahmed, E. 2013b. Enhanced sunlight photocatalytic performance of hafnium doped ZnO nanoparticles for methylene blue degradation. *Integrated Ferroelectrics,* **145:** 108-114.

Ahmad, M., Ahmed, E., Hong, Z.L., Khalid, N.R., Elhissi, E., Ahmed, W. 2013c. Graphene-Ag/ZnO nanocomposite as a high performance photocatalyst under visible light irradiation. *Journal of Alloys and Compounds*, **577:** 717-727.

Ahmad, M., Ahmed, E., Khalid, N.R., Jackson, M.J., Ahmed, W. 2012a. Synthesis and characterization of hexagonal shaped nanocrystalline zinc oxide powders. *International Journal of Manufacturing Materials and Mechanical Engineering,* **2:** 61-76.

Ahmad, M., Ahmed, E., Hong, Z.L., Khalid, N.R. 2012b. Effect of fuel to oxidant molar ratio on the photocatalytic activity of ZnO nanopowders. *Ceramic International,* **39:** 3007-3015.

Anandan, S., Vinu, A., Lovely, K.L.P.S., Gokulakrishnan, N., Srinivasu, P., Mori, T., Murugesan, V., Sivamurugan, V., Ariga, K. 2007. Photocatalytic activity of ZnO for the degratation of monocrotophos in aqueous suspension *Journal of Molecular Catalysis A: Chemical,* **266:** 149-157.

Behnajady, M.A., Modirshahla, N., Shokri, M., Zeininezhad, A., Zamani, H.A. 2009. Enhancement photocatalytic activity of ZnO nanoparticles by silver doping with optimization of photo-deposition method parameters. *Journal of Environmental Science: Health Part A,* **44:** 666-672.

Bouderbala, M., Hamzaoui, S., Amrani, B., Reshak, A.H., Adnane, M., Sahraoui, T., Zerdali, M. 2008.Thickness dependence of structural, electrical and optical behaviour of undoped ZnO thin films. *Physica B: Condensed Matter,* **403:** 3326-3330.

Chen, Y.F., Bagnall, D.M., Koh, H.J., Park, K.T., Hiraga,

K.J., Zhu, Z.Q., Yao, T.F. 1998. Plasma assisted molecular beam epitaxy of ZnO on c-plane sapphire-growth and characterization. *Journal of Applied Physics,* **84:** 3912-3918.

Ciciliat, M.A., Silva, M.F., Fernandes, D.M., de Melo, M.A.C., Hechenleitnar, A.A.W., Pineda, E.A.G. 2015. Fe-doped ZnO nanoparticles: Synthesis by a modified Sol-gel method and characterization. *Materials Letters,* **159:** 84-86.

Culity, B.D., Stock, S.R. 2001. *Elements of X-ray Diffraction,* 3rd edition., pp. 388 Prantice-Hall Inc., New Jersey, USA.

Dole, B.N., Mote, V.D., Huse, V.R., Purushotham, Y., Lande, M.K., Jadhav, K.M., Shah, S.S. 2011. Structural studies of Mn doped ZnO nanoparticles. *Current Applied Physics,* **11:** 762-766.

Elangoran, S.V., Chandramohan, V., Sivakumar, N., Senthil, T.S. 2015. Synthesis and characterization of sodium doped ZnO nanocrystals and its applications to photocatalysis. *Superlattices and Microstructures,* **85:** 901-907

Flickyngerova, S., Shtereva, K., Stenova, V., Hasko, D., Novotny, I., Tvarozek, V., Sutta, P., Vavrinsky, E. 2008. Structural and optical properties of sputtered ZnO thin films. *Applied Surface Science,* **254:** 3643-3647.

Ghouri, M.I., Ahmad, E., Khalid, N.R., Ahmad, M., Ramzan, M., Shakoor, A., Niaz, N.A. 2014. Gadolinium doped ZnO nanocrystalline powders and its photocatalytic performance for degradation of methylene blue under sunlight. *Journal of Ovonic Research,* **10:** 89-100.

Hwang, C.C., Wu, T.Y. 2004. Synthesis and characterization of nanocrystalline ZnO powders by a novel combustion synthesis method. *Materials Science and Engineering B,* **111:** 197-206.

Ismail, B., Abaab, M., Rezig, B. 2001. Structural and electrical properties of ZnO films prepared by screen printing technique. *Thin Solid Films,* **383**: 92-94.

Jia, T., Wang, W., Long, F., Fu, Z., Wang, H., Zhang, Q. 2009. Fabrication characterization and Photocatalytic ctivity of La-doped ZnO nanowires. *Journal of Alloys and Compounds,***484:** 410-415.

Kaneva, N.V., Dimitrov, D.T., Dushkin, C.D. 2011. Effect of nickel doping on the photocatalytic activity of ZnO thin films under UV and visible light. *Applied Surface Science,* **257:** 8113-8120.

Korake, P.V., Dhabbe, R.S., Kadam, A.N., Gaikwad, Y.B., Garadkar, K.M. 2014. Highly active lanthanum doped ZnO nanorods for photodegradation of metasystox. *Journal of Photochemistry and Photobiology B: Biology,***130:** 11-19.

Liqiang, J., Xiaojun, S., Baifu, X., Baiqi, W., Weimin, C., Honggang, F. 2004. The preparation and characterization of La-doped TiO_2 nanoparticles and their photocatalytic activity. *Journal of Solid State Chemistry,* **177:** 3375-3382.

Mukherjee, D. 2011. Development of a Novel TiO_2-Polymeric Film Photocatalyst for Water Purification both under UV and Solar Illumination. *Ph.D. Thesis,* 143 pp., University of Western Ontario, Canada.

Peng, F., Zhu, H., Wang, H., Yu, H. 2007. Preparation of Ag-sensitized ZnO and its photocatalytic performance under simulated solar light. *Korean Journal of Chemical Engineering,* **24:** 1022-1026.

Reddy, A.J., Kokila, M.K., Nagabhushana, H., Rao, J.L., Shivakumara, C., Nagabhushana, B.M., Chakradhar, R.P.S. 2011. Combustion synthesis, characterization and Raman studies of ZnO nanopowders. *Spectrochimica Acta* Part A, **81:** 53-58.

Shinde, V.R., Gujar, T.P., Lokhande, C.D., Mane, R.S., Han, S.H. 2006. Mn doped and undoped ZnO film: A comparative structrual, optical and electrical properties study. *Materials Chemistry and Physics,* **96:** 326-330.

Suwanboon, S., Amornpitoksuk, P. 2011. Preparation and characterization of nanocrystalline La-doped ZnO powders through a mechanical milling and their optical properties. *Ceramics International,* **37:** 3515-3521.

Wan, X., Liang, X., Zhang, C., Li, X., Liang, W., Xu, H., Lan, S., Tie, S. 2015. Morphology controlled synthesis of Cu-doped ZnO, tubular Zn(Cu)O and Ag decorated tubular Zn(Cu)O microcrystals for photocatalysis. *Chemical Engineering Journal,* **272:** 58-68.

Wang, Y., Herron, N. 1991. Nanometre-sized semiconductor cluster: Material synthesis, quantum size effects, and photophysical properties. *Journal of Physical Chemistry,* **95:** 525-532.

Xiao, S., Li, H., Liu, L., Lian, J. 2015. Glucose-assisted generation of assembled mesoporous ZnO sheets with highly efficient photocatalytic performance. *Materials Science in Semiconductor Processing,* **39:** 680-685.

Zhao, T., Fu, Y., Zhao, Y., Xing, L., Xue, X. 2015. Ga-doped ZnO nanowire nanogenerator as self-powered/active humidity sensor with high sensitivity and fast response. *Journal of Alloys and Compounds,* **648:** 571-576

Zhou, X., Li, Y., Peng, T., Xie, W., Zhao, X. 2009. Synthesis, characterization and its visible-light-induced photocatalytic property of carbon doped ZnO. *Materials Letters,* **63:** 1747-1749.

Pak. j. sci. ind. res. Ser. A: phys. sci. 2016 **59** (1) 11-22

Kinetics of Adsorptive Removal of Drimarene Brilliant Red from Aqueous Solution Using Untreated Agricultural Residues

Ch. Tahir Mehmood[a], Muhammad Arshad[a]*, Tayyab Ashfaq[b], Muhammad Bilal[c], Muhammad Shafiq[c] and Kiran Hina[d]

[a]Institute of Environmental Sciences and Engineering (IESE), School of Civil and Environmental Engineering (SCEE), National University of Sciences and Technology (NUST), Sector H-12, Islamabad, 44000, Pakistan

[b]Department of Civil Engineering, COMSATS Institute of Information Technology, University Road, Abbottabad-22060, Pakistan

[c]Department of Environmental Sciences, COMSATS Institute of Information Technology, University Road, Abbottabad-22060, Pakistan

[d]Department of Environmental Sciences, Hafiz Hayat Campus, University of Gujrat, Gujrat, 54000, Pakistan

(received January 6, 2015; revised March 26, 2015; accepted April 2, 2015)

Abstract. The potential of untreated banana and orange peels, and rice husk was tested for drimarene brilliant red (DBR) dye removal from aqueous solution. Kinetics was also studied in a batch experiment. Dose of adsorbents varied from 6 to 12 g/L, particle sizes 0.2 and 0.8 mm and contact time 2–32 h. High dose and small particle size favoured DBR removal efficiency significantly. The highest adsorption capacity was shown by rice husk (10 mg/g), then orange peels (9 mg/g) and the lowest by banana peels (4 mg/g). Langmuir isotherm (R^2=0.99) and pseudo-second order model (R^2=0.99) depicted well the equilibrium and best explained the kinetics for rice husk, respectively. Initial adsorption appeared as pore diffusion in all the cases and film diffusion was controlling the rate, later on. Based upon the analytical data, a simple model has been presented that fitted best to describe rice husk adsorption kinetics.

Keywords: adsorption, drimarene brilliant red, banana peels, orange peels, rice husk

Introduction

Textile sector produces large quantities of wastewater that result in the release of toxic dyes into freshwater bodies. According to estimates, 12-20 tonnes/day production of finished fabric results into generation of 1,000-3,000 m^3. Globally more than 1×10^7 kg/year of dyes stuff is produced and contributes about $1\text{-}2\times10^6$ kg of active dye into freshwater bodies annually (Prigione *et al.,* 2012; Allen *et al.,* 2003). These dyes are considered responsible for dermatitis, allergies, skin irritation, cell mutation and cancer. The dyes also pose serious hazards to aquatic organisms as well as affect photosynthetic activity in aquatic ecosystems. Presence of dyes in water badly affects light penetration, creating problems for photosynthetic activities in aqueous flora (Royer *et al.,* 2009). Degradation of some dyes generates byproducts, as metabolites which are more genotoxic or carcinogenic (Zhang *et al.*, 2011).

*Author for correspondence; E-mail: marshad@iese.nust.edu.pk

Complex molecular structure and synthetic origin of textile dyes make them stable to light, heat, oxidizing agents and microbial degradation (Sun and Yang, 2003). Conventional methods for dye removal include reverse osmosis, coagulation/flocculation, advanced oxidation, micro, ultra, and nano-filtration, and electrochemical as a tertiary treatments, as well as aerobic and anaerobic processes. Many of the aforementioned methods either have the disadvantage of producing toxic sludge, which create disposal issues, or have higher treatment costs. So there is a need for more sustainable option.

Many studies have reported the use of different adsorbents like activated carbon, peat, coir pith, chitin, silica and fly ash to remove contaminants (Royer *et al.,* 2009; Ponnusami *et al.,* 2007; Sun and Yang, 2003). A comprehensive list of adsorbents and target dyes is provided in a recent review (Noroozi and Sorial, 2013). Chitosan was reported as an efficient adsorbent for 90% removal of Food Yellow 3 and Acid Blue 9 (Goncalves *et al.,* 2013). Zhang *et al.* (2014) have reported adsorption capacities up to 84.2, 79.6 and

99.9% for methyl orange, disperse blue and malachite green chloride, respectively, with a synthetic carboxymethyl cellulose-acrylic acid adsorbent. Base treated *Shorea dasyphylla* sawdust has been reported for the removal of acid blue 25 (Hanafiah *et al.,* 2012).

High cost of some adsorbents, like activated carbon, is a major impediment to its application in developing countries like Pakistan. For low cost sustainable solutions, agricultural/plant residues have the potential to offer a replacement to existing costly adsorbents. Considerable efforts have been made to explore the effectiveness of plants and plant materials for textile wastewater treatment (Verma *et al.,* 2012). However, these efforts are fragmented and more research is required using indigenous bio resources. In agricultural countries, like Pakistan, rice husk could prove a good option for sorption processes, since it is available either free of cost or at very low price. Average annual productions of rice, orange and banana during 2009-2013 were 6072, 2149 and 124 thousand tonnes, respectively. These led to estimated waste production of 1214, 516 and 41 thousand tonnes in the form of rice husk, orange and banana peels, respectively. The present study was conducted to compare various low cost adsorbents; banana and orange peels, and rice husk for their efficiency for drimarene brilliant red (DBR) dye removal without prior treatment. Experimental conditions such as particle size, dose and time required for maximum removal of dye were optimized. Furthermore, the mechanism of dye adsorption on various biomass materials was investigated using various isotherms and kinetic models. Finally, a very simple model is proposed which describes the adsorption by rice husk.

Materials and Methods

The adsorption potential of banana and orange peels, and rice husk was investigated for the reactive dye drimarene brilliant red (K-4BL-CDG) (Fig. 1) from aqueous dye solution.

Bio-adsorbent preparation. The banana and orange peels were obtained from a local market of Islamabad, Pakistan. Initially, the peels were washed to remove any adhering dirt and then subjected to drying, crushing and sieving to get different particle sizes (0.2 and 0.8 mm). Rice husk was obtained from Kisan Rice Pvt. Ltd. Gujranwala, Pakistan, then air dried and sieved before use.

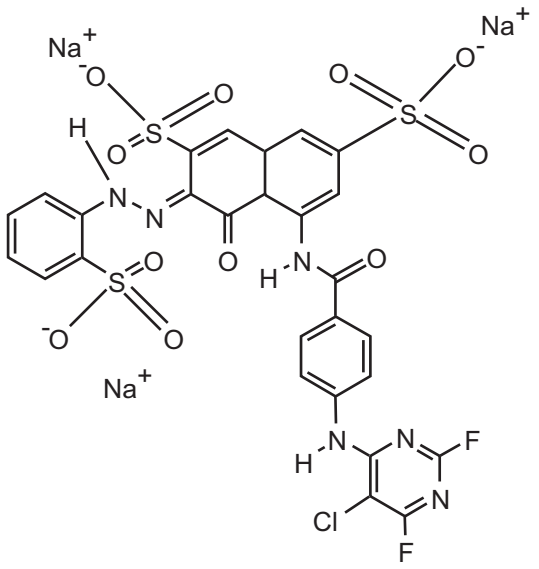

Fig. 1. Structural formula of reactive dye drimarene brilliant red (DBR).

Reagents and solutions. Drimarene brilliant red (DBR) (99% purity), a reactive textile dye widely used in textile industry, was purchased from Hangzhou Weiyi Chemical Co., Ltd. China, through local supplier. The stock solution (500 mg/L) of DBR was prepared by addition of 0.5 g of DBR in 1 L distilled water. The solutions of required concentrations were further prepared through dilution of the stock solution. All the tests were performed at an original solution with pH of 5.3. The chemical oxygen demand (COD) of the resulting dye solution was 580 mg/L.

Adsorption studies. All the adsorption experiments were conducted in 250 mL flasks using 100 mL of dye solution at the original pH. Factorial experimental design was used to perform the experiments and the factors like adsorbent dose (g/L), particle size (mm) and contact time (h) were varied. Calculated quantities of bio-adsorbents were mixed with dye solution, followed by agitation at a rate of 200 rpm in an orbital shaker (Stauart, SSL2, UK). For adsorption kinetics experiments, constant temperature of 25 °C was maintained. Initial adsorbent dose was varied from 6 to 12 g/L for a total contact time from 2 to 32 h. A sample (3 mL) was carefully withdrawn at desired time intervals. Each sample was analyzed after centrifugation at 4000 rpm for 30 min to separate the adsorbent from dye solution. The adsorption capacity (q_e) and colour removal efficiency (R) were calculated using the following equations, respectively:

$$q_e\ (mg/g) = \frac{C_t - C_o}{m} \quad (1)$$

$$R\ (\%) = \frac{C_t - C_o \times 100}{C_o} \quad (2)$$

where:

C_o is the initial dye concentration (mg/L), C_t is the residual dye concentration (mg/L) at time t (h) and m is the mass of an adsorbent (g/L).

Rate constants of decoloration were determined using exponential relation below:

$$\ln\left(\frac{C}{C_o}\right) = -kt \quad (3)$$

where:

C was concentration of dye, time t and C_o was initial dye concentration. A plot of $\ln C/C_o$ versus t without intercept yields slope equals to k.

Analytical procedure. The dye removal was determined at maximum absorption wavelength (530 nm) using visible spectrophotometer (HACH DR2400). The COD was determined through wet digestion by taking 2 mL of dye solution, 1.5 mL of COD reagent and 3.5 mL of H_2SO_4 (Boyd *et al.*, 1947) using closed reflux colorimetric method. The COD reagent was prepared using 500 mL distilled water, 10.22 g $K_2Cr_2O_7$, 167 mL H_2SO_4 and 33.3 g $HgSO_4$ and then diluted to 1000 mL. Afterwards, the solution was digested at 150 ºC for 2 h using block digester (Lovibond, model ET 108, Germany), and finally titrated with ferrous ammonium sulphate (FAS) solution. Solution pH was recorded with digital pH meter (BMS, model pH-200L) after three stage calibration with buffers of pH 4, 7 and 10.

Experimental design and statistical analysis. Main factors; adsorbent dose (A), particle size (B) and, contact time (C) were investigated. An analysis of variance (ANOVA) was performed to analyze the data using SPSS 17 software for the experimental design and statistical significance at 95% confidence interval. Means were also compared using least significant difference (LSD). Multiple regression analysis was performed according to the equation given below:

$$y = \beta_o + \Sigma\ \beta_i \chi_i + \varepsilon \quad (4)$$

where:

y is the response vector for q_e (adsorption capacity) and R (colour removal %). The β_o and β_i are regression coefficients for the intercept, whereas x_i is the independent factor in coded units, and ε is the error term (Chang *et al.* 2011). Coefficients of determination (R^2) were calculated to evaluate the fitness of regression model.

Results and Discussion

Screening factors for dye removal. Experimental design matrix at 32 h contact time is given in Table 1, which shows adsorption capacity (q_e) and colour removal (%) of banana and orange peels, and rice husk. Adsorption capacity of the rice husk was maximum ranging from 6.0 to 10.0 mg/g followed by orange peels i.e. 5.1 to 8.7 mg/g. The lowest q_e was observed in case of banana peels with a maximum value of 3.7 mg/g. Colour removal was also highest with the rice husk showing 84.8% removal.

Effect of adsorbent dose. Dye removal increased with increasing adsorbent doses (Table 1). Statistical significance was determined using analysis of variance (ANOVA) by general linear method of SPSS. The

Table 1. Factorial design matrix for investigated factors for adsorption capacity and colour removal after 32 h contact time at 25 °C

Coded factors		Actual factorial level		Adsorption capacity q_e (mg/g)			Colour removal R (%)		
A	B	Adsorbent dose (g/L)	Particle size (mm)	Banana peels	Orange peels	Rise husk	Banana peels	Orange peels	Rise husk
1	1	6	0.2	3.7	8.7	10.0	22.2	52.3	59.8
1	2	6	0.8	3.1	7.0	6.6	18.6	42.1	39.9
2	1	8	0.2	3.2	6.8	9.5	25.9	54.6	76.1
2	2	8	0.8	2.6	5.6	6.2	21.0	44.4	49.9
3	1	10	0.2	3.1	5.6	8.1	30.8	55.6	80.8
3	2	10	0.8	2.8	5.9	6.2	28.4	59.3	62.5
4	1	12	0.2	2.8	5.3	7.1	33.7	63.4	84.8
4	2	12	0.8	2.6	5.1	6.0	31.5	61.1	72.2

adsorption capacity of banana peels ranged 2.6-3.1 mg/g with the maximum colour removal of 33.7% at the highest adsorbent dose i.e. 12 g/L (Table 1). Higher decolourisation was achieved at higher adsorbent dose i.e. 12 g/L, which was probably due to the presence of unoccupied binding sites for the attachment of dye molecules.

Effect of contact time. Statistically significant colour removal was observed with increasing contact time. Orange peels showed better adsorption capacity and colour removal efficiency (63.4%) as compared to the banana peels with increasing contact time (Fig. 2). Rice husk was the most efficient among the tested adsorbents, achieving colour removal of 84.8% from aqueous dye solution with 12 g/L of an adsorbent dose. Average removal efficiency at 32 h was slightly higher as compared to 16 h contact time, but there was no statistically significant difference. Colour removal was faster initially and decreased with time. In case of banana peel, most decolourisation occurred within 16 h of contact time. In the case of orange peel and rice husk, most decolourisation occurred within 8 h of contact time (Fig. 2). Colour removal rates decreased gradually which could be due to active binding site saturation and probably more time was required to bind further dye molecules with inactive or less active binding sites. Similar trends have been observed by Han *et al.* (2008).

Effect of particle size. Particle size significantly affected the colour removal efficiency of all the bio adsorbents under consideration (Table 1 and Fig. 2). Smaller particle size (0.2 mm) was strongly correlated with colour removal (R^2=0.99) as compared to the larger particle size (0.8 mm) with R^2 value of 0.88. Smaller particle size (0.2 mm) was highly correlated (R^2=0.99) with dye removal as compared to larger particle size (0.8 mm). Similar results have been reported in a study (Punjongharn *et al*., 2008), where increase in adsorption with decrease in particle size was observed.

Regression analysis. Regression analyses displayed the leading effects of an adsorbent dose, contact time (positive) and, particle size (negative), on colour removal as compared to contact time. Following are the codified polynomial regression models for banana peels which correlate to q_e and R (%):

$$q_e \text{ (mg/g)} = + 0.476 + 0.158A - 0.423B + 0.071C \quad (5)$$
$$R\ (\%) = +6.765 + 1.848A - 3.540B + 0.601C \quad (6)$$

where:

A, B, C correspond to adsorbent dose, adsorbent particle size and contact time, respectively. The q_e indicates adsorption capacity and R stands for colour removal. Factors exhibiting the positive values for their coefficients could improve the respective response vector while negative value of the coefficients suggested their inverse relationship with the response vectors. Regression analysis for orange peels revealed that dye removal was strongly affected by the particle size and adsorbent dose. The regression equations for orange peels are given as follows:

$$q_e \text{ (mg/g)} = +0.045 + 0.296A - 1.010B + 0.126C \quad (7)$$
$$R\ (\%) = +5.874 + 3.527A - 8.590B + 1.049C \quad (8)$$

Regression analysis for rice husk shows that coded factor B (particle size) displayed the greatest effect both on colour removal and adsorption capacity followed by the adsorbent dose and least effect of contact time was observed. The regression equations are as follows;

$$q_e \text{ (mg/g)} = +2.024 + 0.512A - 2.823B + 0.064C \quad (9)$$
$$R\ (\%) = +7.366 + 6.025A - 23.91B + 0.532C \quad (10)$$

Regression analysis for rice husk showed that coefficient of determination (R^2) and adjusted R^2 for the model was correlated well (0.99, 0.98).

These findings are in accordance with the theory that larger particles have less surface area compared to the smaller particles having more surface area, for a given volume of particles. The facts are also supported by the correlation values (R^2=0.99) for smaller particle size (0.2 mm). Similar trends have already been reported by Han *et al.* (2008) and Punjongharn *et al.* (2008).

According to chemical composition of banana peels, it contains about 41% carbon by weight, which is an advantage with adsorption processes. This high amount of carbon could be helpful for treating wastewater containing hazardous compounds like dyes (Palma *et al.*, 2011). But in the same research, it has been reported that banana peel was effective only on certain dyes and it had its limitations to remove colour of textile wastewater. Since it was only able to remove 33.7% colour (Table 1) of DBR dye, it was inferred that banana peels cannot be used widely. However, there may be some potential if it is used after pre-treatment with an acid (Xi and Chen, 2014) or alkali and temperature variations (Crini, 2006) that will increase the treatment cost.

Regression analysis for orange peels also revealed that colour removal is strongly influenced by the particle size and adsorbent dose. Similar trends were observed for the adsorption capacity. Fair colour removal efficiency (63.4%) with orange peels is probably due to their citrus content,

Table 2. Isotherm and kinetic models used in present study

Model	Equation	Plot	Parameters	References
Isotherm models				
Langmuir	$q_e = \frac{K_{ads} Q_{max} C_e}{1 + K_{ads} C_e}$ Eq.11	$C_e / q_e \sim C_e$	q_e(mg/g)=equilibrium adsorption capacity K_{ads}(L/mg)=langmuir constant related to free energy of adsorption Q_{max}(mg/g)=maximum adsorbent capacity R_L=separation factor C_o(mg/L)=inititaladsorbate concentration in solution C_e(mg/L)=equilibrium adsorbate concentration in solution	(Langmuir, 1916)
	$\frac{c_e}{q_e} = \frac{1}{1 + K_{ads} C_e E} + \frac{C_e}{Q_{max}}$ Eq.12			
	$R_L = \frac{1}{1 + K_{ads} C_o}$ Eq.13			
Freundlich	$q_e = x/m = K_f C e^n$	$q_e \sim C_e$	q_e(mg/g)=equilibrium adsorption capacity C_e(mg/L)=equilibrium adsorbate concentration in solution K_f(mg/g)(L/g)^n=freubndlich constant h=heterogeneity factor	(Freundlich, 1906)
Kinetic models				
Pseudo 1st order	$Log(q_e - q_e) = log\ q_e - k_1 t/2.303$	$Log\ (q_e - q_t) \sim t$	q_t (mg/g)=amount of adsorbates adsorbed at time t $k_1(h^{-1})$=pseudo 1st order rate constant	(Lagergren, 1898)
Pseudo 2nd order	$\frac{t}{q_t} = \frac{1}{K_2 Q_2^{\ 2}} + \frac{1}{q_2} t$	$t/ qt \sim t$	k_2(gm/g.h)= pseudo 2nd order rate constant h(mg/g.h)=initial adsorption rate	(Mohan *et al.,* 2008)
	$h = k_2 qe^2$			
	$q_t = k_{int} t^{1/2} + C$	$q_t \sim t^{1/2}$		
Intraparticle diffusion (Weber-morris model)	$F = \frac{q_t}{q_e} = 1 - \frac{6}{n^2} \sum_{n=1}^{\infty} \frac{1}{n^2} \exp(-n^2 K_1)$		ki(mg/g $h^{1/2}$)=intraparticle diffusion rate constant C(mg/g)=boundary layer effect $K(h^{-1})$=rate constant of adsorption F=is the fraction of adsorbate in the sorbent at time t (unitless).	(Wang *et al*., 2004)
Dumwald-wagner model	$Log[(1 - F^2]) = -\frac{K_t}{2.303}$	$Log\ (1-F^2) \sim t$		
Double exponential model	$q_t = q_e - \frac{D_2 \exp(-k_1 t)}{m_a} - \frac{D_2 \exp(-k_2}{m_a}$	$Ln(q_e - q_t) \sim t$	D_1& D_2(mg)=diffusion rate parameter for slow and rapid step respectively K_1& $K_2(h^{-1})$= adsorption rate parameter for slow and rapid step respectively ma(g) =mass of adsorbent	(Wilczak and Keinath, 1993)
Boyd model	$In(q_e - q_t) = \frac{In\ D_2}{m_a} - K_2 t$	$Bt \sim t$	$B(h^{-1})$ =Rate coefficient, $D_{eff}(mm^2 h^{-1})$ =liquid film effective diffusion coefficient R (mm) = radius of adsorbent beads	(Boyd *et al.*, 1947)
	$F = \frac{q_t}{q_e} = 1 - \frac{6}{n^2} \sum_{n=1}^{\infty} \frac{1}{n^2} \exp(-n^2 B_t)$			
	$Bt = \left(\sqrt{\pi} - \sqrt{\pi - \left(\frac{\pi^2 F}{3}\right)}\right)^2$ for F<0.85 and Bt=-0.498-ln(1-F) for F>0.85			
	$B = \frac{\pi^2 D_{eff}}{R^2}$			
Proposed model	$q_T = k'(lnt)^n$	$q_e \sim lnt$	k′=rate constant(mg/g.h^n)	This paper

Table 3. First and second order kinetic parameters for adsorption of dye on untreated biomass

Adsorbent	Size (mm)	Dose mg/L	Q_{exp} (mg/g)	First order kinetic model			Second order kinetic model			R^2
				Q_{calc} (mg/g)	K_1 (h^{-1})	R^2	Q_{calc} (mg/g)	K^2 (mg/g.h)	Initial adsorption rate $h=k_2qe^2$ (mg/g.h)	
Rice husk	0.8	6	10.020	7.394	0.160	0.988	11.100	0.030	3.660	0.999
		8	9.550	9.940	0.441	0.956	10.000	0.102	10.200	0.997
		10	8.110	3.683	0.266	0.976	8.403	0.163	11.490	0.999
		12	7.110	2.047	0.155	0.942	7.300	0.174	9.260	0.999
	0.2	6	6.690	3.038	0.139	0.890	7.040	0.087	4.310	0.999
		8	6.270	4.396	0.204	0.998	6.700	0.077	3.460	0.999
		10	6.270	2.053	0.114	0.770	6.490	0.125	5.260	0.999
		12	6.040	3.125	0.232	0.989	6.290	0.159	6.290	0.999
Orange peel	0.8	6	8.796	13.820	0.234	0.940	76.923	8.000	0.311	0.012
		8	6.887	8.521	0.262	0.893	9.461	0.011	0.989	0.895
		10	5.602	7.405	0.344	0.865	7.128	0.020	1.030	0.932
		12	5.324	26.687	0.698	0.907	6.780	0.022	0.995	0.918
	0.2	6	7.099	9.759	0.145	0.972	85.470	0.000	0.263	0.006
		8	5.613	8.656	0.306	0.974	9.074	0.007	0.595	0.542
		10	4.954	8.488	0.290	0.968	7.353	0.012	0.651	0.812
		12	4.128	3.499	0.051	1.000	5.519	0.020	0.595	0.848
Banana peel	0.8	6	3.749	10.703	0.281	0.878	-2.771	0.008	0.062	0.327
		8	3.270	4.242	0.096	0.971	62.112	0.000	0.115	0.005
		10	3.105	3.929	0.182	0.964	5.359	0.010	0.280	0.599
		12	2.832	4.158	0.281	0.981	3.392	0.056	0.647	0.979
	0.2	6	3.178	5.390	0.149	0.878	-2.620	0.008	0.053	0.433
		8	2.689	4.094	0.142	0.936	-33.33	0.000	0.091	0.021
		10	2.861	3.776	0.176	0.923	5.528	0.007	0.222	0.495
		12	2.649	3.926	0.230	0.941	3.577	0.029	0.374	0.932

which is capable of binding dye molecules (Sivaraj *et al.,* 2001). Orange peel contains carboxyl and hydroxyl groups and adsorption capacity improves with increase in carboxyl and hydroxyl content. These properties make it a suitable material for adsorption of a wide range of contaminants. It is found that orange peel contains relatively high content of pectin which plays an important role in adsorption.

Regression analysis for rice husk showed that coefficient of determination (R^2) and adjusted R^2 for the model was correlated well (0.99, 0.98). Minor difference in these values infers that there was a negligible possibility of adding any insignificant term in these regression models (Chang *et al*., 2011). The normal distribution of the predicted values along respective mean values confirmed the appropriateness of the regression models to explain colour removal efficiency and adsorption capacity according to eq. (9) and eq. (10).

Adsorption isotherms. Various isotherm models as well as kinetic models used in present study are shown in Table 2. Langmuir and Freundlich isotherms were selected from several isotherm equations, eq. 11, 12 and 13 already used in the literature (Langmuir, 1916; Freundlich, 1906). In the Langmuir isotherm, it is supposed that adsorption occurs at specific homogeneous sites on surface of an adsorbent and there are no significant interactions within adsorbed species. The adsorbent surface is saturated by a single layer of adsorbent molecules. The linearized Langmuir isotherm equation also known as Hanes-Woolf plot is represented by eq. 11 (Table 2). Linear relationships of rice husk for both particle sizes were found (R^2 =0.99). This indicates suitability of the model to explain the adsorption process equilibrium (Wu *et al.*, 2007) for rice husk. The closeness of calculated q_m (7.2 mg/g) and experimental adsorption capacity (6.7 mg/g) confirmed the validity of this model for the adsorbent.

Langmuir isotherm's characteristics are expressed by equilibrium parameter R_L which is a dimension less

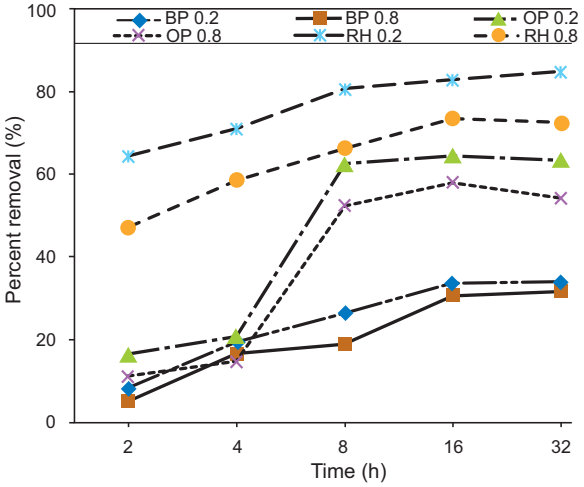

Fig. 2. Effect of contact time on adsorption capacity of different bioadsorbents. BP = banana peel; OP = orange peel; RH = rice husk; 0.2 and 0.8 mm sizes.

constant that measures the favourability and shape of the adsorption isotherm of using eq. 13 (Table 2).The R_L value determines either the isotherm is linear (R_L= 1), favourable (0 <R_L< 1), unfavourable (R_L> 1) or irreversible (R_L= 0). The Freundlich model can be used to explain multilayer and heterogeneous adsorption on surfaces (Freundlich, 1906). Power series regression analysis of the plot of q_e against C_e resulted into correlation coefficients' (R^2) value of less than 0.944. This indicated that the Freundlich plots did not agree well with the experimental data.

For similar adsorption studies, Langmuir model has been applied and reported (Low *et al.*, 2011). Orange and banana peel did not follow the Langmuir model (Table 2). Also, the parameters for Langmuir model came out to be negative, which does not have any physical significance. All the values of R_L calculated from the Langmuir equation ranged between 0-1 for rice husk highlighting the fact that adsorption process was favourable for both particle sizes. This provided the evidence that, rice husk can be used for the commercial scale treatment of dye wastewater. In all the other cases Langmuir model gave fairly low R^2 value in most cases indicating that this model cannot be applied on other biomass materials.

Adsorption kinetics. Kinetics is a significant aspect in assessment of sorption potential of any substance. The kinetic constants can help to adjust residence conditions for dye adsorption. For the adsorption of

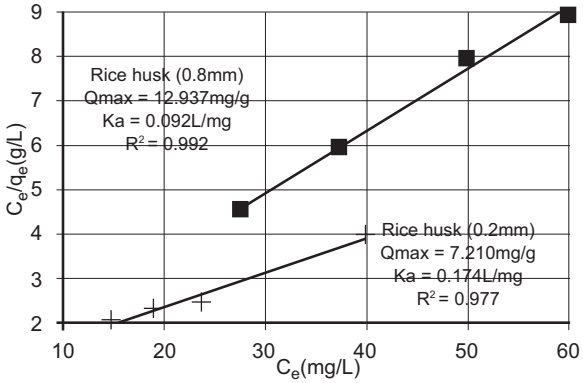

Fig. 3. Langmuir isotherm plot for the adsorption of DBR dye on rice husk (contact time = 32 h; pH = 5.3; temperature = 25 °C).

DBR dye on rice husk after 32 h of contact time, Langmuir isotherm plot is presented in Fig. 3. The rate of achieving equilibrium on the large particle size of rice husk was quicker than that of smaller particle size. Kinetic models usually used in literature are divided into following two categories: (a) Adsorption reaction models (b) Adsorption diffusion models;

The adsorption capacities of larger particle size were lesser than those of small particle size. Large sized particles reached equilibrium earlier because of small surface area as compared to fine particles having large surface area. Three mass transport steps are linked in adsorption process (Wu *et al*., 2007). In the first step, adsorbate moves through the solution to reach external surface of adsorbent by molecular diffusion (film or external diffusion). Then solute movement takes place by pore diffusion from surface of the particle into interior site. In the final step, adsorption of adsorbate takes place on the active sites. The phenomenon requires relatively longer contact time (Crini, 2006).

Orange and banana peels seem to follow pseudo 1st order kinetics with correlation coefficient. Rice husk did not give a strong correlation (R^2=0.77-0.99) in most cases. Pseudo-first order reaction model also indicates film diffusion as rate controlling process. Hence, in case of orange peel and banana peel film diffusion seemed to be rate controlling. The rice husk seems to follow pseudo-second order kinetics quite well. The R^2 values for two particle sizes were found as 0.99 which shows that the adsorption of DBR on rice husk followed pseudo-second order kinetic model (Arami *et al.*, 2005). The average percentage error between calculated and experimental capacity was less than 5%. There seems to be strong correlation between experimental and

calculated capacity (Table 3). Hence, this model can be used to calculate adsorption capacity of rice husk for DBR. Usually initial adsorption rate decreases with particle size except at low solids concentration (6 g/L). The initial faster rate of dye adsorption onto rice husk could be due to the presence of higher number of unused binding sites.

Dumwald-Wagner Model, Boyd, double exponential and Weber-Morris models were used to get mechanisms of adsorption kinetics. Dumwald-Wagner model gave good correlations for most of the combinations like 0.85 to 0.96 for the banana peel. However, in no case, the plot passed through the origin, which shows that the intra-particle diffusion was not the sole process controlling adsorption.

Weber-Morris model showed that the intercept did not pass through the origin (Fig. 4), which indicated the existence of boundary layer effect to some extent, and there was difference in mass transfer rate during initial and final stages of adsorption process (Akar *et al.*, 2008). The value of C1 in case of orange and banana peel came out to be negative which does not have any physical significance and indicates that diffusion through the boundary layer was not rate limiting in initial stages of adsorption (Table 4). There seems to be two (rice husk and orange peel) or three (banana peel) different regimes involved (Fig. 4). In the first regime (0-8 h) boundary layer effect is small and adsorption seems to

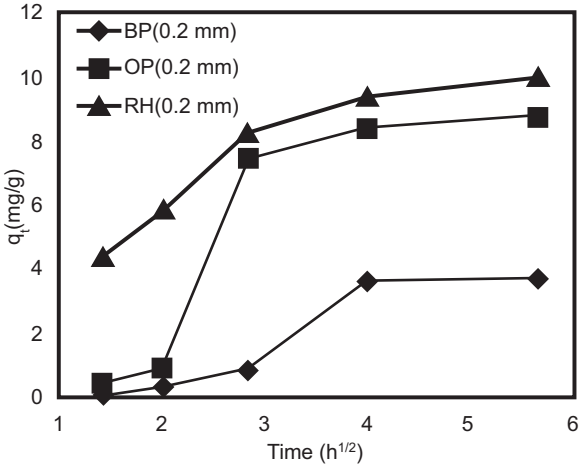

Fig. 4. Intra-particle diffusion model of DBR adsorption for biomasses at 6 g/L dose of 0.2 mm particle size. BP = banana peel; OP =orange peel; rice husk = RH, 0.2 and 0.8 mm sizes.

be mainly controlled by pore diffusion. This represented surface adsorption and immediate use of readily available sorption sites (Chang *et al.,* 2003). There is strong correlation (average R^2=0.98) for first regime in case of rice husk. However, banana and orange peel did not give strong correlations (average R^2=0.91) in most cases. In the second regime (8-32 h) there was a large boundary layer effect, which was indicated by a marked increase in y-intercept of curve for second regime. This could be due to very slow adsorbate diffusion and more time required reaching inner pores from the surface (Mohan *et al.*, 2008). The second regime did not give strong correlation (R^2=0.70) for all biomass used. In the case of banana peel, there is an additional transition region (8-16 h) in many cases.

Adsorption reaction models. Adsorption reaction models originating from chemical reaction kinetics are dependent on the complete adsorption process without considering the actual mechanism of transport of contaminant due to diffusion. The kinetic adsorption data is treated first to find out the order of rate constant. The following reaction models were used:

Lagergren's pseudo first order reaction model. This model (Table 3) is the earliest known and adsorption capacity is considered to describe the adsorption rate. A pseudo first order model has been generally used for description of pollutants adsorption mainly from wastewater. For example, methylene blue adsorption using broad bean peels from aqueous solution and malachite green removal from aqueous solutions with oil palm trunk fibre (Hameed and El-Khaiary, 2008). It was first used to treat kinetic data. Values of the equilibrium adsorption capacity (q_e), rate constant (k_1) and the correlation coefficients (R^2) were calculated from log (q_e-q_t) versus t plots as shown in Table 5. Orange and banana peels seem to follow psuedo 1st order kinetics (R^2 = 0.91-0.98).

Pseudo second order rate expressions. In next step, pseudo-second order model was tested. In this model, it is assumed that the chemisorption may be the rate-limiting step. Chemisorption involves valence forces through exchange or sharing of electrons between sorbate and sorbent. Rate constant of this model is a complex function of the initial solute concentration. The driving force, (q_e-q_t), is directly proportional to the available fraction of active sites. The equation for this model has the advantages like; there is no problem in assigning the effective adsorption capacity, i.e., the rate constant of pseudo second order, the

adsorption capacity, and the initial adsorption rate, these can be calculated from the equation, without any need to know any particular parameter beforehand. This model was applied by plotting t/q_t vs t. The parameters; rate constant (k_2) and initial adsorption rate ($h = k_2 q_e^2$), were determined from the intercept and the slope of plot.

Adsorption diffusion models. On the basis of previous studies, it can be claimed that adsorption kinetics are always controlled by intra-particle diffusion or liquid film diffusion (Meng, 2005). So adsorption diffusion models are developed to explain the film diffusion and/or the process of intra particle diffusion.

Dumwald-Wagner model. Dumwald-Wagner proposed another intra-particle diffusion model (Wang *et al.,* 2004). This model gave fairly good correlations for most of the combinations and R^2 value was above 0.90, whereas, for banana peels it ranged from 0.85 to 0.96 (Table 5).

Boyd's model. The Boyd's model (Boyd *et al.*, 1947) is often used to explain the adsorption kinetics mechanism. Originally proposed for intra-particle diffusion in a spherical particle, it is better known as the Boyd's film-diffusion model. It allows identification of the slowest stage between intra-particle diffusion and film-diffusion. Although the plot of B_t versus t is linear but does not pass through the origin, which indicates that the process is controlled by film diffusion. The effective diffusion coefficient, D_{eff} (mm^2 /h) is as calculated in Table 5.

Double-exponential model (DEM). A double-exponential function proposed was used to describe lead and copper adsorption onto activated carbon (Wilczak and Keinath, 1993). In this model, the uptake process is divided into two steps, a rapid phase for external and internal diffusions and then a slow phase involving intra-particle diffusion. It was demonstrated

Table 4. Kinetic parameters for Weber-Morris model and proposed model for adsorption of dye on untreated biomass at different dosage level

Adsorbent	Size	Dose	Weber - Morris model						Proposed model		
	(mm)	(mg/L)	K_{id1} ($mg/g.h^{1/2}$)	C_1 (mg/g)	R^2	K_{id2} ($mg/g.h^{1/2}$)	C_2 ($mg/g.h^{1/2}$)	R^2	K' ($mg/g.h^{1/2}$)	N	R^2
Rice husk	0.8	6	2.734	0.493	0.998	0.602	6.724	0.929	5.278	0.539	0.979
		8	2.186	3.026	0.987	0.075	9.247	0.145	6.920	0.304	0.915
		10	1.100	0.452	0.989	0.136	7.433	0.516	6.510	0.195	0.937
		12	0.928	4.070	1.000	0.145	6.301	0.983	5.720	0.182	0.977
	0.2	6	1.615	1.554	0.977	0.232	5.376	1.000	4.359	0.371	0.979
		8	1.308	1.654	0.996	0.299	4.672	0.813	3.970	0.383	0.967
		10	1.270	2.283	0.948	0.181	5.212	0.925	4.489	0.285	0.967
		12	1.091	2.528	0.956	0.162	5.233	0.495	4.440	0.281	0.972
Orange peel	0.8	6	5.161	-7.781	0.872	0.448	6.364	0.894	0.869	2.087	0.887
		8	3.763	-4.492	0.956	0.160	6.010	0.943	1.910	1.089	0.924
		10	2.998	3.307	0.924	0.048	5.342	0.919	1.870	1.011	0.886
		12	2.825	-3.075	0.893	0.021	5.250	0.093	1.830	0.980	0.850
	0.2	6	2.782	-3.885	0.963	0.952	2.286	0.556	0.600	2.111	0.971
		8	2.692	-2.650	0.804	0.365	3.708	0.704	1.309	1.450	0.837
		10	2.455	-2.885	0.983	0.226	4.027	0.158	1.256	1.321	0.943
		12	2.517	-3.026	0.887	0.119	4.956	0.206	1.330	1.103	0.828
Banana peel	0.8	6	0.408	-0.380	0.949	0.043	3.471	1.000	0.178	2.538	0.969
		8	0.517	-0.397	0.990	0.713	-0.614	0.913	0.309	1.949	0.995
		10	0.795	-0.334	0.883	0.411	0.920	0.793	0.643	1.447	0.917
		12	0.754	0.000	0.981	0.210	1.734	0.714	1.660	0.899	0.960
	0.2	6	0.285	-0.309	0.990	0.904	-1.617	0.786	0.155	2.366	0.933
		8	0.528	-0.641	0.967	0.610	-0.572	0.827	0.252	1.904	0.959
		10	0.773	-0.573	0.643	0.484	0.300	0.773	0.541	1.489	0.908
		12	0.770	-0.461	0.808	0.353	0.799	0.724	0.761	1.105	0.951

Table 5. Kinetic parameters for Dumwald-Wagner, double exponential and Boyd model for adsorption of dye on untreated biomass at different dosage level

Adsorbent	Size	Dose	Dumwald-wagner model		Double exponential model			Boyds model	
	(mm)	(mg/L)	K_1 (h^{-1})	R^2	K_2 (h^{-1})	D_2 (mg)	R^2	D_{eff} (cm^2/h)	R^2
Rice husk	0.8	6	0.140	0.993	0.160	4.437	0.988	1.327E-06	0.991
		8	0.411	0.950	0.441	7.953	0.956	6.678E-06	0.953
		10	0.248	0.973	0.265	3.683	0.976	3.645E-06	0.975
		12	0.148	0.947	0.155	2.456	0.942	3.237E-06	0.943
	0.2	6	0.126	0.904	0.139	1.823	0.890	3.209E-05	0.897
		8	0.188	0.994	0.204	3.270	0.998	6.103E-05	0.996
		10	0.103	0.781	0.114	2.053	0.770	4.399E-05	0.775
		12	0.209	0.994	0.232	3.749	0.989	4.582E-05	0.991
Orange peel	0.8	6	0.187	0.963	0.233	8.292	0.940	8.700E-07	0.959
		8	0.225	0.908	0.262	6.817	0.893	2.911E-06	0.904
		10	0.310	0.876	0.344	7.405	0.865	1.560E-06	0.869
		12	0.620	0.900	0.698	32.028	0.907	1.791E-06	0.9
	0.2	6	0.074	0.928	0.145	5.761	0.972	3.488E-06	0.923
		8	0.272	0.964	0.306	6.924	0.974	7.157E-05	0.968
		10	0.211	0.939	0.290	8.488	0.968	1.150E-05	0.936
		12	0.022	1.000	0.051	4.207	1.000	4.183E-06	1.000
Banana peel	0.8	6	0.233	0.850	0.280	6.421	0.878	5.497E-07	0.848
		8	0.073	0.919	0.111	3.394	0.971	2.267E-07	0.913
		10	0.148	0.944	0.182	3.929	0.964	4.913E-07	0.944
		12	0.252	0.964	0.281	4.990	0.981	1.261E-06	0.968
	0.2	6	0.105	0.888	0.148	3.234	0.878	4.137E-06	0.846
		8	0.101	0.838	0.142	3.275	0.936	2.684E-06	0.883
		10	0.142	0.899	0.176	3.776	0.923	6.334E-06	0.897
		12	0.203	0.916	0.230	4.710	0.941	1.394E-05	0.917

that the two-step mechanism can be described fairly well with the double-exponential model (Table 5). If $K_1>K_2$, this means that the contribution of rapid process on the overall kinetics can be assumed to be negligible hence, this can be simplified as and be rearranged to a linear form.

Weber-morris model. This model ($q_t=k_{int}\, t^{1/2}+C$) helps us to understand intra-particle diffusion. In this model, k_{int} is the intra-particle diffusion rate constant (μg/g $min^{1/2}$) and C (μg/g) is a constant linked to thickness of the boundary layer. Its higher value means larger boundary layer effect and vice versa. The plot of q_t versus $t^{1/2}$ would result in a linearised relationship. Diffusion would be the rate limiting step if the line passes through the origin. If it is not so, the intra-particle diffusion is responsible for the sorption but it might not be the only step controlling sorption rate. Boundary layer control and some other processes occurring at the same time may also be responsible. In all the cases it is clear that adsorption is not diffusion controlled and boundary layer has significant effect on the overall adsorption rate as well as capacity.

Proposed kinetic model. It was found that in most cases the adsorption kinetic seems to follow the empirical model "$q_t=K'(lnt)^n$"

where:

"q_t" is the adsorption capacity at time "t". This model gave a very good correlation in most of the cases as shown in Table 4.

Conclusion

Out of the three bio adsorbents used, rice husk was the most effective for removal of DBR dye. The optimised conditions for the maximum colour removal efficiency at 25 °C using rice husk were 0.2 mm particle size, 12 g/L dose of adsorbent and 16 h contact time. In the case of rice husk, initial adsorption seemed to be intra-

particle pore diffusion controlled, while later on, film diffusion appeared as the rate limiting mechanism. Adsorption models and kinetic studies indicated the potential of using untreated rice husk as an effective adsorbent. These findings can help us in developing cost-effective remediation process for coloured/textile wastewater. The utilization of such biomass in fixed bed reactor designs for dyes removal from wastewaters needs to be tested.

Acknowledgement

The research was supported and funded by Science and Technology Fund, National University of Sciences and Technology (NUST), Islamabad, Pakistan. We thank Dr. M. Ali Awan for his support and guidance on technical issues during the study. Authors would also like to thank Dr. James Hanly, Institute of Agriculture and Environment, Massey University, New Zealand for critical review and corrections at first stage.

References

Akar, T., Ozcan, S.A., Tunali, S., Ozcan, A. 2008. Biosorption of a textile dye (Acid Blue 40) by cone biomass of *Thuja orientalis*: Estimation of equilibrium, thermodynamic and kinetic parameters. *Bioresource Technology,* **99:** 3057-3065.

Allen, S.J., Gan, Q., Matthews, R. Johnson, P.A. 2003. Comparison of optimised isotherm models for basic dye adsoption by kudzu. *Bioresource Technology*, **88:** 143-152.

Arami, M., Limaee, N.Y., Mahmoodi, N.M., Tabrizi, N.S. 2005. Removal of dyes from colored textile wastewater by orange peel adsorbent: equilibrium and kinetic studies. *Journal of Colloid and Interface Science,* **288:** 371-376.

Boyd, G.E., Adamson, A,W., Myers Jr., L.S. 1947. The exchange adsorption of ions from aqueous solutions by organic zeolites, II, Kinetics. *Journal of the American Chemical Society*, **69:** 2836-2848.

Chang, C.Y., Sai, W.T.T., Ing, C.H., Chang, C.H. 2003. Adsorption of polyethylene glycol (PEG) from aqueous solution onto hydrophobic zeolite. *Journal of Colloid and Interface Science,* **260:** 273-279.

Chang, S.H., Teng, T.T., Ismail, N. 2011. Screening of factors influencing Cu (II) extraction by soybean oil-based organic solvents using fractional factorial design. *Journal of Environmental Management,* **92:** 2580-2585.

Crini, G. 2006. Non-conventional low-cost adsorbents for dye removal: A review. *Bioresource Technology,* **97:** 1061-1085.

Freundlich, H.M.F. 1906. Over the adsorption in solution. *Journal of Physical Chemistry A,* **57:** 385-470.

Gonçalves, J.O., Duarte, D.A., Dotto, G.L., Pinto, L.A.A. 2014. Use of Chitosan with different deacetylation degrees for the adsorption of food dyes in a binary system. *CLEAN - Soil, Air, Water,* DOI. 10. 1002/clean.20120065.

Hameed, B.H., El-Khaiary, M.I. 2008. Sorption kinetics and isotherm studies of a cationic dye using agricultural waste: Broad bean peels. *Journal of Hazardous Materials,* **154:** 639-648.

Han, R., Han, P., Cai, Z., Zhao, Z., Tang, M. 2008. Kinetics and isotherms of Neutral Red adsorption on peanut husk. *Journal of Environmental Sciences,* **20:** 1035-1041.

Hanafiah, M.A.K.M., Ngah, W.S.W., Zolkafly, S.H., Teong, L.C., Majid, Z.A.A. 2012. Acid Blue 25 adsorption on base treated (Shorea dasyphylla) sawdust: Kinetic, isotherm, thermo dynamic and spectroscopic analysis. *Journal of Environmental Sciences,* **24:** 261–268.

Lagergren, S. 1898. About the theory of so-called adsorption of soluble substances. *Kungliga Svenska Vetenskapsa kademiens Handlingar,* **24:** 1-39.

Langmuir, I. 1916. The constitution and fundamental properties of solids and liquids. Part I. Solids. *Journal of the American Chemical Society,* **38:** 2221-2295.

Low, L.W., Teng, T.T., Ahmad, A., Morad, N., Wong, Y.S. 2011. A novel pretreatment method of lignocellulosic material as adsorbent and kinetic study of dye waste adsorption. *Water, Air, & Soil Pollution,* **218:** 293-306.

Meng, F.W. 2005. Study on a Mathematical Model in Predicting Breakthrough Curves of Fixed-bed Adsorption onto Resin Adsorbent. *MS Thesis*, pp. 28-36, Nanjing University, China.

Mohan, S.V., Ramanaiah, S.V., Sarma, P.N. 2008. Biosorption of direct azo dye from aqueous phase onto *Spirogyra* sp. I02: Evaluation of kinetics and mechanistic aspects. *Biochemical Engineering Journal,* **38:** 61-69.

Noroozi, B., Sorial, G.A. 2013. Applicable models for multi-component adsorption of dyes: A review. *Journal of Environmental Sciences,* **25:** 419-429.

Palma, C., Contreras, E., Urra, J., Martinez, M.J. 2011. Eco-friendly technologies based on banana peel use for the decolourization of the dyeing process wastewater. *Waste*

and Biomass Valorization, **2:** 77-86.

Ponnusami, V., Krithika, V., Madhuram, R. Srivastava, S.N. 2007. Biosorption of reactive dye using acid-treated rice husk: Factorial design analysis. *Journal of Hazardous Materials,* **142:** 397-403.

Prigione, V., Grosso, I., Tigini, V., Anastasi, A., Varese, G.C. 2012. Fungal waste-biomasses as potential low-cost biosorbents for decolorization of textile wastewaters. *Water,* **4:** 770-784.

Punjongharn, P., Meevasana, K., Pavasant, P. 2008. Influence of particle size and salinity on adsorption of basic dyes by agricultural waste: dried Seagrape (*Caulerpa lentillifera*). *Journal of Environmental Sciences,* **20:** 760-768.

Royer, B., Cardoso, N.F., Lima, E.C., Vaghetti, J.C., Simon, N.M., Calvete, T.,Veses, R.C. 2009. Applications of Brazilian-pine fruit shell in natural and carbonized forms as adsorbents to removal of methylene blue from aqueous solutions-kinetic and equilibrium study. *Journal of Hazardous Materials,* **164:** 1213-1222.

Sivaraj, R., Namasivayam, C., Kadirvelu, K. 2001. Orange peel as an adsorbent in the removal of acid violet 17 (acid dye) from aqueous solutions. *Waste Management,* **21:** 105-110.

Sun, Q., Yang, L. 2003. The adsorption of basic dyes from aqueous solution on modified peat-resin particle. *Water Research,* **37:** 1535-1544.

Verma, A.K., Dash, R.R., Bhunia, P. 2012. A review on chemical coagulation/flocculation technologies for removal of colour from textile wastewaters. *Journal of Environmental Management,* **93:** 154-168.

Wang, H.L., Chen, J.L., Zhai, Z.C. 2004. Study on thermodynamics and kinetics of adsorption of *p*-toluidine from aqueous solution by hyper-cross-linked polymeric adsorbents. *Environmental Chemistry,* **23:** 188-192.

Wilczak, A., Keinath, T.M. 1993. Kinetics of sorption and desorption of copper(II) and lead(II) on activated carbon. *Water Environment Research,* **65:** 238-244.

Wu, X,. Wu, D., Fu, R. 2007. Studies on the adsorption of reactive brilliant red X-3B dye on organic and carbon aerogels. *Journal of Hazardous Materials,* **147:** 1028-1036.

Xi, Z., Chen, B. 2014. Removal of polycyclic aromatic hydrocarbons from aqueous solution by raw and modified plant residue materials as biosorbents. *Journal of Environmental Sciences,* **26:** 737-748.

Zhang, G., Yi, L., Deng, H., Sun, P. 2014. Dyes adsorption using a synthetic carboxymethyl cellulose-acrylic acid adsorbent. *Journal of Environmental Sciences,* **26:** 1203-1211.

Zhang, W., Yan, H., Li, H., Jiang, Z., Dong, L., Kan, X., Yang, H., Li, A., Cheng, R. 2011. Removal of dyes from aqueous solutions by straw based adsorbents: Batch and column studies. *Chemical Engineering Journal,* **168:** 1120-1127.

Pak. j. sci. ind. res. Ser. A: phys. sci. 2016 **59** (1) 23-29

Synthesis and Application of Highly Active Dithiooxamide Functionalised Multi-Walled Carbon Nanotubes Toward Mercury Removal from Aqueous Solution

Mirabi Ali[a]*, Shokuhi Rad Ali[b], Siadati Seyyed Amir[a] and Alavi Tabari Seyyed Ali[a]

[a]Department of Chemistry, Qaemshahr Branch, Islamic Azad University, Qaemshahr, Iran

[b]Department of Chemical Engineering, Qaemshahr Branch, Islamic Azad University, Qaemshahr, Iran

(received January 20, 2015; revised July 31, 2015; accepted August 3, 2015)

Abstract. Highly sensitive and accurate method has been applied for removal of toxic mercury(II) ions in aqueous solution, using synthesised nanosorbent. Determination of mercury(II) was carried out by flame atomic absorption spectrometer. A nanosorbent multi-walled carbon nanotubes (MWCNT) was synthesised by the reaction of dithiooxamide with functionalised multi-walled carbon nanotubes. Initially, the surface of the multi-walled carbon nanotubes was oxidised by a mixture of nitric and sulphuric acids and then was functionalised using thionyl chloride. The ligand has been attached to the multi-walled carbon nanotubes in somewhat shorter time and lower temperature than previous reported methods. The sorbent was characterised by Fourier transmission infrared and scanning electron microscopy. In this research study, the effect of different parameters in removal of mercury(II) ions by nanosorbent, such as pH, amount of nanosorbent, time and concentration of Hg(II), was investigated. Experiments show that the new MWCNT with loading amount of 1.02 mmol/g is a powerful sorbent for removing the Hg(II) ions from water.

Keywords: carbon nanotubes, mercury removal, aqueous solution, dithiooxamide

Introduction

Mercury is considered as a highly toxic element because of its accumulative and persistent character in the environment (Wu *et al*., 2007). It is one of the famous agents in wide range of human disorders especially in breath cancer (Mishra *et al*., 2005). Although mercury is not an abundant chemical element in nature, it has become dangerously widespread as a result of many industrial and agricultural applications and its threat is rising day-by-day. The major sources of mercury pollution to the environment are waste effluents from the metal plating industry, mining operations, fertilizer industry, tanneries, and textile industry (Farajim *et al*., 2010; Sukocheva *et al*., 2005). The major effects of mercury poisoning are neurological and renal disturbances as well as impairment of pulmonary function. Natural inputs of mercury to the environment are related to weathering of mercuriferous areas, the degassing from surface water and from the crust through volcanic eruptions, naturally-caused forest fires, and biogenic emissions of the earth (Jones *et al*., 2007; Liu *et al*., 2007; Green-Ruiz, 2006; Manohar *et al*., 2002; Boening, 2000), therefore, elimination of the Hg(II) ions from water is essentially required. In this regard, different types of sorbents such as resins, activated chars(Klasson *et al*., 2010), polymers (Zong *et al*., 2001), metal nanooxides, oxidized carbon nanotubes and fibre biosorbents (Johari *et al*., 2014) were evaluated. Sorbents with high surface area, which can lead to high removal of Hg(II) ions, are interesting to the researchers. Discovery of multi-walled carbon nanotubes (MWCNT) in 1991 has generated extensive activity in most areas of science and engineering due to molecular electronics, sensoring, nerve cell stimuli, drug delivery, cancer therapy and chemical properties (El-Sheikh *et al*., 2011). They have become attractive materials for their novel structure characters and high surface area. The unique tubular structure makes CNTs promising absorbent materials, and thus may be used in removal of many pollutants.

In particular, chemical functionalization of carbon nanotubes (CNTs) can modify their physical and chemical properties, leading to the improvement of their performance for specific applications. Thus, the extensive research has been focused on the functionalization of CNTs which can be cited fluorination (Pourrezar *et al*., 2009), carbene addition (Malic *et al*., 2010), esterification (Hu *et al*., 2004) and amidation (Venkatesan *et al*., 2005).

One method for functionalizing of the carbon nanotubes is its oxidation by a strong and concentrated nitric and sulphuric acids mixture (Kalita *et al*., 2008; Yu *et al*., 2008).

*Author for correspondence; E-mail: mirabi2012@yahoo.com

The produced MWCNT-COOH was reacted with thionyl chloride in the presence and absence of dimethylformamide (DMF) (Yu *et al*., 2008b). Moreover, the MWCNT-COCl reacts with various ligands which mostly take more than 80 h (Sone and Yagi, 2009; Teixeira *et al*., 2006; Wang *et al*., 2006).

In this study, oxidation of MWCNT was performed by a mixture of nitric and sulphuric acids. Thionyl chloride was then used to produce the acid chloride functional group on the CNT. Finally the MWCNT-COCl was reacted with dithiooxamide in shorter time and under lower temperature than previous reported methods (Tahermansouri *et al*., 2013; Barbara *et al*., 2011; Yang *et al*., 2009) and then the dithiooxamide functionalised MWCNT was used as a sorbent to remove the toxic Hg(II) ions in different aqueous solutions.

Materials and Methods

Reagents. All chemicals were in analytical grade reagents. All solutions were prepared using double distilled water. A stock standard solution containing 1000 mg/L of Hg(II) was prepared via dissolving appropriate amounts of its nitrate salt $Hg(NO_3)_2$ (obtained from Merck company, Darmstadt, Germany) in distilled water and 0.5 mL concentrated nitric acid that was purchased from Merck company. The multi-walled carbon nanotubes (MWCNT), thionylchloride, triethanolamine, dimethylformamide (DMF), dithiooxamide (ligand), sulphuric acid, and nitric acid were used without further purification.

Instrumentation. Thermo Scientific (model: M5) flame atomic absorption spectrometer with a mercury hollow cathode lamp as a radiation source, operated at 15 mA with a monochromator spectral band pass of 1.0 nm was used for the determination of the exact mercury amount. The wavelength selected for mercury was 253.6 nm. An air-acetylene flame was used for the determination of mercury ions and their flow rates were 10.0 L/min and 0.8 L/min, respectively. Also, this device was equipped with a 50 mm burner head and deuterium background correction. The pH was measured using a Metrohm pH meter (model 744) with a combined pH glass electrode calibrated against two standard buffer solutions (pH 4.0 and 7.0). Other instruments which have been used were: Fourier transmission infrared spectrophotometer (Shimadzu, model 1280), scanning electron microscope (LEO 440i, leo electron microscopy, Cambridge, England) and UV-Vis spectrophotometer (Jenway model 6505).

Functionalisation of carbon nanotubes sorbent. The MWCNT (4.0 g) were added to 30.0 mL of a mixture of sulphuric acid and nitric acid (3:1 v/v), and then the mixture was heated at 80 °C for 2 h. The resulted MWCNT-COOH was centrifuged at 4000 rpm for 5 min to remove excess acids and then was eluted by distilled water and dried at 80 °C. Dried 3.0 g of the MWCNT-COOH was dispersed in 15.0 mL of thionyl chloride and refluxed at 70 °C for 1 h. After synthesis of MWCNT-COCl it was eluted with anhydrous toluene and then dried in oven at 70 °C for 48 h. 3.0 g of MWCNT-COCl has been dispersed using ultrasonic in DMF as solvent and 0.5 g of dithiooxamide and 0.3 mL of triethanolamine were added to the mixture, subsequently (Scheme 1). The mixture was heated at 80 °C for 30 h. The synthesised MWCNT-CO-dithiooxamide was separated from the reaction mixture by centrifugation and washed with distilled water.

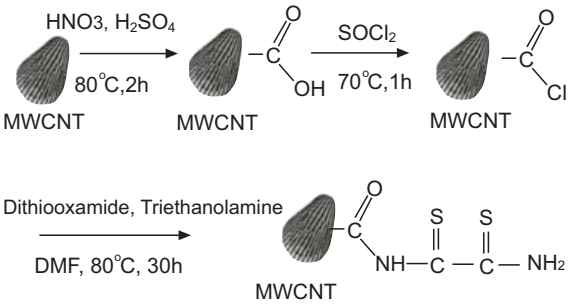

Scheme 1. Preparation of dithiooxamide functionalised multi walled carbon nanotubes.

Procedure for removal of Hg(II) ion. The effect of different parameters such as pH, sorbent dosage, time and the mercury concentration on removal of mercury ions were studied. The pH effect was studied within the pH range of 4.0-9.0. In other hand the effect of the sorbent dosage was studied by different absorbent values between 20-100 mg. Also the effect of the time was studied by different times between 10-70 min. Moreover, the effect of mercury concentration was observed within the concentration range of 40-300 mg/L. Conventional one factor- at-a-time method was used, and optimised amount of any parameter was used to next optimisation of other amounts.

Dithiooxamide functionalized multi walled carbon nanotubes (70 mg) was added to 100 mL of mercury(II) ions solution (150 mg/L). The pH value was adjusted

by adding 0.5 mL of ammonia/ammonium chloride buffer solution (1.0×10^{-3} mol/L, pH 9.0). Afterwards, the solution was stirred at room temperature for 30 min and then the MWCNT sorbent separated from the solution using centrifuge for 5 min at 4000 rpm. For determination of residual mercury(II) ions, the supernatant was analysed by flame atomic absorption spectrometer (FAAS). Our calculation for mercury removal and loading amount has been done based on eq.1 and eq.2.

$$R\% = C_i - C_e / C_i \times 100 \quad \text{..... (1)}$$

where:

R% = mercury removal percent; C_i and C_e (mg/L) = the initial and equilibrium concentrations of Hg(II), respectively.

$$L.A. = V \times C \times \%R / M_{Hg} \times m_s \quad \text{..... (2)}$$

where:

L.A. = loading amount; V = volume of solution sample (L); C = concentration of Hg (mg/L); M_{Hg} = the atomic weight of Hg (g) and m_s = the mass of nanosorbent (g).

Results and Discussion

Synthesis of dithiooxamide functionalized MWCNT as sorbent. In order to verify the linkage between MWCNT and the dithiooxamide ligand, the Fourier transmission infrared spectroscopy (FT-IR) was used (Fig. 1a-b). Comparison of the FT-IR spectra of MWCNT-COOH with that of MWCNT-dithiooxamide, gives important results to identify the groups substitution. The FT-IR spectra of MWCNT-COOH (Fig. 1a) identified the peaks of C=O at 1704.96 cm^{-1} and O-H at 3386.77 cm^{-1}, respectively. In the FT-IR spectra of MWCNT-dithiooxamide (Fig. 1b), the sharp peak of N-H bond appeared at the area of 3425.34 cm^{-1} instead of wide peak of O-H group which proves attachment of dithiooxamide to the carbon nanotubes (see Scheme 1).

Surface morphology. The size and morphology of dithiooxamide functionalized MWCNT before and after absorbing the mercury(II) ions are illustrated in (Fig. 2a-b) by using SEM. After precipitating with mercury ions, Fig. 2b indicates a significant change which was observed along the tube walls. This significant change on the surface of CNT proves the precipitation of mercury ions on this sorbent.

Optimisation of adsorption conditions. ***Effect of pH.*** The pH value of the solution is one of the most important

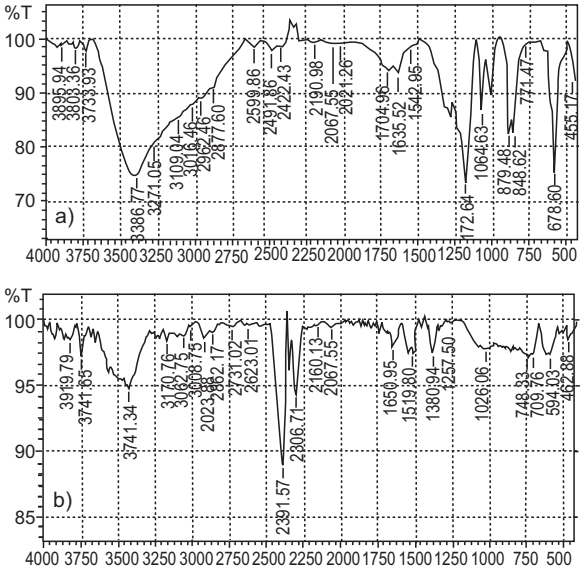

Fig. (1a-b). FT-IR spectrum of (a) MWCNT-COOH and (b) MWCNT-CO-dithiooxamide.

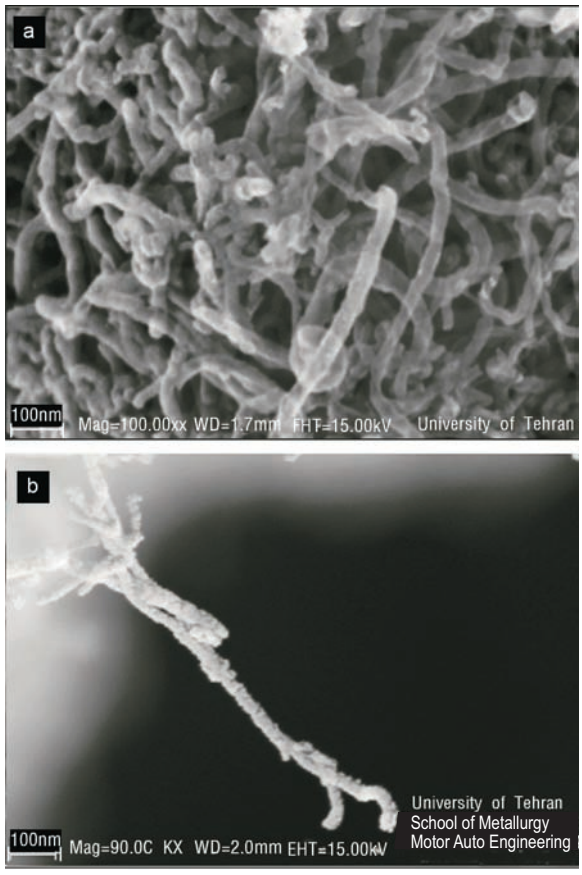

Fig. 2(a-b). SEM image of dithiooxamide multi walled carbon nanotubes (a) before absorption of mercury (II) ions, (b) after absorption of mercury(II) ions.

factors which affect the adsorption behaviour of mercury ions on sorbents. It is not only due to the surface structure of sorbents, but it may also influence the interaction between sorbents and mercury ions. In this case, due to the presence of amide functional group in the ligand structure, the decrease in pH can also significantly reduce the activity of sorbent (Scheme 2). The effect of pH was studied within the pH range of 4.0-9.0. At low pH values the surface of dithiooxamide gives positive charge because of acidic situation. So repeal interaction will occur between the positive surface and Hg^{2+} resulting decrease in adsorption. In contrast at higher pH values, reveres interaction happens resulting increase in adsorption. According to Fig. 3, the most suitable pH value for this sorbent was found to be 9.0 which results in the highest amount of mercury removal.

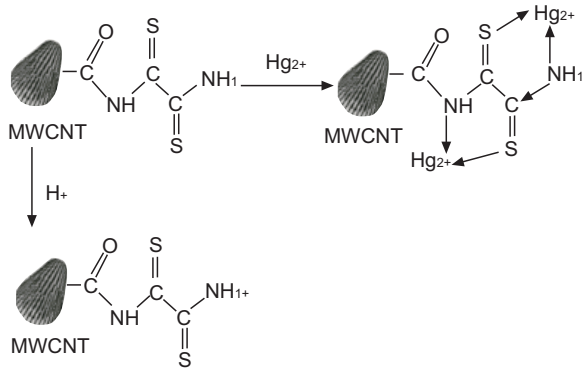

Scheme 2. Suggested binding model of dithiooxamide functionalised multi walled carbon nanotubes and mercury(II) ions.

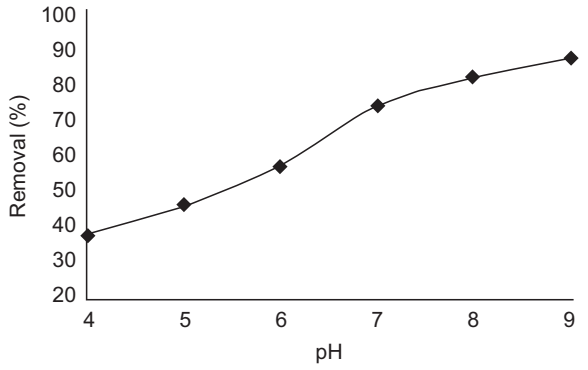

Fig. 3. The effect of pH on the sorbent activity. Removal conditions: aqueous solution volume (100.0 mL); sorbent dosage (70 mg); time of adsorption (30 min); concentration of mercury (150 mg/L).

***Effect of the sorbent dosage*.** The effect of the sorbent dosage on the adsorption of Hg(II) was studied by different absorbent values between 20-100 mg. The results in Fig. 4 show that, Hg(II) was approximately, adsorbed on the surface of sorbent. According to these results, after about 70 mg of sorbent, the value of adsorption for Hg(II) does not change significantly. So, 70 mg of the sorbent was selected for further studies.

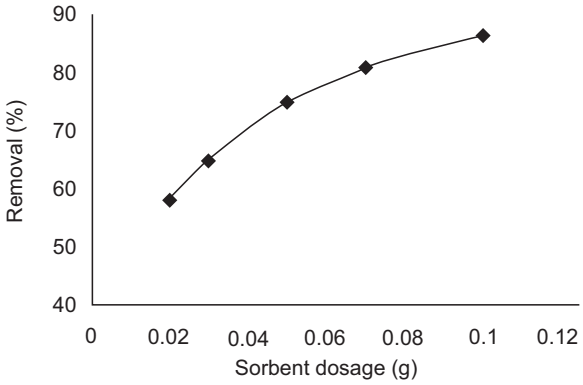

Fig. 4. The effect of sorbent dosage on adsorption. Removal conditions: aqueous solution volume (100.0 mL); pH (9.0); time of adsorption (30 min); concentration of mercury (150 mg/L).

***Effect of time*.** The effect of time on the adsorption of Hg(II) was studied by different times between 10-70 min and illustrated in Fig. 5. The results show that, after about 30 min of adsorption process, the value of adsorption does not change significantly. So, this time is the contact time required for achieving the adsorption equilibrium which is lower than the required contact time (120 min) (Johari *et al*., 2014).

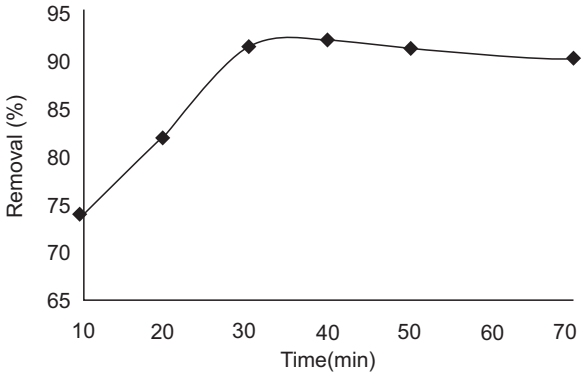

Fig. 5. The effect of time of adsorption. Removal conditions: aqueous solution volume (100.0 mL); sorbent dosage (70 mg); pH (9.0); concentration of mercury (150 mg/L).

Effect of Hg(II) concentration. To study the possibility of our proposed sorbent toward different concentrations of Hg(II), the effect of different concentrations of this cation was studied within the range of 40 – 300 mg/L. There was a high value of adsorption at the low concentration of mercury ions. But when the ions dosage increased to 200 mg/L, the activity of sorbent decreased. According to Fig. 6, the most appropriate concentration value for Hg(II) was found to be 150 mg/L based on the removal percent and also the loading amount for the applied sorbent is 1.02 mmol/g which is higher than as per the values of 0.720 mmol/g (Johari *et al*., 2014) and 0.351 mmol/g (Karthika and Sekar, 2012). Comparison of the presented method with other reported methods for removal of mercury show that presented method has better loading amount (Karthika and Sekar, 2012).

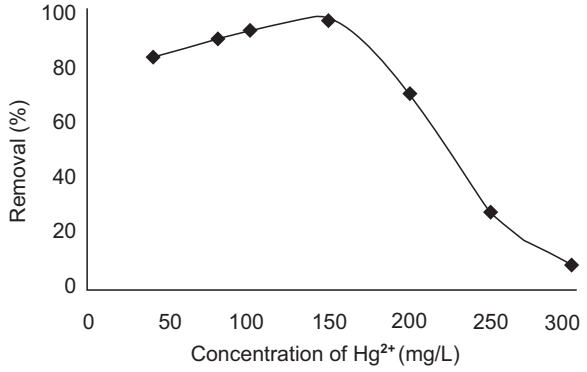

Fig. 6. The effect of mercury concentration on the sorbent activity. Removal conditions: aqueous solution volume (100.0 mL); time of adsorption (30 min); sorbent dosage (70 mg); pH (9.0).

The amount of absorbed Hg(II) at the time of equilibrium based on the mass of sorbent was calculated using eq. 3.

$$q_e = (C_o - C_e) \times V/W \quad \text{..... (3)}$$

where:

q_e = amount of absorbed Hg(II) at the time of equilibrium (mg/g);
C_o = initial concentration of Hg(II) (mg/L);
C_e = residual concentration of Hg(II) in solution (mg/L)
V = volume of the solution (L) and
W = mass of sorbent (g).

A scattered graph of Hg(II) removed amount, per gram of sorbent as a function of equilibrium Hg(II) concentration is given in Fig. 7. It can be seen that, at Hg(II) concentration of 150 mg/L maximum amount of q_e is achieved which is totally in accordance to results of Fig. 6.

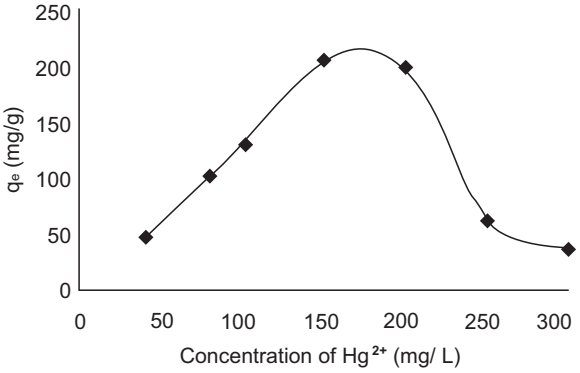

Fig. 7. A scattered graph of Hg(II) removed amount, per gram of sorbent as a function of equilibrium Hg(II) concentration. Removal conditions: aqueous solution volume (100.0 mL); time of adsorption (30 min); sorbent dosage (70 mg); pH (9.0).

Effect of other ions. The effects of other familiar ions in aqueous samples on the removal of mercury were studied. In these experiments, 100.0 mL of solutions containing 150 mg/L of mercury and various amounts of interfering ions were treated according to the presented procedure. An ion was considered to interfere when its

Table 1. Effect of other ions on the removal of mercury

Ion	Ion/Hg(II) (w/w)	Removal (%)
Li^+	7	97.6
Na^+	7	96.1
Cu^{2+}	3	98.7
Ni^{2+}	2	95.5
Al^{3+}	2	97.3
Zn^{2+}	2	99.5
Pb^{2+}	2	97.9
Cd^{2+}	2	97.2
Co^{2+}	3	99.1
Cr^{3+}	3	95.3
Fe^{2+}	2	99.3
NO_3^-	7	98.6
Cl^-	5	96.7
SO_4^{2-}	3	95.4

presence produced a variation of more than 5% in the removal of mercury in aqueous sample. The results of Table 1, indicate that the removal of mercury is almost quantitative in the presence of interfering ions.

Conclusion

A new effective sorbent was synthesised by functionalization of the MWCNT. Experiments show that the new modified MWCNT with a loading amount of 1.02 mmol/g is a powerful sorbent for removing the Hg(II) ions from water. This method indicates that 95.7% removal of Hg^2 + is possible at optimal conditions of pH = 9, mercury ion concentration = 150 mg/L, and the sorbent dosage = 0.07 g. The results showed that, MWCNT-dithiooxamide is an excellent absorbent for moderate concentrations of mercury ions. This proposed method applies an environment friendly non-toxic absorbent which does not threaten human health. Also this method is simple, highly sensitive, selective and relatively fast.

Acknowledgement

The authors thank the Research Council at the Qaemshahr Branch, Islamic Azad University for technical and financial support.

References

Barbara, C.F., Bonalume, G.W.L., Jesualdo Luiz, R. 2011. Functionalized carbon nanotubes for nanocomposites. In: *16th International Conference on Composite Structures ICCS 16*, A.J.M. Ferreira (ed), Porto, Portugal.

Boening, D.W. 2000. Ecological effects, transport, and fate of mercury: a general review. *Chemosphere*, **40:** 1335-1351.

Chiarle, S., Ratto, M., Rovatti, M. 2000. Mercury removal from water by ion exchange resins absorption. *Water Research*, **34:** 2971-2978.

El-Sheikh, A.H., Al-Degs, Y.S., Al-Asad, R.M., Sweileh, J.A. 2011. Effect of oxidation and geometrical dimensions of carbon nanotubes on Hg(II) sorption and preconcentration from real waters. *Desalination*, **270:** 214-220.

Ghambarian, M., Khalili-Zanjani, M.R., Yamini, Y., Esrafili, A., Yazdanfar, N. 2010. Preconcentration and speciation of arsenic in water specimens by the combination of solidification of floating drop microextraction and electrothermal atomic absorption spectrometry. *Talanta*, **81:** 197-201.

Green-Ruiz, C.R. 2006. Mercury(II) removal from aqueous solutions by nonviable *Bacillus* sp. from a tropical estuary. *Bioresource Technology*, **97:** 1907-1911.

Hu, H., Ni, Y., Montana, V., Haddon, R.C., Parpura, V. 2004. Chemically functionalized carbon nanotubes as substrates for neuronal growth. *Nano Letter*, **4:** 507-511.

Johari, K., Saman, N., Song, S.T., Heng, J.Y.Y., Mat, H. 2014. Study of Hg(II) removal from aqueous solution using lignocellulosic coconut fiber biosorbents: Equilibrium and kinetic evaluation. *Chemical Engineering Communications*, **201:** 1198-1220.

Jones, A.P., Hoffmann, J.W., Smith, D.N., Feeley, T.J.3rd, Murphy, J.T. 2007. DOE/NETL's phase II mercury control technology field testing program. Preliminary economic analysis of activated carbon injection. *Environmental Science and Technology*, **41:** 1365-1371.

Kalita, G., Adhikari, S., Aryal, H.R., Ghimre, D.C., Afre, R., Soga, T., Sharon, M., Umeno, M. 2008. Flourination of multi-walled carbon nanotubes (MWNTs) via surface microwave (SW-MW) plasma treatment. *Physica E*, **41:** 299-303.

Karthika, C., Sekar, M. 2012. Removal of Hg(II) ions from aqueous solution by acid acrylic resin–A study through absorption isotherms analysis. *I Research Journal of Environment Sciences*, **1:** 34-41.

Klasson, K.T., Lima, I.M., Boihem, J.L.L., Wartelle, L.H. 2010. Feasibility of mercury removal from simulated flue gas by activated chars made from poultry manures. *Journal of Environmental Management*, **91:** 2466-2470.

Liu, S.H., Yan, N.Q., Liu, Z.R., Qu, Z., Wang, H.P., Chang, S.G., Miller, C. 2007. Using bromine gas to enhance mercury removal from flue gas of coal-fired power plants. *Environmental Science and Technology*, **41:** 1405-1412.

Malic, E., Maultzsch, J., Reich, S., Knorr, A. 2010. Excitonic absorption spectra of metallic single-walled carbon nanotubes. *Physical Review B*, **82:** 035433.

Manohar, D.M., Krishnan, A.K., Anirudhan, T.S. 2002. Removal of mercury(II) from aqueous solutions and chlor-alkali industry wastewater using 2-mercaptobenzimidazole-clay. *Water Research*, **36:** 1609-1619.

Mishra, S., Tripathi, R.M., Bhalke, S., Shukla, V.K., Puranik, V.D. 2005. Determination of methylmercury and mercury(II) in a marine ecosystem using solid-

phase microextraction gas chromatography-mass spectrometry. *Analytica Chimica Acta*, **551:** 192-198.

Pourreza, N., Parham, H., Kiasat, A.R., Ghanemi, K., Abdollahi, N. 2009. Solid phase extraction of mercury on sulfur loaded with N-(2-chloro benzoyl)N'-phenylthiourea as a new adsorbent and determination by cold vapor atomic absorption spectrometry. *Talanta*, **78:** 1293-1297.

Sone, K., Yagi, M. 2009. Chemical adsorption onto an ITO substrate of single-wall carbon nanotube functionalized by carboxylic groups as an efficient support for electrocatalyst. *Electroanalysis*, **21:** 144-149.

Sukocheva, O.A., Yang, Y., Gierthy, J.F., Seegal, R.F. 2005. Methyl mercury influences growth-related signaling in MCF-7 breast cancer cells. *Environmental Toxicology*, **20:** 32-44.

Tahermansouri, H., Aryanfar, Y., Biazar, E. 2013. Synthesis, characterization, and the influence of functionalized multi-walled carbon nanotubes with creatinine and 2-aminobenzophenone on the gastric cancer cells. *Bulletin of Korean Chemical Society*, **34:** 149-153.

Teixeira Tarley, C.R., Barbosa, A.F., Segatelli, M.G., Figueiredo, E.C., Luccas, P.O. 2006. Highly improved sensitivity of TS-FF-AAS for Cd(II) determination at ng L^{-1} levels using a simple flow injection minicolumn preconcentration system with multiwall carbon nanotubes. *Journal of Analytical Atomic Spectrometry*, **21:** 1305-1313.

Venkatesan, N., Yoshimitso, J., Ito, Y., Shibata, N., Takada, K. 2005. Liquid filled nanoparticles as a drug delivery tool for protein therapeutics. *Journal Biomaterials*, **26:** 7154-7163.

Wang, X., Li, W., Chen, Z., Waje, M., Yan, Y. 2006. Durability investigation of carbon nanotube as catalyst support for proton exchange membrane fuel cell. *Journal of Power Sources*, **158:** 154-159.

Wu, G., Wang, Z., Wang, J., He, C. 2007. Hierarchically imprinted organic-inorganic hybrid sorbent for selective separation of mercury ion from aqueous solution. *Analytica Chimica Acta*, **582:** 304-310.

Yang, K., Gu, M., Guo, Y., Pan, X., Mu, G. 2009. Effects of carbon nanotubes functionalization on the mechanical and thermal properties of expoxy composites. *Carbon*, **47:** 1723-1737.

Yu, J.G., Huang, K.L., Liu, S.Q., Tang, J.C. 2008a. Preparation and characterization of soluble methyl- β-cyclodextrin functionalized single-walled carbon nanotubes. *Physica E: Low-Dimensional Systems & Nanostructures*, **40:** 689-692.

Yu, J.G., Huang, K.L., Tang, J.C. 2008b. Chemical attachment of dibromocarbene to carbon nanotubes. *Physica E: Low-Dimensional Systems & Nanostructures*, **41:** 181-184.

Zong, G., Chen, H., Qu, R., Wang, C., Ji, N. 2011. Synthesis of polyacrylonitrile-grafted cross-linked N-chlorosulfonamidated polystyrene via surface-initiated ARGET ATRP, and use of the resin in mercury removal after modification. *Journal of Hazardous Materials*, **186:** 614-621.

Pak. j. sci. ind. res. Ser. A: phys. sci. 2016 **59** (1) 30-33

Remote Controlling and Monitoring of Microscopic Slides

Ghulam Mustafa[a]*, Muhammad Tahir Qadri[b] and Umar Daraz[c]

[a]PCSIR Laboratories Complex, Karachi-75280, Pakistan

[b]Department of Electronics Engineering, Sir Syed University of Engineering & Technology, Karachi, Pakistan

[c]Pathological Department of Civil Hospital, Karachi, Pakistan

(received December 18, 2014; revised May 11, 2015; accepted May 21, 2015)

Abstract. Remotely controlled microscopic slide was designed using especial Graphical User Interface (GUI) which interfaces the user at remote location with the real microscope using site and the user can easily view and control the slide present on the microscope's stage. Precise motors have been used to allow the movement in all the three dimensions required by a pathologist. The pathologist can easily access these slides from any remote location and so the physical presence of the pathologist is now made easy. This invention would increase the health care efficiency by reducing the time and cost of diagnosis, making it very easy to get the expert's opinion and supporting the pathologist to relocate himself for his work. The microscope is controlled with computer with an attractive Graphical User Interface (GUI), through which a pathologist can easily monitor, control and record the image of a slide. The pathologist can now do his work regardless of his location, time, cost and physically presence of lab equipment. The technology will help the specialist in viewing the patients slide from any location in the world. He would be able to monitor and control the stage. This will also help the pathological laboratories in getting opinion from senior pathologist who are present at any far location in the world. This system also reduces the life risks of the patients.

Keywords: pathology, remote monitoring, microscope, motor control, LabVIEW, Arduino, teamviewer

Introduction

Health care is the most important sector these days and many scientists are busy in their research using the new era technologies to provide health facilities to human beings (John *et al.,* 2009; Kamel- Boullos and Wheeler 2007; Eysenbach, 2001). In the recent time there is a rapid development in information technologies i.e., growth of internet through high speed networks, communication technologies, web technologies, etc. Combination of new age technologies gave birth of a new field which is remote monitoring and controlling which rises the technological change in the field of control industries, communication industries, automotive industries, medical, agriculture etc. The aim of present study is to facilitate the personnels working in medical field, specifically a pathologist and to reduce the time of diagnosis of a disease. This research paper introduces a new solution for monitoring and controlling the microscopic slides regardless of the location of the pathologist.

Facilitating a pathologist has always remained an important issue of discussion, because in an emergency diagnosis can be delayed due to unavailability of the pathologist which is a high risk of patient's life. So there have been several methods used previously to resolve this matter. But monitoring and controlling the slides from any location in the world is a great achievement. This research shows the real implementation of the method that could be used for remote monitoring of slides and control of the stage in up-down, right-left and in and out movements.

The machine is composed of a visualization system which is interfaced with the microscope, a control board that controls and interfaces the user interface with motors, a graphical user interface which contains the graphical push buttons providing the control in three dimensions and a software through which the doctor can interact with the user interface remotely.

This is a low cost and very effective method by which the time to diagnose a disease would be readily decreased. Microscopic examination cost is very high for the underdeveloped countries where the slides are being sent to other cities to the specialist. Now, using this technique the pathologist can give his report in a few minutes. Also this will reduce the health care cost that was previously bared by the patients and the pathological laboratories. Also the pathologists will be free from moving into different labs and can easily perform their task from any location even from their home. This will facilitate them physically as well as economically.

*Author for correspondence; E-mail: mustafabme@gmail.com

Materials and Methods

This system model is described as follows: The system consists of five parts. The first part is the image acquisition whose purpose is to acquire the real time video signal using LabVIEW (NILS, 2014) based graphical user interface (GUI). The second part is to process the video signal using image processing tools in LabVIEW. The GUI is designed for this purpose which is the medium of communication between the physician and the microscopic unit. The third part is the design of controlling circuitry in order to control the movement of microscopic slides using stepper motors. The fourth part is the arduino (Arduino, 2014a) based controlling unit which is interfaced with the GUI to move the slides accordingly. The last part of the system is to publish the GUI on internet for remote monitoring and controlling of the microscopic slides. The overall block diagram of the system is illustrated in Fig. 1.

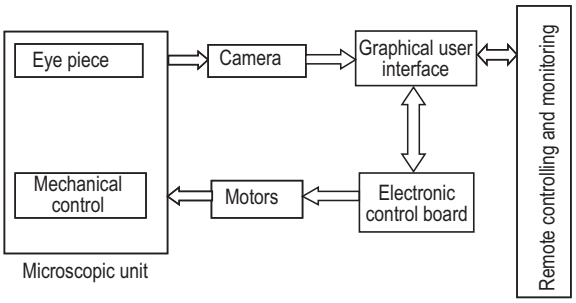

Fig. 1. Overall block diagram of the system.

Image acquisition. The most important part of the microscope is the eye piece from where the image of the slide is seen by the pathologist. In order to acquire the image from the eye piece, a digital camera of high resolution is attached on the eye piece. The camera is interfaced at the USB port of the system and is able to transmit live video of the slide to the attached computer. For this purpose LabVIEW software (NILS, 2014) is used.

To interface the camera in LabVIEW an additional tool kit is required. LabVIEW provides a solution known as vision acquisition software (NIVAS, 2014) which makes it very easy to interface any USB camera in LabVIEW. After interfacing the camera the live video of the slide of microscope was viewed as shown in Fig. 2.

LabVIEW based GUI. To get the user's input and translate it into machine understandable format, an interface is required to communicate. This interface must be easy to understand and simple to use, so that the user can perform its task very easily. The interface developed here is named

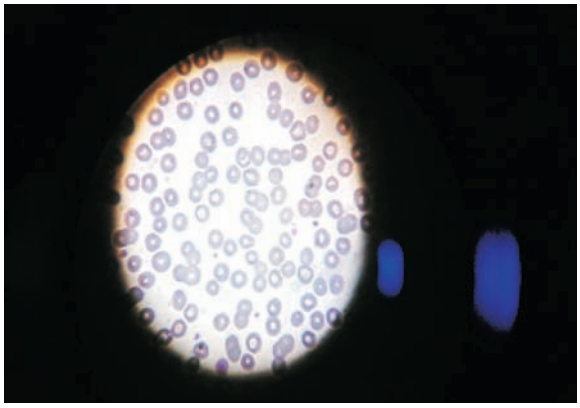

Fig. 2. Snapshot of the microscopic slide video.

as a graphical user interface. This is the main link of the whole system as it provides the communication between the user's interface and the central control board, which is arduinio based system. The task of the GUI is to handle the following operations.

i. Image acquisition.
ii. To process the user's input.
iii. Communicating the data to the control board.

The image was acquired in LabVIEW using the Vision Acquisition Software, which provides the opportunity to interface any USB imaging device having direct show support. In order to view the slide continuously, the camera is used in a live video display mode.

As the slide can be moved in all the three dimensions, therefore, the user is provided with the control buttons on the front panel to move it accordingly. These controls are simply made by using push buttons. The GUI contains the push buttons to adjust the position of slide and a control which displays the live video of the slide. The hardware interfaced gets the input corresponding specific button pressed by the user, as illustrated in Fig. 3.

Finally, the control board is made by using Arduino mega2560 (Arduino, 2014b) microcontroller board. This board is interfaced with LabVIEW on HyperTerminal (HTS, 2014) on USB port.

Microscopic slides controlling. The slide is placed on the microscope called as 'Stage'. After placing a slide on the stage of microscope, the stage is moved 'up', 'down', 'in' and 'out' and the slide can be moved in right and left directions. These all actions are performed using the mechanical knobs present for the tasks in microscope. In order to control these movements through a computer, especial stepper motors are required to be attached with

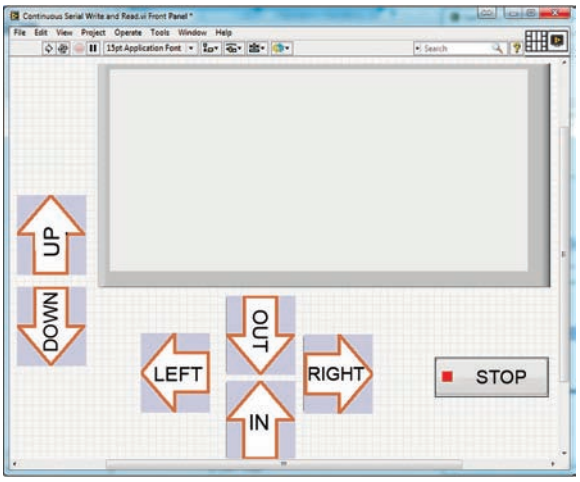

Fig. 3. LabVIEW based GUI.

individual knob. Since our requirement is two dimension accurate movement in each dimension. A stepper motor of 1.8° step is feasible for the task. The torque of the motor is dependent upon the mechanical force required to move the knob. An easily available stepper motor can provide enough torque to rotate it.

Electronic circuit is required to control the rotation of the motors. 'Arduino Motor Control Shield' was used to control the stepper's movement. The Arduino shield can be easily attached with the Arduino main board and provide the additional library of motor control through which the user can control the acceleration, direction and torque of the motor easily.

The arduino shield has the capacity to control two stepper motors at a time. Therefore, an additional circuit developed on ULN2003 was used which was directly attached with the Arduino main board and the stepper motor. With these attachments it became easy to have a control on the movement of slide of microscope. In order to view the sample of the slide especial arrangement has to be made through which the slide moves accurately and precisely.

In order to control the slide's direction on the stage, an especial control circuitry is required to accurately move the slide in three dimensions. The slide placed by the technician on the stage of microscope could only be seen easily by the doctor when he can view the whole span of the slide. In order to achieve the target, three stepper motors were used to control the up-down, right-left and in-out motion of it. Each stepper motor with the accuracy of 1.8° was used, which was providing accurate linear motion in all dimensions.

Arduino based controlling unit. A central control board was required to get the signal from the user and then to control the required motor in specified direction and with specific speed. There are several options to perform the task, but an Arduino board is a good option. The Arduino board is developed around Atmega AVR Microcontrollers and provides the opportunity to use its ports. The Arduino also provides an easy to learn and programme code that could be used to run the microcontroller used in the board. The Arduino board is USB powered and is supplied with its own compiler, so it gets very easy for the user to write, compile and upload the code. The Arduino Board comes in variety and the user can select specific board according to their requirements. Due to Arduino Motor Shield with a facility to drive three stepper at a time Arduino mega 2560 board was used in the present study. This board has 8 bit microcontroller having 86 digital I/O pins to cope with present requirement.

The Arduino mega board was programmed to control the motor and to communicate with the GUI. The Central Control board communicates with computer and gets the control signals from the user and transmits this into the motor control signal to specific motor.

Remote monitoring and controlling of the slides. Accurate software through which the remote monitoring and controlling could be done was the most important part of this solution. To access any system remotely it is always important to provide a secure access so that only that person can use it having the full authority. Remote computer controlling software was used for this purpose which provides a secure access to the user present at the remote location. There are many softwares available in the market that provides the remote desktop sharing option, they also provide the control of the desktop. Team viewer software (TVS) is one of them. Team viewer software was used to share the desktop of the computer on which the GUI was present. Figure 4 shows the front panel view from the remote location.

Results and Discussion

The operation of the complete remote controlled microscope is divided into two ends. One end is the microscope interfaced with the PC and the other end is the remote computer on which the pathologist is present to view the slide.

At the first end a PC is interfaced with the microscope through its camera and Arduino board connected at the

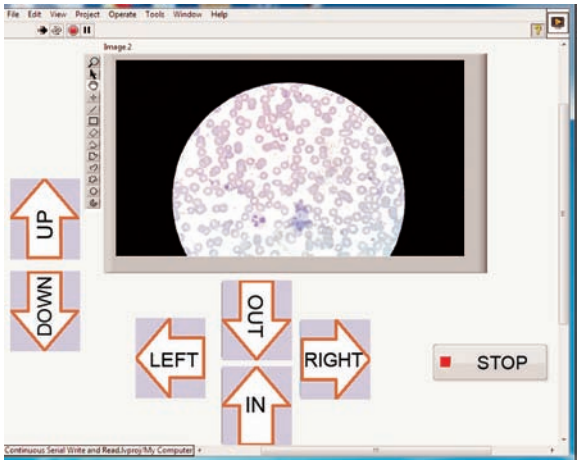

Fig. 4. Front panel to view and control the microscopic slides from remote location.

USB port of the PC, the graphical user interfaces the hardware which displays the live video of the slide to be examined. A remote desktop sharing and control software must be installed on both sides so that the screen could be easily shared, also a fast internet connection is required to connect this system with the remote system and to give a look of live monitoring of the slide.

The other end from which the pathologist views the slide does not need anything other than a remote controlling software and an internet connection. The pathologist can view the slide at any time just by logging into the system and can easily adjust it in three dimentional operating system.

Conclusion

Microscopes with camera are already used all around the world but this is very new technique in which the control of stage and movements of slides are controlled by pathologist. This is a novel idea that will help the remote areas to get specialist opinion regarding the critical cases in hematology, urine analysis, microbiology and histopathology on time.

It will reduce cost and time and pathologist can examine different cases from a places without moving anywhere so it will help a lot to patients and pathologist too. This equipment is totally dependent on the analysis of a pathologist, so if a diagnostic software is developed which helps them in detecting abnormal cells would be a great achievement and very helpful for them.

Acknowledgement

The author wishes to thank Mr. Asad Ali, CEO, Husaini Blood Bank for providing facility to carry out this research.

References

Arduino, 2014a. Arduino basics, available at http:// arduino. cc/en/ main/ software, last visited December 2014.

Arduino, 2014b. Arduino mega 2560 specifications, available at http://arduino.cc/en/Main/arduino BoardMega2560, last visited December 2014.

Eysenbach, G. 2001. What is e-health?. *Journal of Medical Internet Research,* **3:** e20.

HTS, 2014. HyperTerminal Software trial package, available at http://www.hilgraeve.com/hyper-terminal-triall/, last visited December 2014.

John, C.M., David, P.S., Joel, M.G.., Raquel, M.S., Kelly, J.B. 2009. Emergency department crowding, Part 2-Barriers to reform and strategies to overcome them. *Annals of Emergency Medicine,* **53:** 612-617.

Kamel Boulos, M.N., Wheeler, S. 2007. The emerging Web 2.0 social software: An enabling suite of sociable technologies in health and health care education. *Health Information and Libraries Journal,* **24:** 2-23.

NILS, 2014. National Instruments Labview Software, available at http://www.ni.com/labview/, last visited December 2014.

NIVAS, 2014. National Instruments Vision Acquisition Softwere available at http://sine.ni.com/nips/cds/ view/p/lang/en/ nid/12892, last visited December 2014.

TVS, Team Viewer Software, available at http:// www. team viewer.com

Pak. j. sci. ind. res. Ser. A: phys. sci. 2016 **59** (1) 34-42

Seasonal and Temporal Variations of Criteria Air Pollutants and the Influence of Meteorological Parameters on the Concentration of Pollutants in Ambient Air in Lahore, Pakistan

Amtul Bari Tabinda[a], Saleha Munir[a]*, Abdullah Yasar[a] and Asad Ilyas[b]
[a]Sustainable Development Study Centre, GC University Lahore, Pakistan
[b]IB & M, University of Engineering and Technology Lahore, Pakistan

(receivd September 6, 2013; revised December 19, 2014; accepted December 31, 2014)

Abstract. Criteria air pollutants have their significance for causing health threats and damage to the environment. The study was conducted to assess the seasonal and temporal variations of criteria air pollutants and evaluating the correlations of criteria air pollutants with meteorological parameters in the city of Lahore, Pakistan for a period of one year from April 2010 to March 2011. The concentrations of criteria air pollutants were determined at fixed monitoring stations equipped with HORIBA analyzers. The annual average concentrations ($\mu g/m^3$) of $PM_{2.5}$, O_3, SO_2, CO and NO_x ($NO+NO_2$) for this study period were 118.94±57.46, 46.0±24.2, 39.9±8.9, 1940±1300 and 130.9±81.0 (61.8±46.2+57.3±22.19), respectively. $PM_{2.5}$, SO_2, CO and NO_x had maximum concentrations during winter whereas O_3 had maximum concentration during summer. Minimum concentrations of $PM_{2.5}$, SO_2 and NO_x were found during monsoon as compared to other seasons due to rainfall which scavenged these pollutants. The O_3 showed positive correlation with temperature and solar radiation but negative correlation with wind speed. All other criteria air pollutants showed negative correlation with wind speed, temperature and solar radiation. A significant ($P<0.01$) correlation was found between NO_x and CO ($r = 0.779$) which showed that NO_x and CO arise from common source that could be the vehicular emission. $PM_{2.5}$ was significantly correlated ($P<0.01$) with NO_x ($r = 0.524$) and CO ($r = 0.519$), respectively. High traffic intensity and traffic jams were responsible for increased air pollutants level especially the $PM_{2.5}$, NO_x and CO.

Keywords: $PM_{2.5}$, O_3, SO_2, CO, NO_x, seasonal variations, air pollution, meteorological parameters

Introduction

Among the current environmental problems faced by the society, air quality issues are most problematic to handle as more and more studies report the human health and environmental impact of air pollution (Desauziers, 2004). Lahore is the second largest city in Pakistan, it stands at number 40 in the ranking of world's most populated urban cities. The population of Lahore is growing at a rapid rate and has now reached 10 million (Hameed and Nazir, 2011). Lahore is situated in east of Pakistan (latitude 31.470 N and longitude 74.253 E) and has an altitude of 702ft from sea level (Fig. 1). It is commercial, industrial, cultural and educational hub of Pakistan. The selected site is ideal for the study as it represents the local and distant air pollution sources. Lahore city has arid and hot climate and it presents four seasons. The winter season starts from November and ends at February. The temperature is lowest during winter having an average of 12.14 ± 4.12 °C. Spring season comprises of two months March and April. The summer season is from May to July and temperature is highest during these months having an average of 34.8±11.8 °C.

Lahore receives bulk of rainfall during July to September and the fall season is in October. During the last 10 years the rainfall varied from 333-1232 mm and relative humidity in this area was 17% to 70%. The growing volume of population and traffic are major factors for rise in air pollution. The Lahore city has 1.4 million registered vehicles (Ali and Athar, 2008). Many earlier studies show that Lahore is one of the world's most polluted cities (Mehta *et al*., 2009; Hopke, 2009; Biswas *et al*., 2008; Wahid, 2006; Barletta *et al*., 2002; Parekh *et al*., 2001; Harrison *et al*., 1997; Hussain*et al*., 1990). In 1992 WHO conducted an air quality monitoring programme which revealed that total concentration of suspended particulate in Lahore was among the highest in the world (Smith *et al*., 1996; WHO and UNEP, 1992).

Air pollution is caused mainly by fossil fuel (oil, coal and natural gas) use in industry, domestic sector, power generation and transport (Jaffary and Faridi, 2006). In addition; animal waste, agricultural waste and biomass

*Author for correspondence; E-mail: salimunir@gmail.com

burning also contribute in polluting air. The pollutant emission into ambient air has direct and indirect effects like eutrophication, stratospheric ozone depletion, acidification and production of ground level ozone. This may in turn worsen the air quality and leave its impact on the ecosystem, buildings, agriculture and human health (Schwella, 2008). Meteorological parameters have an important role in dispersion, dilution, formation and transport of pollutants in air (Ying *et al*., 2012). For understanding atmospheric air quality the accurate measurement and monitoring of meteorological parameter is a principal requirement (Seaman, 2003). The ambient weather conditions influence the chemical reaction of air pollutants (Elminir, 2005). The air quality of cities is correlated with the various meteorological factors like wind speed, air temperature and solar radiation (Gupta *et al*., 2004). This study was conducted to assess the seasonal and temporal variations of criteria air pollutants and evaluating the correlations of criteria air pollutants with meteorological parameters in the city of Lahore, Pakistan.

Materials and Methods

Description of study site. Complete monitoring data for the criteria air pollutants $PM_{2.5}$, O_3, SO_2, CO and NO_x ($NO+NO_2$) was obtained with the courtesy of Environment Protection Department (EPD) Lahore, Pakistan for a period of one year from April 2010 to March 2011. Figure 1 represents the map of Lahore. Environment Protection Agency Punjab is continuously monitoring the air quality of Lahore at two sites through fixed monitoring stations. One of them is located at Town Hall on lower Mall Area Lahore, Pakistan. This is a general air quality monitoring station situated on the roof top (25 f from ground level) of local EPA office. Its distance from the main busiest roads like Mall Road, Lower Mall, Bank Road and Anarkali Road is about 200 meter. Lower Mall Area is situated in the centre of the city. It is surrounded by busiest road of city and commercial activities. About 3 kilometers away from this site is an industrial centre named Badami Bagh industrial area. The dominant industrial activity in this area is steel scrap processing units and plastic industry. The other fixed monitoring station is located in Township in south of Lahore. It has residential area as well as small industrial area.

Instrument and statistical analysis. $PM_{2.5}$ was monitored with HORIBA instrument APDA-371. It works on the principle of betaray attenuation. The lower

Fig. 1. Map of Lahore, Pakistan.

detection limit for 1 h is < 4.8 µg/m^3 and for 24 h is < 1.0 µg/m^3. CO monitoring was done with HORIBA instrument APMA-370. It uses solenoid valve cross flow modulation, non-dispersive infrared (NDIR) absorption technology (Detection limit 0.02 ppm). NO_x (NO_2+NO) were monitored with APNA-370. The principle of measurement is cross flow modulation type reduced pressure chemiluminescence (CLD) with lower detection limit of 0.5 ppb. O_3 was monitored with APOA-370. The instrument operates on cross flow modulation type, Ultra-violet-absorption method (NDUV) and the lower detection limit is 0.5 ppb. SO_2 was monitored with APSA-370. The instrument works on Ultra Violet Florescence Technology (lower detection limit 0.5 ppb).

Pearson correlation was used to correlate between criteria air pollutants and meteorological parameters using SPSS Statistics v20.

Results and Discussion

Monthly average concentrations of criteria air pollutants $PM_{2.5}$, O_3, SO_2, CO and NO_x ($NO+NO_2$) are presented in Fig. 2(a-e). and monthly ranges along with simultaneously measured meteorological data is represented in Table 1. The seasonal variation is presented in Fig. 3. Highest

and lowest $PM_{2.5}$ levels were observed in winter and monsoon, respectively. The highest $PM_{2.5}$ concentration in winter months can be attributed to residential heating. The $PM_{2.5}$ concentration in winter was 2.2 times higher than the $PM_{2.5}$ concentration in summer and 3.7 times higher than the $PM_{2.5}$ concentration in monsoon season. The $PM_{2.5}$ level during the winter season was 7.7 times higher than the WHO prescribed limit of 25 µg/m³ (WHO, 2006) and 4.8 times greater than the Pak-EPA limit of 40 µg/m³ (Pak-EPA, 2009). During the summer season the $PM_{2.5}$ level was 3.4 times higher than the standard WHO limit (WHO, 2006) and 2.1 times greater than the Pak-EPA standards (Pak-EPA, 2009). The $PM_{2.5}$ level during the spring and fall also violated the standards. The $PM_{2.5}$ concentration was 4.2 times in excess the WHO standard (WHO, 2006) and 2.6 times in excess than Pak-EPA standard (Pak-EPA, 2009) during spring and 5.4 times in excess than WHO limit (WHO, 2006) and 3.4 times in excess than Pak-EPA limits (Pak-EPA, 2009) during fall. During monsoon the $PM_{2.5}$ level was 2 times greater than the WHO limit (WHO, 2006) and 1.3 times in excess the Pak-EPA standard (Pak-EPA, 2009). The $PM_{2.5}$ levels in air reduced during the monsoon season because the rain scavenges the particulate matter in air and wash it out (McCully *et al*., 1956). Yaseen (2000) reported similar results in Malaysia where rainfall drops washout the particulate in air and thus reduces its concentration in ambient air.

The first study on particulate matter in Lahore was carried out by Global Environment Monitoring System (GEMS) which reported that the annual mean suspended particulate matter (SPM) concentration in Lahore was 332 µg/m³ in 1978 at commercial city centre and 749 µg/m³ and 690 µg/m³ during 1979 and 1980, respectively at the suburban residential site (WHO, 1984). Similarly Smith *et al*. (1996) studied annual mean total suspended particulate (TSP) level in Lahore and reported that 838, 590 and 607 µg/m³ of particulate was present at rural, industrial and city site in Lahore, respectively. Pak-EPA/JICA (2001) reported the hourly average concentration of suspended particulate matter (SPM) at Lahore was 895 µg/m³. Waheed *et al*. (2005) reported that the particulate matter in Lahore was in the range of 1, 128-1, 870 µg/m³. Hussain *et al*. (2007) studied $PM_{2.5}$ level in Lahore during 2005-2006 and the $PM_{2.5}$ level was in range of 53-476 µg/m³. Ghauri *et al*. (2007) reported that, total suspended particulate (TSP) in Lahore during 2003-2004 was 482 µg/m³ and the level of PM_{10} in Lahore during 2003-2004 was 200 µg/m³. Lodhi

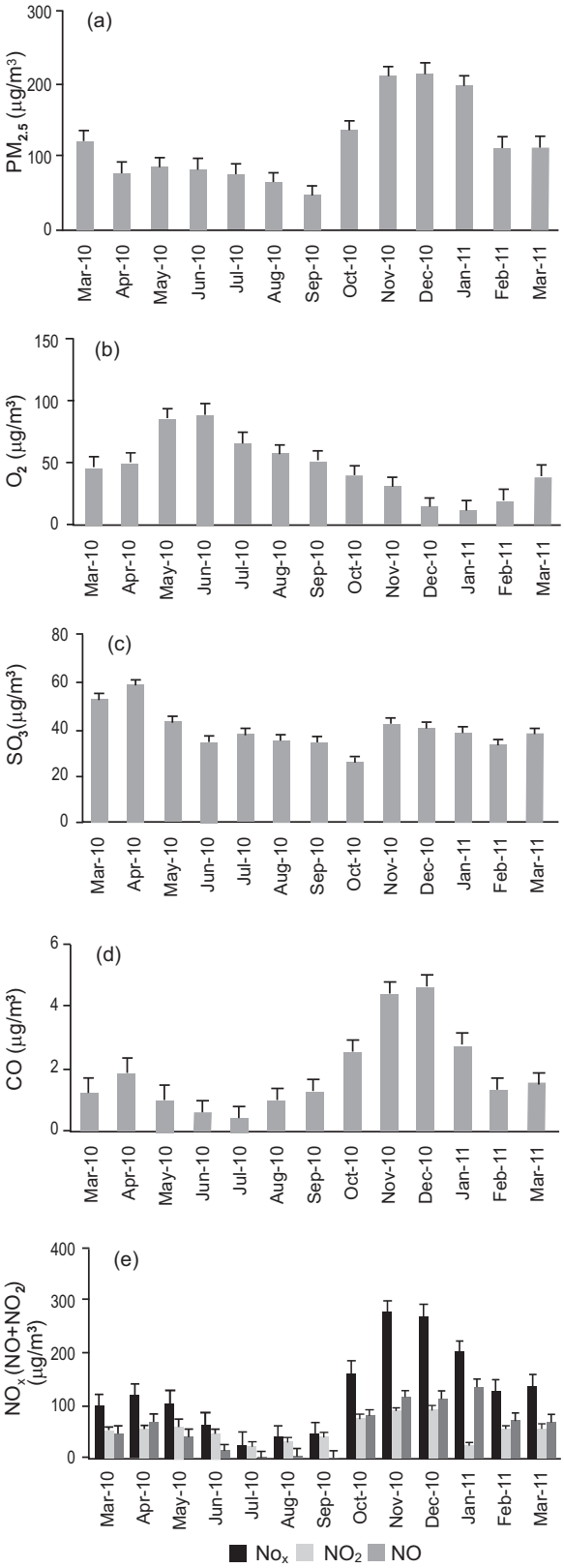

Fig. 2(a-e). Monthly average concentrations of criteria air pollutants in Lahore, Pakistan.

et al. (2009) reported that $PM_{2.5}$ annual arithmetic mean during 2007 was 103 µg/m^3.

In the present study (2010-2011), the observed annual mean of $PM_{2.5}$ is 118.9 µg/m^3. This level is 4.8 times in excess the WHO standard (WHO, 2006) and 3 times greater than the Pak-EPA limit (Pak-EPA, 2009). From this, it is obvious that Lahore is facing alarming particulate matter levels. This is due to excessive increase in vehicle use, outdated unfit vehicles, poorly maintained old vehicles, old buses model, fuel adulteration and lack of paved areas, road side vegetation and soil erosion. The number of vehicles in Lahore has reached up to 2.48 million (Haider, 2010). Motor vehicles emit a mixture of pollutants i.e. PM_{10}, CO, O_3 and NO_x (Kadiyali, 2008).To combat the excessive particulate matter concentration in air the government has encouraged the use of compressed natural gas (CNG) instead of diesel and petrol. Now, Pakistan ranks third in the world for using CNG and it is the largest CNG user in Asia (GOP, 2005). Although particulate matter levels are still elevated due to poor CNG technology use (Narain and Krupnick, 2007).

Seasonal O_3 variation showed inverse trend as compared to other gaseous pollutants monitored in study. The monthly concentrations are represented in Fig. 2b. The seasonal concentrations are presented in Fig. 3b. Ozone concentrations were lowest during winter season and greater during summer season. The highest O_3 concentration was found in June (88.6±56.8 µg/m^3) and lowest O_3 concentration was observed in January (11.3±10.9 µg/m^3). However, the O_3 concentration throughout the year was within the permissible limits of Pak-EPA (2009). The higher concentration of O_3 during summer as compared to winter is due to the high

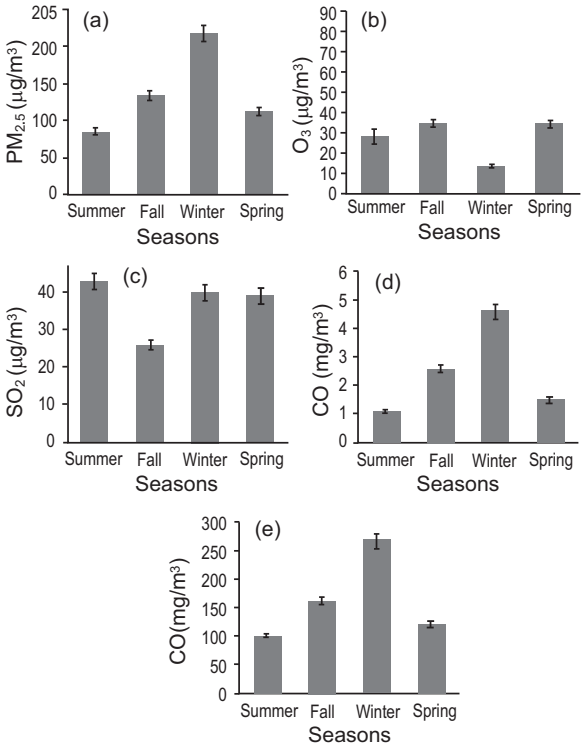

Fig. 3(a-e). Seasonal variations of criteria air pollutants in Lahore, Pakistan.

Table 1. Monthly ranges of criteria air pollutants and simultaneously measured meteorological data (March 2010 to March 2011) in Lahore, Pakistan

Months	$PM_{2.5}$	SO_2	CO	O_3	NO_x	NO_2	NO	Temperature (°C)	Wind speed (m/s)	Radiation (W/m^2)
	(µg/m^3)									
Apr-2010	0.27-336.00	7.50-247.60	270-16100	1.20-227.70	7.50-679.10	8.60-211.50	1.20-584.30	16.90-41.50	0.16-2.90	1.50-896.20
May-2010	17.67-443.00	4.77-316.20	250-13620	8.26-345.94	7.81-747.66	6.59-186.88	0.97-613.47	20.72-44.27	0.37-3.17	1.40-541.10
Jun-2010	19.50-391.80	3.20-262.80	150-10100	8.90-248.00	5.50-636.10	5.42-224.80	0.70-515.40	24.80-45.20	0.10-2.70	1.50-532.60
Jul-2010	10.10-399.50	1.03-43.90	70-4010	4.40-207.20	5.00-141.90	4.85-132.80	0.10-40.30	26.10-39.70	0.20-4.00	1.30-917.40
Aug-2010	15.00-174.00	1.70-56.10	20-6600	0.03-199.70	3.35-235.70	3.30-120.60	0.10-128.20	27.70-36.40	0.40-3.14	1.40-760.50
Sep-2010	5.00-113.30	1.80-44.50	40-9800	0.80-197.40	4.30-430.70	3.09-268.00	0.05-170.30	20.70-34.90	0.03-2.03	1.40-172.20
Oct-2010	18.00-430.01	0.24-140.77	250-18170	0.28-268.67	11.19-759.36	9.37-244.40	0.80-632.74	16.59-32.14	0.17-3.18	1.40-150.30
Nov-2010	21.1-825.00	9.40-193.80	330-19900	1.60-228.20	15.10-818.20	25.08-217.00	2.20-635.80	11.70-28.20	0.14-1.24	1.50-68.50
Dec-2010	30.33-560.00	10.95-305.34	490-20010	0.10-154.73	31.34-746.26	34.91-192.66	3.23-647.06	6.68-22.47	0.13-1.31	1.40-76.90
Jan-2011	1.79-413.00	6.01-230.50	300-21400	0.10-108.20	15.80-726.40	24.10-183.60	3.60-625.20	5.70-19.90	0.19-1.23	1.30-87.50
Feb-2011	21.00-377.30	7.07-134.90	150-10700	0.10-108.80	15.40-704.50	12.50-171.10	2.90-618.60	9.70-23.70	0.10-2.07	1.30-144.60
Mar-2011	24.00-347.00	6.68-183.66	160-10540	0.01-250.58	12.33-602.77	9.81-135.91	2.16-536.81	11.75-30.46	0.22-1.52	1.40-680.70

solar radiation during summer months. Selvaraj *et al*. (2010) reported similar results where high level of O_3 was present during summer months due to high solar radiations. Pak-EPA/ JICA (2011) also reported similar results where low concentration of O_3 during winter season was linked with low solar radiation.

Pak-EPA/JICA (2001) reported that hourly average concentration of O_3 was 17 µg/m^3. Ghauri *et al*. (2007) reported that level of O_3 in Lahore was 44 µg/m^3 (48 h mean) during 2003-2004. In the present study, the observed annual mean of O_3 was 46.04 µg/m^3. The O_3 concentration in Lahore was within the permissible limit of Pak-EPA of 130 µg/m^3 (Pak-EPA, 2009). However, as a result of rise in CNG vehicles use in Lahore the concentration is likely to rise due to emission of NO_2 from vehicles.

The concentration of SO_2 remained high throughout the year. The monthly concentrations are represented in Fig. 2c and seasonal variation is shown in Fig. 3c. Low concentration of SO_2 was observed during the monsoon season. This is due to the fact that SO_2 has been converted to H_2SO_4 due to the rainfall (Ravindra *et al*., 2003). Gupta *et al*. (2008) reported similar results in Kolkata, India where, the SO_2 concentration decreased in air due to monsoon precipitation.

GEMS study showed that SO_2 annual concentration in Lahore was 49 µg/m^3 in 1978 at city center and 40 µg/m^3 in 1979 at suburban residential area (WHO, 1984). Pak-EPA/JICA (2001) reported that hourly average concentration of SO_2 was 44.6 µg/m^3. Ghauri *et al*. (2007) found concentration of SO_2 in Lahore was 57.6 µg/m^3 (48 h mean) during 2003-2004.

In the present study, the observed SO_2 annual mean was 39.9 µg/m^3. The annual mean concentration of SO_2 (2010-2011) was below the permissible limit of 80 µg/m^3 of Pak-EPA (2009). The presence of SO_2 in air in Lahore is due to 1% (10,000 ppm) sulphur in diesel. The SO_2 level is low in air due to the use of CNG based public transport vehicles. According to Haider (2010) the number of total CNG vehicles in Lahore (628269) is about three folds higher in number as compared to diesel vehicles (207656). Moreover, a CNG bus emits 5.45 times less SO_2 than the diesel bus and CNG wagon emits 5 times less SO_2 than diesel wagon (Haider, 2010). Narain and Krupnick (2007) reported similar results in Delhi, India where, SO_2 levels decreased from 1997 to 2005 due to conversion of vehicles from diesel to CNG.

High CO concentrations were prevalent in winter months. The maximum CO monthly average was observed in December (4690±3910) and minimum CO concentration was recorded in July (540±490). Monthly variation in CO concentration is represented in Fig. 2d. The seasonal trends are shown in Fig. 3d, it reveals very high CO concentrations in winter months as compared to summer season. The concentration of CO in winter months in 2010-2011 approached the Pak-EPA standard of 5000 µg/m^3 (5 mg/m^3) (Pak-EPA 2009). These elevated CO level in colder days was due to residential heating.

Pak-EPA/JICA (2001) reported 2820 µg/m^3 hourly average concentration of CO. Ghauri *et al*., (2007) studied CO in Lahore and found its concentration as 4000 µg/m^3 (48 h mean) during 2003-2004. In present study, the observed annual mean of CO was 1940 µg/m^3. The level of CO is a result of burning of solid waste, increase in vehicular number and poorly maintained mass transit system. Lahore is a city with high pollution level per vehicle. The international and public pressure has forced the government so it took measures to control the pollution level through conver-sion of public transport to CNG, ban on two stroke vehicle production, subsidy on four stroke rickshaws and installation of CNG kits in diesel buses. Therefore, decrease in CO concentration seems to be due to shifting of vehicles on CNG. Kim and Chung (2008) reported similar results where CO level decreased in Korea due to switching to CNG fuel. In Delhi, India CO level declined from 1997-2005 due to shift in vehicle from diesel to CNG (Narain and Krupnick, 2007).

NO_x is mainly comprised of nitrogen dioxide and nitric oxide. Fig. 2e, illustrates the seasonal variation of NO_x ($NO+NO_2$). The maximum and minimum NO_x monthly average concentration was observed in December (279.8±233.9 µg/m^3) and in July (28.3±23.9 µg/m^3), respectively. The seasonal concentrations are represented in Fig. 3e. The highest NO_x concentration was during winter season and lowest NO_x level was during summer and monsoon season. The cold season has 3.7 times greater concentration of NO_x as compared to hot season. The anthropogenic sources of NO_x include power plants, residential combustion units industry and motor vehicles. In our study, NO_x showed elevated concentration during cold season mainly due to residential heating. During the cold season, the NO_x concentration was 5.7 times higher than the WHO limits of 40 µg/m^3 (WHO, 2006) and 2.9 times greater than the Pak-EPA

standards of 80 µg/m^3 (Pak-EPA 2009). The lower NO_x concentration in monsoon is due to washout of NO_x by rainfall (Ravindra *et al*., 2003). Gupta *et al*. (2008) reported similar results in Kolkata, India where the NO_x level decreased in air due to monsoon.

Pak-EPA/JICA (2001) reported the hourly average concentration of NO 88.4 µg/m^3 and NO_x 156.6 µg/m^3. Ghauri *et al*. (2007) studied NO_x in Lahore and found its concentration to be 55 µg/m^3 (48 h mean) during 2003-2004. In the present study, the observed annual mean of NO_x, NO_2 and NO was 130.9, 57.3 and 61.8 µg/m^3, respectively. This NO_x level is 3.3 times greater than the WHO standard (WHO, 2006) and 1.6 times greater than the Pak-EPA limit (Pak-EPA, 2009). A study was carried out in Brazil which revealed that conversion of vehicle from gasoline to CNG reduced CO by 53% but increased NO_x by 171% (LuzDondero and Goldemberg, 2005). Narain and Krupnick (2007) reported similar results in Delhi, India where, NO_x levels increased from 1990-2005 due to use of CNG vehicles.

Correlation of criteria air pollutants with meteorological parameters. Concentration of all the criteria air pollutants was correlated with wind speed, temperature and solar radiation (Table 2).

Wind is the air in motion and wind speed is rate of air motion. No seasonal fluctuations were observed with varying wind speed and low wind speed values were dominant ranging from 0.03 to 3.18 m/s. The average wind speed was 1.14 m/s. Significant inverse correlation was observed between wind speed and criteria air pollutants ($P<0.01$). The inverse relationship between variables can be explained on the basis of fact that when wind speed is low, it will not influence the distribution of air pollutants in an area but when the wind speed will be high it will disperse the pollutants and thus reducing the concentration of air pollutants in an area. Tasdemir *et al.* (2005) reported similar results.

$PM_{2.5}$, NO_x, CO and SO_2 were negatively correlated ($P<0.01$) with air temperature and solar radiation. The SO_2 showed lowest correlation value with air temperature and solar radiation. This can be linked with the burning of coal containing sulphur, used for the heating purpose but the 'r' values were not high enough. The lower burning efficiency of coal also contributed to elevated CO and $PM_{2.5}$ emissions. $PM_{2.5}$ was significantly correlated with NO_x ($r = 0.524$, $P<0.01$) and CO ($r = 0.519$, $P<0.01$). Positive correlation depicts a similar source for these gases. High traffic intensity and traffic jams were responsible for increased air pollutants level especially the $PM_{2.5}$, NO_x and CO.

Table 2. Correlations of criteria air pollutants with meteorological parameters

Parameters		$PM_{2.5}$	NO_x	O_3	CO	SO_2	Wind speed	Temperature	Radiation
$PM_{2.5}$	Pearson coefficient (r)	1	-	-	-	-	-	-	-
	Significance (P)	-	-	-	-	-	-	-	-
NO_x	Pearson coefficient (r)	.524**	1	-	-	-	-	-	-
	Significance (P)	.000	-	-	-	-	-	-	-
O_3	Pearson coefficient (r)	-.330**	-.450**	1	-	-	-	-	-
	Significance (P)	.000	.000	-	-	-	-	-	-
CO	Pearson coefficient (r)	.519**	.779**	-.422**	1	-	-	-	-
	Significance (P)	.000	.000	.000	-	-	-	-	-
SO_2	Pearson coefficient (r)	.316**	.331**	-.176**	.261**	1	-	-	-
	Significance (P)	.000	.000	.000	.000	-	-	-	-
Wind speed	Pearson coefficient (r)	-.253**	-.332**	-.284**	-.327**	-.117**	1	-	-
	Significance (P)	.000	.000	.000	.000	.000	-	-	-
Temperature	Pearson coefficient (r)	-.324**	-.264**	.469**	-.253**	-.039*	.179**	1	-
	Significance (P)	.000	.000	.000	.000	.044	.000	-	-
Radiation	Pearson coefficient (r)	-.161**	-.244**	.369**	-.232**	-.030	.314**	.304**	1
	Significance (P)	.000	.000	.000	.000	.121	.000	.000	-

In the present study, a high correlation was found between NO_x and CO ($r = 0.779$, $P<0.01$). A positive correlation between CO and NO_x indicates that they arise from same source. Kimmel *et al*. (2002); Bogo *et al*. (1999) and Cardens *et al*. (1998) suggested that NO_x and CO arise from common source(s) that could be the vehicular emission. NO_x and CO are emitted from incomplete combustion of organic fuel in motor vehicles (Goyal and Sidhartha, 2003).

The O_3 showed positive relation with solar radiation and air temperature ($P<0.01$). This is due to the fact that the reaction between nitrogen oxides, volatile organic compounds and carbon monoxide take place in the presence of sunlight to produce ozone. So, the availability of high amount of solar radiation contributes to the production of ozone at ground level and increased its concentration in ambient air (Selvaraj *et al*. 2010). The negative correlation of NO_x with O_3 ($r = -0.450$, $P<0.01$) also support this argument. Shan *et al.* (2008) and Tu *et al*. (2007) reported the positive correlation of ozone concentration with air temperature. Pulikesi *et al*. (2006) linked the ozone concentration with intense solar radiation.

Conclusion

Criteria air pollutants are known to cause serious health issues and damage to environment. Keeping this fact in mind, the present study was conducted in Lahore, Pakistan for the assessment as well as correlation of criteria air pollutants with meteorological parameters. Results showed that O_3 concentration increased in summer season while the concentration of $PM_{2.5}$, SO_2, CO and NO_x raised during winters. $PM_{2.5}$ concentration was highest in winter due to heating but its elevated levels were also found during summer due to poorly maintained out dated vehicles, lack of paved areas and vegetation. O_3 remained highest in summer season due to high solar radiations which enhance the production of ground level ozone. SO_2 and CO level remained within the permissible limit due to shifting in vehicle from petrol and diesel to CNG. Level of NO_x remained high and its elevated level was contributed by CNG vehicles. $PM_{2.5}$, SO_2 and NO_x remained lowest during monsoon due to washout from rains. O_3 remained lowest in winter due to less solar radiation. CO remained lowest during summer due to decreased residential burning. The concentration of air pollutants was negatively correlated with wind speed showing that the increase in wind speed causes dispersion of pollutants. O_3 showed positive correlation with temperature and solar radiation but negative correlation with wind speed. All other criteria air pollutants showed negative correlation with wind speed, temperature and solar radiation.

References

Ali, M., Athar, M. 2008. Air pollution due to traffic, air quality monitoring along three sections of National Highway N-5, Pakistan. *Environmental Monitoring and Assessment*, **136:** 219-226.

Barletta, B., Meinardi, S., Simpson, I.J., Khwaja, H.A., Blake, D.R., Rowland, F.S. 2002. Mixing ratios of volatile organic compounds (VOCs) in the atmosphere of Karachi, Pakistan. *Atmospheric Environment*, **36:** 3429-3443.

Biswas, K.F., Ghauri, B., Husain, L. 2008. Gaseous and aerosol pollutants during fog and clear episodes in South Asian urban atmosphere. *Atmospheric Environment*, **42:** 7775-7785.

Bogo, H., Negri, M., Roman, E.S. 1999. Continuous measurement of gaseous pollutants in Buenos Aires city. *Atmospheric Environment*, **33:** 2587-2598.

Cardenas, L.M., Austin, J.F., Burgess, R.A., Clemitshaw, K.C., Dorling, S., Penkett, S.A., Harrison, R.M. 1998. Correlations between CO, NO_x, O_3 and non-methane hydrocarbons and their relationships with meteorology during winter 1993 on the North Norfolk Coast, UK. *Atmospheric Environment*, **32:** 3339-3351.

Desauziers, V. 2004. Traceability of pollutant measurements for ambient air monitoring. *Trends in Analytical Chemistry*, **23:** 252-260.

Elminir, H.K. 2005. Dependence of urban air pollutants on meteorology. *The Science of the Total Environment*, **350:** 225-237.

Ghauri, B., Lodhi, A., Mansha, M. 2007. Development of baseline (air quality) data in Pakistan. *Environmental Monitoring and Assessment*, **127:** 237-252.

GOP, 2005. *Pakistan Millennium Development Goals Report*, Government of Pakistan Planning Commission. Islamabad, Pakistan.

Goyal, P., Sidhartha, 2003. Present scenario of air quality in Delhi: A case study of CNG implementation. *Atmospheric Environment*, **37:** 5423-5431.

Gupta, A.K., Karar, K., Ayoob, S., John, K. 2008. Spatio-temporal characteristics of gaseous and particulate pollutants in an urban region of Kolkata, India. *Atmospheric Research*, **87:** 103-115.

Gupta, A.K., Patil, R.S., Gupta, S.K. 2004. Influence

of meteorological factors on air pollution concentration for a coastal region in India. *International Journal of Environment and Pollution*, **21:** 253-262.

Hameed, R., Nazir, S. 2011. Improving secondary collection of solid waste. The experience of performance based system in Lahore. *The Journal of American Science*, **7:** 157-164.

Haider, R. 2010. Usefulness of CNG as vehicular fuel over gasoline and diesel in the city of Lahore. *M. Phil Thesis*, 34 pp., Government College University, Lahore, Pakistan.

Harrison, R.M., Smith, D.J.T., Piou, C.A., Castro, L.M. 1997. Comparative receptor modeling study of airborne particulate pollutants in Birmingham (United Kingdom), Coimbra (Portugal) and Lahore (Pakistan). *Atmospheric Environment*, **31:** 3309-3321.

Hopke, P.K. 2009. Contemporary threats and air pollution. *Atmospheric Environment*, **43:** 87-93.

Hussain, L., Dutkiewicz, V.A., Khan, A.J. 2007. Characterization of carbonaceous aerosols in urban air. *Atmospheric Environment*, **41:** 6872-6883.

Hussain, K., Riffat, R., Shaukat, A., Siddiqui, M. 1990. A study of suspended particulate matter in Lahore (Pakistan). *Advances in Atmospheric Sciences*, **7:** 178-185.

Jaffary, Z.A., Faridi, I.A. 2006. Air pollution by roadside dust and automobile exhaust at busy road-crossings of Lahore. *Pakistan Journal of Physiology*, **2:** 31-34.

Kadiyali, L.R. 2008. *Traffic Engineering and Transport Planning*, 256 pp., 7th edition, Khanna publishers, New Delhi, India.

Kimmel, V., Tammet, H., Truuts, T. 2002. Variation of atmospheric air pollution under conditions of rapid economic change-Estonia 1994-1999. *Atmospheric Environment*, **36:** 4133-4144.

Kim, H., Chung, Y. 2008. Satellite and ground observations for large scale air pollution transport in the yellow sea region. *Journal of Atmospheric Chemistry*, **60:** 103-116.

Lodhi, A., Ghauri, B., Khan, M.R., Rahmana, S., Shafiquea, S. 2009. Particulate matter ($PM_{2.5}$) concentration and source apportionment in Lahore. *Journal of Brazilian Chemical Society*, **20:** 1811-1820.

LuzDondero, Goldemberg, J. 2005. Environmental implications of converting light gas vehicles: the Brazililian experience. *Energy Policy*, **33:** 1703-1708.

McCully, C.R., Fisher, M., Langer, G., Rosinski, J., Glaess, H., Werle, D. 1956. Scavenging action of rain on air-borne particulate matter. *Industrial and Engineering Chemistry*, **48:** 1512-1516.

Mehta, B., Venkataraman, C., Bhushan, M., Tripathi, S.N. 2009. Identification of sources affecting *fog* formation using receptor modeling approaches and inventory estimates of sectoral emissions. *Atmospheric Environment*, **43:** 1288-1295.

Narain, U., Krupnick, A. 2007. The impact of CNG programme on Delhi air quality. 1 pp., Resources for the future discussion paper. http://www.rff.org/documents/RFF-DP-07-06.pdf. Washington DC 20036, USA.

Pak-EPA/JICA, 2011. *Comprehensive Environmental Monitoring Report for Selected Pilot Areas in Pakistan*. Japan International Cooperation Agency-Pakistan Environment Protection Agency, Pakistan.

Pak-EPA/JICA, 2001. *Report. 3 Cities Investigation of Air and Water Quality (Lahore, Rawalpindi and Islamabad)*. Japan International Cooperation Agency-Pakistan Environment Protection Agency, Pakistan.

Pak-EPA, 2009. National Environmental Quality Standards (NEQS) for ambient air. http://www.environment.gov.pk/act-rules/NEQS%20for%20Ambient%20Air.pdf

Parekh, P., Khwaja, P., Khan, H.A., Naqvi, A.R., Malik, A., Shah, S.A. 2001. Ambient air quality of two metropolitan cities of Pakistan and its health implications. *Atmospheric Environment*, **35:** 5971-5978.

Pulikesi, M., Baskaralingam, P., Rayudu, V.N., Elango, D., Ramamurthi, V., Sivanesan, S. 2006. Surface ozone measurement at urban coastal site Chennai, in India. *Journal of Hazardous Material*, **137:** 1554-1559.

Ravindra, K., Mor, S., Ameena, Kamyotra, J.S., Kaushik, C.P. 2003. Variation in spatial pattern of criteria air pollutants before and during initial rain of monsoon. *Environmental Monitoring and Assessment*, **87:** 145-153.

Schwella, D. 2008. Air pollution and health in urban areas. *Reviews on Environment Health*, **15:** 13-42.

Seaman, N.L. 2003. Future directions of meteorology related to air-quality research. *Environment International*, **29:** 245-252.

Selvaraj, R.S., Selvi, S.T., Priya, S.P.V. 2010. Association between surface ozone and solar activity. *Indian Journal of Science and Technology*, **3:** 332-334.

Shan, W.P., Yin, Y.Q., Zhang, J.D., Ding, Y.P. 2008. Observational study of surface ozone at an urban site in East China. *Atmospheric Research*, **89:** 252-261.

Smith, D.J.T., Harrison, R.M., Luhana, L., Pio, C.A., Castro, L.M., Tariq, M.N. 1996. Concentrations of particulate airborne polycyclic aromatic hydrocarbons and metals collected in Lahore, Pakistan. *Atmospheric Environment*, **30:** 4031-4040.

Tasdemir, Y., Siddik, C., Fatma, E. 2005. Monitoring of criteria air pollutants in Bursa, Turkey. *Environmental Monitoring and Assessment*, **110:** 227-241.

Tu, J., Xia, Z.G., Wang, H.S., Li, W.Q. 2007. Temporal variations in surface ozone and its precursors and meteorological effects at an urban site in China. *Atmospheric Research*, **85:** 310-337.

Waheed, S., Rahman, A., Khalid, N., Ahmad, S. 2005. Assessment of air quality of two metropolitan cities in Pakistan: Elemental analysis using INAA and AAS. *Radiochimica Acta*, **94:** 161-166.

Wahid, A. 2006. Productivity losses in barley attributable to ambient atmospheric pollutants in Pakistan. *Atmospheric Environment*, **40:** 5342-5354.

WHO, 2006. *Air Quality Guidelines Global Update, 2005*. WHO Regional Office for Europe, Copenhagen, Denmark.

WHO, 1984. *Urban Air Pollution 1973-1980*. World Health Organization, Geneva, Switzerland.

WHO & UNEP, 1992. *Urban Air Pollution in Megacities of the World*. 196 pp., Oxford, Blackwell, USA.

Yaseen, M.E. 2000. The relationships between dust particulates and meteorological Parameters in Kualalumpur and Petalingjaya, Malaysia. http://nargeo.geo.uni.lodz.pl/~icuc5/text/P_3_4.pdfAccessed 26 March 2012.

Ying, T.Y., Fook, L.S., Glasow, R.V. 2012. The influence of meteorological factors and biomass burning on surface ozone concentrations at Tanah Rata, Malaysia. *Atmospheric Environment*, **70:** 435-446.

Pak. j. sci. ind. res. Ser. A: phys. sci. 2016 **59** (1) 43-51

Evaluation of Groundwater Quality of Selected Boreholes in Ohaozara and Ivo Council Areas of Ebonyi State, Nigeria

Omaka Ndukaku Omaka[a], Ifeanyi Francis Offor [a]*, David Obasi Igwe[b] and Ewuzie Ugochukwu[c]

[a]Department of Chemistry, Federal University, Ndufu-Alike, Ikwo, P.M.B. 1010, Ebonyi State, Nigeria

[b]Department of Industrial Chemistry, Ebonyi State University, P.M.B. 053, Abakaliki, Ebonyi State, Nigeria

[c]Department of Pure and Industrial Chemistry, Abia State University, P.M.B. 2000, Uturu, Abia State, Nigeria

(received October 13, 2014; revised January 26, 2015; accepted January 31, 2015)

Abstract. Groundwater quality in study areas was evaluated by measuring the physicochemical parameters including selected ions in water samples collected from 12 boreholes in Akaeze, Okposi and Uburu towns of Ebonyi State, Nigeria in April, 2013 and analysed using standard methods. Results obtained showed that, except for As^{5+} content, all other parameters investigated fall within WHO standards for potable water. Regression analysis showed that conductivity, SO_4^{2-} and As^{5+} levels are important variables in predicting the TDS values of the samples while NO_3^-, Cl^-, PO_4^{3-} and TDS are important in predicting the As^{5+} content of the water samples. One-way ANOVA at $P < 0.05$ showed F_{cal} (1.862) > F_{tab} (0.619), implying a significant difference between the parameters for all locations.

Keywords: borehole water, water quality, physicochemical parameters

Introduction

Water is essential for the sustenance of life. It occupies 71% of the entire earth's surface and biologically makes up a large percentage of the total body fluids of all living things (Obasi and Akudinobi, 2013). Quality of water is determined by its physicochemical makeup and the amount of trace contaminants it contains.The use of poor quality water is associated with significant health implications hence, require adequate treatment before use (Centeno *et al*., 2005; Carter and Stewart, 2000; Smith *et al*., 2000). The human health is directly related to the quality of water used for drinking and other purposes, because about 75% of all diseases suffered by human beings may be partially caused by consumption of contaminated water (Pink, 2006).

Review of relevant literature reveals that, geogenic and anthropogenic processes both contribute to the degradation of natural water quality (Jan, 2011; Ayeni *et al.*, 2009; Obasi and Balogun, 2001; Ovrawah and Hymore, 2001; Ojekunle, 2000).

According to available statistics, an average water consumption rate of 10 L per person per day has been recommended for small rural communities (UNICEF, 1989). However, this quantity still falls below the WHO recommended standard of at least 20 L per person per day (WHO, 1984). According to relevant statistics, only about 61% of urban dwellers in developing countries have access to safe water supply sources (Igwenyi and Aja-Okorie, 2014). It is also estimated that 1.2 billion people around the world lack access to safe water, and close to 2.5 billion people are not provided with adequate sanitation (WWC, 2003). In Nigeria, 75-80% of the total population of about 160 million people live in rural areas, and less than 50% of that number have access to potable water (Obasi and Akudinobi, 2013).

In most local investigations of groundwater quality, physicochemical parameters are mostly measured and in some cases, trace metal constituents. However, it has been observed that most of these local researches on groundwater quality in Nigeria tend to neglect the possible contamination of the water by arsenic from both natural and anthropogenic sources.

Arsenic occurs in various forms in nature but its most toxic forms are arsenate and arsenite which comes from anthropogenic sources such as application of As-containing herbicides/pesticides, phosphorus fertilizers on cultivated lands and the discharge of industrial effluents containing As into water bodies (Okorie, 2010; Feng *et al.*, 2009; Jung *et al*., 2009; Williams and Silver, 1984).

*Author for correspondence; Email:offorifeanyi@gmail.com

Therefore, the aim of this study is to determine the physicochemical parameters and ionic (including As^{5+}) content of selected boreholes within Uburu, Okposi and Akaeze Communities in Ohaozara and Ivo Council Areas of Ebonyi State, Nigeria and to compare data obtained with existing permissible limits set by different regulatory bodies.

Materials and Methods

Study area. Okposi, Uburu and Akaeze are all rural communities in Ebonyi South Senatorial zone of Ebonyi State. Okposi and Uburu are located in Ohaozara Local Government Area (LGA) while Akaeze is located in Ivo LGA; both LGAs forming part of the 13 LGAs that make up Ebonyi State. Okposi, Uburu and Akaeze communities are located within longitudes 5° 52' N and 6° 07' N and latitudes 7° 40' E to 7° 54' E and they all fall within the Imo-Cross River Basin province of Southeastern Nigeria. The study site consists mainly of undulating land and sedimentary rocks from the Albian age. The introduction of As into drinking water can occur as a result of its natural geological presence in local bedrock (Garelick *et al.,* 2008). Ground waters are generally more vulnerable to As contamination than surface water because of their interaction with aquifer minerals, and the increased potentials in aquifer for the generation of physicochemical conditions favourable for As release (Smedley, 2008). The lithology of Uburu Salt Lake shows that it consists of sandstone beds with intercalation of fine-grained bands of silts and shales, whereas, that of Okposi Salt Lake is a mud filled depression surrounded by sandstone exposures (Okoyeh and Egboka, 2013). Smedley and Kinniburgh (2002) stated that the highest arsenic concentrations (20–200 mg/kg) are typically found in organic-rich and sulphide-rich shales, sedimentary iron stones, phosphatic rocks, and some coals. This is definitely a source of As in the water samples within the study sites. They further opined that in sedimentary rocks, As is concentrated in clays and other fine-grained sediments. High concentration of naturally occurring As are also found in oxidizing conditions where groundwater pH values are high (ca. >8) (Smedley and Kinniburgh, 2002). The pH results (8.3-8.8) of this study, lucidly support the above finding, and buttress the rationale for high As level of the samples. Also, salt harvesting by the rural women, could as well lead to increasing As concentration.

Mechanisms by which As is released from minerals are varied, and are accounted for by many (bio)geochemical processes: oxidation of As-bearing sulphides, desorption from oxides and hydroxides, reduction dissolution, evaporation concentration, leaching from sulphide by carbonates, and microbial mobilisation (Garelick *et al.,* 2008).

Surface drainage pattern within the area consists of small rivers such as Asumgbom, Atte, Azuu, Ovum, Enu and Oshi rivers which tends to dry up by flowing into the larger Asu river (Obasi and Akudinobi, 2013; Okoyeh and Egboka, 2013). A map of the study area indicating the 12 sampling locations is shown in Fig. 1.

Sampling and laboratory analyses. Groundwater samples were collected from 12 hand-dug boreholes in April, 2013 from various locations within the study areas. Six samples were collected from Akaeze town in Ivo LGA and three samples each were collected from Uburu and Okposi towns both located in Ohaozara LGA of Ebonyi State. Sampling was done at the beginning of the dry season under good weather conditions in order to avoid rain water contamination, which would have impacted on the quality of the water samples. All chemical reagents used were of analytical grade and purchased from Fisher Scientific UK. Ltd. (Loughborough, Leicestershire). All sample vessels were first washed, soaked overnight in 5% nitric acid and rinsed in high purity deionised water (Okorie, 2010). To maintain the integrity of the water samples, parameters that are sensitive to environmental changes, which include pH, dissolved oxygen (DO), electrical conductivity (EC) and temperature were measured and recorded *in-situ* using portable digital meters.

Furthermore, water samples used for determination of SO_4^{2-}, NO_3^-, Arsenate (As^{5+}) and selected physical parameters were collected in plastic containers while those for the determination of chemical oxygen demand (COD), biochemical oxygen demand (BOD) and PO_4^{3-} were collected in specialised glassware. The samples were transported to the laboratory in ice chest and then analysed for different parameters such as physicochemical properties [total hardness, total alkalinity, total dissolved solids (TDS), turbidity], Arsenate (As^{5+}) and anions (SO_4^{2-}, Cl^-, NO_3^-, PO_4^{3-}) using standard methods.

Analyses of water samples were carried out using either the American Public Health Association (APHA *et al*., 2012) or the American Standard for Testing Material (ASTM, 2012) standard procedure.

The pH was determined *in-situ* using Jenway pH meter, model 350 after calibration with buffers 4 (potassium hydrogen phthalate) and 9 (sodium borate decahydrate) (ASTM D1293-12). TDS determination was performed using APHA 2540C method, while EC was determined using APHA 2510B.

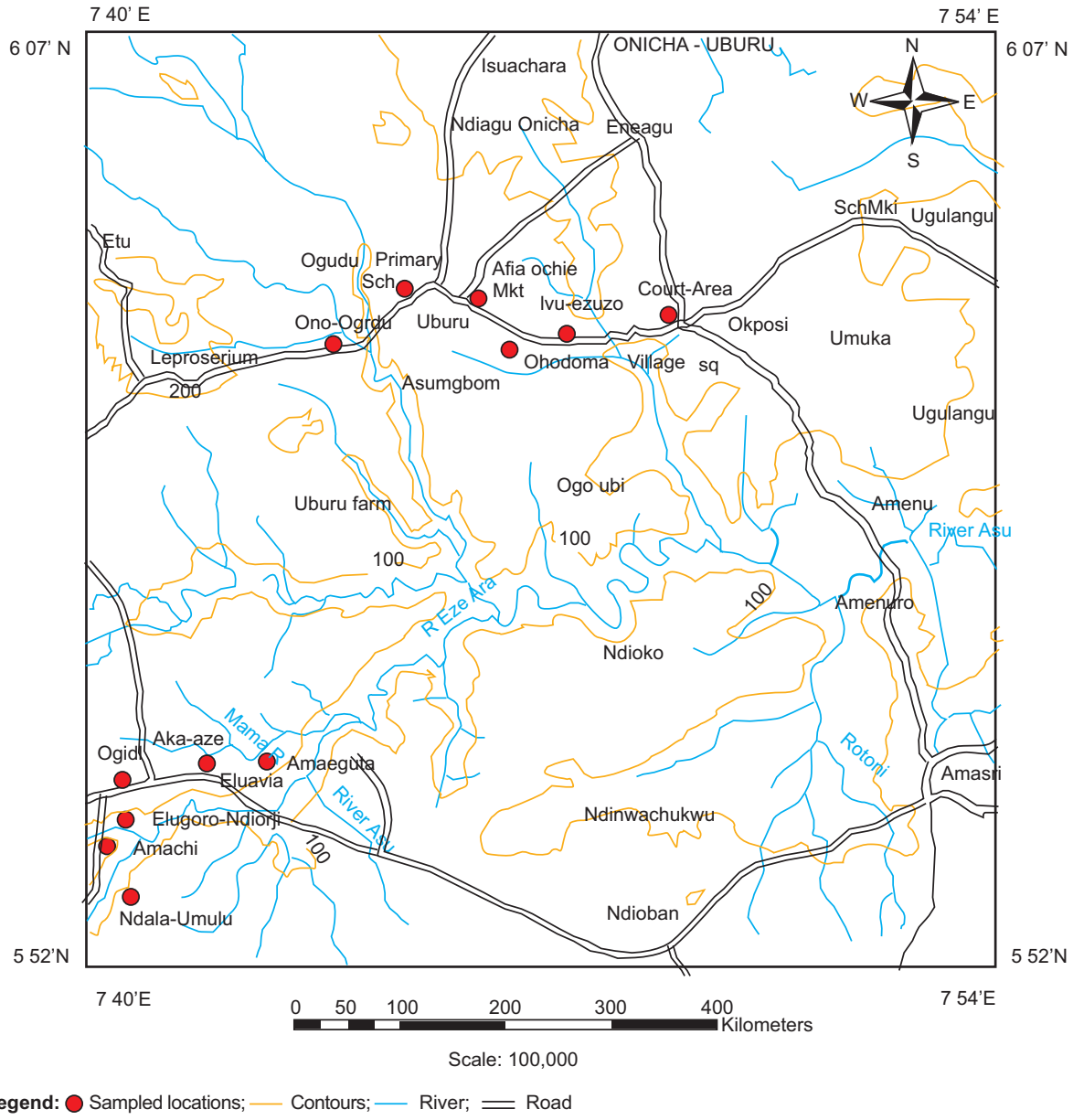

Fig. 1. Map of the study area showing 12 sampling stations in Uburu, Okposi and Akaeze towns, Nigeria.

Determinations of SO_4^{2-}, Cl^- and PO_4^{3-} were performed according to ASTM D 4327-03 method, while temperature and NO_3^- were determined following APHA 2550 and ASTM D3867-90A methods, respectively. Analysis of water samples for As^{5+} determination was done by Atomic Absorption Spectrophotometry–Hydride Generation (ASTM D2972-08B). APHA 2130B and 2340-B methods were employed in the determination of turbidity (HACH 2100AN turbidimeter) and total hardness of water samples, respectively. COD, BOD and alkalinity determinations were done according to ASTM D6238-98 and D1067-11 standard methods, respectively.

Statistical analysis. Statistical analyses of data were carried out using SPSS 16.0 for windows (SPSS Inc., Polar Engineering and Consulting 2007) and Excel 2007 statistical package programmes. For regression analysis, simultaneous method of the multiple linear regression was adopted while for ANOVA, one-way ANOVA approach was chosen.

A multiple linear regression model of the form: $Y_i = \beta_0 + \beta_1 X_{1i} + \beta_2 X_{2i} + \ldots\ldots\ldots + \beta_m X_{mi} + \xi_1$ was obtained;

where:

Y_i = dependent variable as predicted by regression model; β_0 = intercept or constant; $\beta_1 = i^{th}$ coefficient of X_i, $X_i = i^{th}$

independent variable from total set of m variables and ξ_1 = random errors.

The multiple linear regression analysis was conducted to investigate the effects of arsenic (V) content and total dissolved solids (TDS) as dependent variables on independent variables such as electrical conductivity (EC), Cl^-, NO_3^-, SO_4^{2-} and PO_4^{3-} levels in order to predict the water quality of different boreholes while analysis of variance test was conducted to check for significant differences between the physicochemical parameters of borehole water from different locations.

Results and Discussion

Physicochemical analysis. A comparison of analytical data generated in this study with national and global drinking water standards like the Nigerian Institute of Standards (NIS, 2007) and World Health Organization (WHO, 2011) water standards for drinking and public health purposes are presented in Table 1. Also, a summary of the data for physicochemical parameters, arsenate, sulphate, chloride, nitrate and phosphate contents of the borehole water samples are given in Table 2.

The pH of the water samples ranged from 8.3-8.8 with a mean value of 8.5, which was within the WHO stipulated tolerable pH range of 6.5-8.5 for potable water (WHO, 2011). This indicated that most of the groundwater samples were mildly alkaline, which can be attributed to the nature of bedrock geology of the study sites. Comparable pH ranges: 5.8-6.9, 3.84-7.72 and 8.3-9.6 were observed in similar researches by Okiongbo and Douglas (2013), Talabi *et al*. (2013) and Nwankwoala and Udom (2011), respectively.

Furthermore, reports from Iran (Mosaferi *et al.,* 2014), Pakistan (Iqbal *et al.,* 2013) and South Africa (Mpenyana-Monyatsi *et al*., 2012) had indicated pH values of 6.09-8.02, 6.44-7.27, and 7.1-8.0, respectively, which were all less than the result of this study. In the same vein, Nag and Lahiri (2012) reported pH values ranging from 6.1 to 7.9 for both pre- and post- monsoon periods.

The temperature of the water samples ranged between 22 and 28 °C, with mean temperature of 25 °C, which was below the mean atmospheric temperature of 28 °C. This relatively low temperature implied that the concentration of dissolved oxygen in the water samples was higher than normal, which might improve the water's taste (Olajire and Imeokparia, 2001; Deas and Lowny, 2000). The result of this study was comparable with that of Mpenyana-Monyatsi *et al*. (2012) which ranged from 19.4 to 24.9.

Table 1 shows that the electrical conductivity (EC) of the water samples ranged from 0.370-1.722 dS/m. OVSOB had the lowest EC value (0.370 dS/m) while, OOUB recorded the highest EC value (1.722 dS/m). Two out of twelve samples of locations namely; OVSOB (0.370 dS/m) and NUIAB (0.418 dS/m) had EC values below the WHO minimum limit of 0.500 dS/m, while all other locations had EC values above the WHO minimum limit. However, only three locations (OOUB, OPSUB and EIUB) recorded EC values that were above the WHO maximum limit of 1.250 dS/m (WHO, 2011). Nevertheless, electrical conductivities (0.110-1.750 dS/m) and (0.040-3.400 dS/m) reported by Nag and Lahiri (2012) and Mosaferi *et al.* (2014), respectively were relatively comparable with our study, whereas the EC ranged of 2.860-3.860 dS/m reported

Table 1. Descriptive statistics of analysed borehole water samples compared with NIS and WHO Standards for drinking water quality

Parameter	Minimum	Maximum	Mean± SD	NIS (2007) limit	WHO (2011) limit
Temp. (°C)	22.0	28.5	24.65±0.56	25	-
pH	8.3	8.8	8.53±0.04	6.5-8.5	6.5-8.5
DO (mg/L)	9.82	10.04	9.92±0.04	-	4
TDS (mg/L)	204	947	517.33±74.14	500	1200
EC(dS/m)	0.370	1.722	0.940±0.135	1.000	1.250
TA (mg/L)	60.70	578.70	272.48±47.87	-	-
TH (mg/L)	43.30	222.00	113.39±16.61	150	-
As^{5+} (mg/L)	2.63	5.53	4.53±0.33	0.01	0.01
Cl^- (mg/L)	100.53	147.89	130.08±3.41	250	250
SO_4^{2-} (mg/L)	16.59	65.41	38.17±4.18	100	500
NO_3^- (mg/L)	0.65	0.86	0.78±0.02	50	50
PO_4^{3-} (mg/L)	0.02	0.19	0.10±0.01	-	10

by Mosaferi *et al.* (2014) was above that of our study and WHO limit.

All the borehole water samples contained dissolved oxygen (DO) ranging from 9.55-10.04 mg/L with an average DO of 9.92 mg/L. In each case, the WHO maximum allowable limit for DO in water (4 mg/L) was exceeded (WHO, 2011). The high level of DO concentration in the water samples may be attributed to the absence of organic matter in the underground water samples, thus, improving the water taste while also posing as a source of corrosion to water pipes in these areas (Narasimha *et al*., 2011; Adekunle *et al*., 2007).

Total dissolved solids (TDS) of the water samples varied from 112 to 832 mg/L. All the samples recorded TDS values below the WHO recommended maximum limit of 1200 mg/L (WHO, 2011). Appreciable concentrations of carbonates, bicarbonates, cations and anions might have contributed to the presence of TDS in the samples (Adejuwon and Mbuk, 2011). Of similar studies in South Africa. (Mpenyana-Monyatsi *et al*., 2012) Iran, (Mosaferi *et al.,* 2014), Pakistan (Iqbal *et al.,* 2013), and India (Nag and Lahiri, 2012), only TDS values (107.1-439 mg/L) of samples studied in South Africa were comparable with our result; others: 71.5-1137.5 mg/L, 1916-2586 mg/L and 30-1365 mg/L, respectively, were averagely higher than the result of this study.

All the borehole water samples were clear (turbidities were very low) implying that there were little or no suspended solids in the samples. They were all below the WHO recommended turbidity limit (5 NTU) in drinking water (WHO, 2011).

Total alkalinity values of the water samples ranged between 60.7 and 574.7 mg/L with a mean value of 272.5 mg/L. The samples showed total alkalinity values that were within the WHO acceptable limits (WHO, 2011). Presence of carbonates, bicarbonates and hydroxides in the samples might have contributed to the concentration of total alkalinity recorded. Chloride content in the water samples ranged from 100.53 mg/L to 147.89 mg/L, implying that they all fell within the WHO recommended chloride limit of 250 mg/L in drinking water. Sources of chloride in drinking water include natural sources, sewage and industrial effluents, urban run-off containing de-icing salt and saline intrusion. Total alkalinity affects the chloride content of potable water, which may lead to a detectable taste if chloride is in excess (WHO, 2011).

Sulphate content in the water samples varied from 16.59 mg/L to 65.41 mg/L, which was well below the WHO maximum recommended limit of 500 mg/L in drinking water. The low values recorded for SO_4^{2-} in these water samples could be due to its removal from the water by bacteria (Freeze and Cherry, 1979). Sulphates are discharged into water through industrial wastes and atmospheric depositions, however their highest concentrations are found in groundwater and from natural sources. Drinking of potable water with high sulphate levels may lead to gastrointestinal effects (WHO, 2011). Mosaferi *et al.* (2014) and Nag and Lahiri (2012) reported SO_4^{2-} concentrations of 11.6-163.9 and 1.8-220.5 mg/L, respectively, which were relatively higher than sulphate contents of this study but less than the WHO limits.

In the case of nitrates, its level in the water samples varied from 0.65 mg/L to 0.86 mg/L, which was relatively low

Table 2. Hydrogeochemical analysis of groundwater samples from selected boreholes within Ivo and Ohaozara LGAs, Ebonyi State, Nigeria

S. no.	Sample location	Temp. (°C)	pH	DO (mg/L)	TDS (mg/L)	EC (dS/m)	TH (mg/L)	TA (mg/L)	SO_4^{2-} (mg/L)	Cl^- (mg/L)	NO_3 (mg/L)	PO_4^{3-} (mg/L)	As^{5+} (mg/L)
1.	Afia Ochie (AOUB)	26.2	8.6	10.0	441	0.801	43.3	60.7	16.59	133	0.81	0.11	4.59
2.	Onu-Ogudu (OOUB)	22.0	8.3	10.0	947	1.722	207.4	304.2	45.04	125	0.84	0.11	5.01
3.	Ogudu Primary School (OPSUB)	26.1	8.6	9.99	913	1.659	97.0	315.7	45.46	138	0.78	0.09	4.47
4.	Obodoma Village Square (OVSOB)	22.4	8.6	9.89	204	0.370	93.0	86.2	17.74	132	0.79	0.10	3.58
5.	Ivu-ezuzor Okposi-Okwu (IOOB)	23.3	8.7	9.92	356	0.648	222.0	183.7	22.26	127	0.76	0.13	2.98
6.	Court Area Isi-Okposi (CAIOB)	24.8	8.3	9.55	315	0.573	83.0	183.7	50.39	148	0.66	0.14	2.63
7.	Amaeguta, Akaezeukwu (AAB)	28.5	8.5	10.0	408	0.742	90.0	311.7	38.95	100	0.86	0.03	6.66
8.	Eluavia Ihenta, Umoihe (EIUB)	25.4	8.8	10.0	810	1.472	101.0	578.7	65.41	141	0.82	0.02	3.74
9.	Ogidi Omoihe (OUB)	26.0	8.6	9.94	636	1.156	183.0	479.0	28.56	130	0.84	0.19	5.53
10.	Elugoro Ndiorji Umoihe (ENUB)	25.0	8.5	9.88	562	1.022	92.0	454.2	38.22	131	0.83	0.02	5.00
11.	Amachi Umoihe (AUB)	23.5	8.4	9.82	386	0.701	85.0	211.2	45.25	134	0.68	0.12	5.25
12.	Ndala Umulu, Iyioji Akaeze (NUIAB)	22.6	8.4	10.04	230	0.418	64.0	100.7	44.20	122	0.65	0.09	4.96

DO = dissolved oxygen,; EC = electrical conductivity; TDS = total dissolved solids; TA = total alkalinity; TH = total hardness.

as compared to the WHO limit of 50 mg/L. Sources of nitrate contamination of surface and groundwater include agricultural activities like excess application of inorganic nitrogenous fertilizers and manures, wastewater disposal, oxidation of nitrogenous waste products and leaching from natural vegetation (WHO, 2011). Nitrate concentrations of 0.4-59.4 and 21-127 mg/L were reportedly obtained by Mosaferi *et al.* (2014) and Iqbal *et al.* (2013) from the study of groundwater samples in Iran and Pakistan, respectively. In a similar study in India, nitrate concentration in 73.68% of samples exceeded the guideline value (50 mg/L) (Balakrishnan *et al*., 2011).

Table 3. Regression statistics for predicting total dissolved solids (TDS) in selected boreholes from Ohaozara and Ivo LGAs

Water quality predictor variable	Unstandardised coefficients		Standardised coefficients (Beta)	t-values	Sig.	95% confidence interval for B (P-values)	
	B	Std. error				Lower bound	Upper bound
Constant	-3.482	3.780	-	-0.921	0.399	-13.199	6.236
EC	0.239	0.149	0.01	1.602	0.170	-0.145	0.623
NO_3^-	-2.252	2.962	0.00	-0.760	0.481	-9.867	5.363
Cl^-	-0.861	2.951	0.00	-0.292	0.782	-8.447	6.726
SO_4^{2-}	0.029	0.016	0.001	1.818	0.129	-0.012	0.070
PO_4^{3-}	-0.01	0.014	0.000	-0.752	0.486	-0.046	0.025
As^{5+}	0.550	0.00	1.000	1.199	0.000	0.549	0.551
R	-	-	-	1.000	-	-	-
R square	-	-	-	1.000	-	-	-
Adjusted R square	-	-	-	1.000	-	-	-
Standard error	-	-	-	0.348	-	-	-
F-test Statistics	-	-	-	9.985	-	-	-
Overall significance	-	-	-	0.000	-	-	-

Table 4. Regression statistics for predicting arsenic (V) content in selected boreholes from Ohaozara and Ivo LGAs

Water quality predictor variable	Unstandardised coefficients		Standardised coefficients (Beta)	t-values	Sig.	95% confidence interval for B (P-values)	
	B	Std. error				Lower bound	Upper bound
Constant	6.308	6.876	-	0.917	0.401	-11.368	23.984
EC	-0.435	0.272	-0.001	-1.601	0.170	-1.133	0.263
NO_3^-	4.104	5.384	0.000	0.762	0.480	-9.736	17.943
Cl^-	1.583	5.364	0.000	0.295	0.780	-12.207	15.372
SO_4^{2-}	-0.053	0.029	-0.001	-1.815	0.129	-0.127	0.022
PO_4^{3-}	0.019	0.025	0.001	0.755	0.484	-0.045	0.083
As^{5+}	1.818	0.002	1.000	1.199	0.000	1.814	1.822
R	-	-	-	1.000	-	-	-
R square	-	-	-	1.000	-	-	-
Adjusted R square	-	-	-	1.000	-	-	-
Standard error	-	-	-	0.633	-	-	-
F-test statistics	-	-	-	9.984	-	-	-
Overall significance	-	-	-	0.000	-	-	-

Phosphate levels in the water samples ranged from 0.02 mg/L to 0.19 mg/L, which was relatively low as compared to the WHO limit of 10 mg/L in drinking water (WHO, 2011). This implied that phosphate pollution due to percolation of agricultural fertilisers, detergents and pharmaceuticals were very minimal. In addition, it showed that the underlying rocks of the study area contained little or no phosphate (Edeogu, 2007).

Arsenic content of the water samples ranged from 2.63 mg/L to 6.66 mg/L, which was above the WHO limit of 0.01mg/L (WHO, 2011). Thus, with respect to As (V) content, the water samples are not too safe for consumption. Arsenic is mainly present as As (V) in water but in anaerobic conditions, it is likely to be present as As (III). In natural waters, they are found in concentrations of less than 1-2 µg/L but in groundwater, they are found at slightly elevated concentrations due to sulphide mineral deposits and sedimentary deposits derived from volcanic rocks (WHO, 2011).

A Schoeller diagram depicting logarithmic data plots for the major ions investigated in the study, is shown in Fig. 2 with the peaks and troughs of the individual water samples indicating their dominant and less dominant ions, respectively. In Fig. 2, chloride is depicted as the most abundant ion followed by sulphate and arsenate while nitrate and phosphate ions are the least dominant ions.

Regression analysis. The multiple linear regression models for predicting TDS and As (V) content of boreholes around Ohaozara and Ivo LGAs of Ebonyi State were shown in equation (1) and (2), respectively:

$$TDS = -3.482 + 0.239\ EC - 2.252\ NO_3 - 0.861Cl^- + 0.029\ SO_4 - 0.01\ PO_4^{3-} + 0.550\ As \quad \text{---------- (1)}$$

$$As = 6.308 - 0.435\ EC + 4.104\ NO_3^- + 1.583\ Cl^- - 0.053\ SO_4 + 0.019\ PO_4^{3-} + 1.818\ TDS \quad \text{---------- (2)}$$

Equation (1) showed that positive relationships existed between TDS and EC, as well as between TDS-SO_4^{2-} and TDS-AS^{5+} constituents of the water samples, while a negative relationship was maintained between TDS and other parameters (NO_3^-, Cl^- and PO_4^{3-}). However, from equation (2), it could be deduced that positive relationship existed among the pairs of As^{5+}-NO_3^-, As^{5+}-Cl^-, As^{5+}-PO_4^3, and As^{5+}-TDS, while negative relationship existed between the pairs of As^{5+}-EC and As^{5+}-SO_4^{2-}. This is in line with literature assertion that in oxidising conditions where groundwater pH values are high, inorganic As (V) predominates, and arsenic concentrations are positively correlated with those of other anion-forming species such as F^-, Cl^-, etc (Smedley and Kinniburgh, 2002). The regression statistics for the models represented in equations (1) and (2) have been summarised in Tables 3- 4. The high *t*-values and low P-values suggested that EC, SO_4^{3-} and As^{5+} levels were important factors in the prediction of the TDS value for different water samples (Table 3). Similarly, high *t*-values and low P-values indicated that NO_3^-, Cl^-, PO_4^{3-} and TDS were important variables in the prediction of As (V) content of different water samples. Furthermore, comparison of the adjusted R square and the R square values for the two regression models (Tables 3- 4) indicate that they accounted for almost 100% of the variance (except for minimal errors) in the TDS and As (V) levels of the water samples.

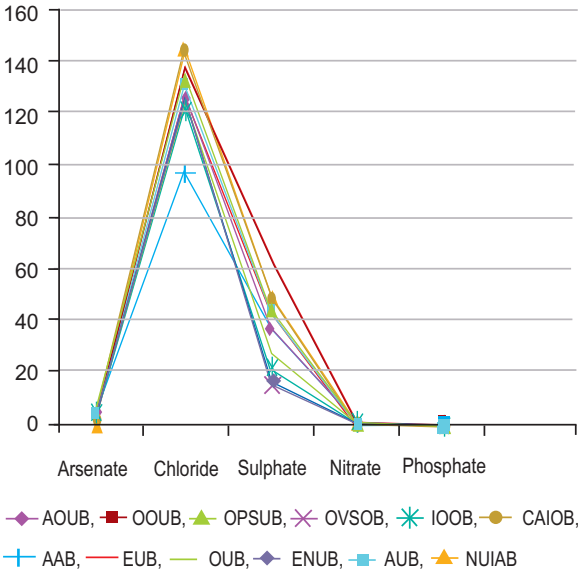

Fig. 2. Schoeller diagram depicting ionic species investigated.

Analysis of variance. One-way ANOVA at $P < 0.05$ (95% confidence level) showed that F_{cal} (1.862) was greater than F_{tab} (0.619) implying that a significant difference existed among the physicochemical parameters in water samples from the 12 different locations investigated. This might be due to the influence of natural and anthropogenic factors on the physicochemical parameters found in the aquatic environment.

Conclusion

The hydrochemical assessment of groundwater resources in Ivo and Ohaozara LGAs, Nigeria revealed that the water in these areas was generally alkaline, non-turbid, moderately hard and saline in nature. With the exception of arsenic

content level, all other physicochemical parameters investigated in the water samples were within the stipulated NIS and WHO limits for contaminants in potable water. This implied that the water in these areas might be fit for other domestic uses apart from drinking, and would require further standard treatment before it could be fit for drinking purposes. It is recommended that certain strategies such as proper sewage disposal, proper siting of boreholes and installation of point-of-use water treatment devices be adopted in order to improve the quality of groundwater located in the study areas. Generally, the water samples are deemed fit for domestic uses; though its high arsenic level may pose potential health threats for children. Point-of-use water treatment devices should be installed in the boreholes to improve water quality.

References

Adejuwon, J.O., Mbuk, C.J. 2011. Biological and physiochemical properties of shallow wells in Ikorodu town, Lagos, Nigeria. *Journal of Geology and Mining Research,* **3:** 161-168.

Adekunle, I.M.N., Adetunji, M.T., Gbadebo, A.M., Banjoko, O.B. 2007. Assessment of groundwater quality in a typical rural settlement in Southwest, Nigeria. *International Journal of Environmental Research and Public Health,* **4:** 307-318.

APHA, AWWA, WPCF, 2012. *Standard Methods for the Examination of Water and Wastewater.* 22th edition, American Public Health Association. American Water Works Association. Water Pollution Control Federation. Washington DC., USA.

ASTM, 2012. *American Society Testing Materials*. Annual Book of (ASTM) Standards. vol. **11.01**. Available in: http://www.astm.org. Access in: Oct. 2014.

Ayeni, A.O., Soneye, A.S.O., Balogun, I.I. 2009. State of water supply sources and sanitation in Nigeria: Implication of Muslims. In Ikare-AKOKO Township. *The Arab World Geographer,* **12:** 95-104.

Balakrishnan, P., Saleem, A,. Mallikarjun, N.D. 2011. Groundwater quality mapping using geographic information system (GIS): A case study of Gulbarga City, Karnataka, India. *African Journal of Environmental Science Technology,* **5:** 1069-1084.

Carter, E., Stewart, A.G. 2000. Environmental geochemistry and health: an integrated future in medical and geochemical studies, the example of Iodine. *Journal of the Geological Society of London,* **157:** 835-836.

Centeno, A., Millic, F.G., Finkleman, R.I., Sellinus, O. 2005. Medical geology. *Military Medical Technology online,* **9:** 1-5.

Davies, S.N., De-Wiest, R.M.J. 1966. *Hydrogeology,* 463 pp. John Wiley & Sons, Inc., New York, USA.

Deas, M.L., Lowney, C.L. 2000. *Water Temperature Modeling Review,* Technical Report to Bay Delta Modeling Forum, 113 pp.

Edeogu, C.O. 2007. Nitrate, sulphate, phosphate and chloride status of stable food crops, soils and water as indicator of environmental base anion pollution load in Ebonyi State, Nigeria. *Journal of Biological Sciences,* **7:** 745-751.

Feng, L., Yuan-Ming, Z., Ji-Zheng, H. 2009. Microbes influence the fractionation of arsenic in paddy soils with different fertilization regimes. *The Science of the Total Environment,* **407:** 2631-2640.

Freeze, R.A., Cherry, J.A. 1979. *Groundwater,* pp. 250-263, Prentice-Hall, Englewood Cliffs, New Jersey, USA.

Garelick, H., Jones, H., Dybowska, A., Valsami-Jones, E. 2008. Arsenic pollution sources. *Reviews of Environmental Contamination Toxicology,* **197:** 17-60.

Igwenyi, I.O., Aja-Okorie, 2014. Physicochemical properties and heavy metal analysis of major water sources in Dhaozara, Ebonyi State, Nigeria. *IOSR Journal of Environmental Science, Toxicology and Food Technology,* **8:** 41-44.

Iqbal, F., Ali, S., Tauqeer, H.M., Shakoor, M.B., Farid, M., Iftikhar, U., Nazir, M.M. 2013. Assessment of ground water contamination by various pollutants from sewage water in Chakera village, Faisalabad. *International Journal of Environmental Monitoring and Analysis,* **1:** 182-187.

Jan, M.H. 2011. Characterization of the inorganic chemistry of surface waters in South Africa. *Water S.A,* **37:** 401-410.

Jung, U.L.S., Sang, W.L., Hyo, T., Kyoung, W.K., Jin, S.L. 2009. Enhancement of arsenic mobility by indigenous bacteria from mine tailings as response to organic supply. *Environment International,* **35:** 496-501.

Mosaferi, M., Pourakbar, M., Shakerkhatibi, M., Fatehifar, E., Belvasi, M. 2014. Quality modeling of drinking groundwater using GIS in rural communities, northwest of Iran. *Journal of Environmental Health Science & Engineering,* **12:** 99.

Mpenyana-Monyatsi, L., Onyango, M.S., Momba, M.N.B. 2012. Groundwater quality in a South African rural community: A threat to public health. *Polish Journal of Environmental Studies,* **21:** 1349-1358.

Nag, S.K., Lahiri, A. 2012. Hydrochemical characteristics

of groundwater for domestic and irrigation purposes in dwarakeswar watershed area, India. *American Journal of Climate Change,* **1:** 217-230.

Narasimha, R.C., Dorairaju S.V., Bujasendra, R.M., Chalapathi, P.V. 2011. Statistical analysis of drinking water quality and its impact on human health in Chandragiri near Tirupati, India. Retrieved October 05, 2014 from www.ecowbeb.com/edi/11121.

NIS, 2007. *Nigerian Industrial Standard for Drinking Water Quality.* Standards Organization of Nigeria, Abuja, Nigeria.

Nwankwoala, H.O., Udom, G.J. 2011. Hydrogeochemical evaluation of groundwater in parts of eastern Niger Delta, Nigeria. *Journal of Academic and Applied Studies,* **1:** 33-58.

Obasi, P.N., Akudinobi, B.E. 2013. Hydrochemical evaluation of water resources of the Ohaozara areas of Ebonyi State, southeastern Nigeria. *Journal of Natural Sciences Research,* **3:** 75-80.

Obasi, R.A., Balogun, O. 2001. Water quality and environmental impact assessment of water resources in Nigeria. *African Journal of Environmental Studies,* **2:** 228-231.

Ojekunle, I.A. 2000. *Transport and Urban Environmental Quality in Nigeria in Contemplary to AD 2000,* Frankad Publishers, Lagos, Nigeria.

Okiongbo, K.S., Douglas, R. 2013. Hydrogeochemical analysis and evaluation of groundwater quality in Yenagoa city and environs, Southern Nigeria. *Ife Journal of Science,* **15:** 209-222.

Okorie, I.A. 2010. Determination of potentially toxic elements (PTEs) and an assessment of environmental health risk from environmental matrices. *PhD. Thesis,* pp. 20-35, Northumbria University, UK.

Okoyeh, E.I., Egboka, B.C.E. 2013. Evaluation of hydrochemical parameters of Okposi and Uburu salt lakes, Nigeria. *International Journal of Scientific and Engineering Research,* **4:** 2882-2889.

Olajire, A.A., Imeokparia, F.E. 2001. Water quality assessment of Osun River: Studies on inorganic nutrients. *Environmental Monitoring and Assessment,* **69:** 17-28.

Ovrawah, I., Hymore, F.K. 2001. Quality of water from hand-dug wells in the Warri environs of Niger delta region. *African Journal of Environmental Studies,* **2:** 169-173.

Pink, D.H. 2006. *Investing in Tomorrow's Liquid Gold,* Retrieved October 03, 2014 from: www. finance. yalow.com

Smedley, P.L. 2008. Sources and distribution of arsenic in groundwater and aquifers. In: *Arsenic in Groundwater: A World Problem,* Appelo, Tony (ed.) pp 4-32.IAH, Utrecht, The Netherlands.

Smedley, P.L., Kinniburgh, D.H. 2002. A review of the source, behaviour and distribution of arsenic in natural waters. *Applied Geochemistry,* **17:** 517-568.

Smith, A.H., Lingas, E.O., Rahman, M. 2000. Contamination of drinking water by arsenic in Bangladesh. Public *Health Emergency Bulletin of World Health Organization,* **78:** 1093-1103.

Talabi, A.O., Afolagboye, O.L., Tijani, M.N., Aladejana, J.A., Ogundana, A.K. 2013. Hydrogeochemical assessment of surface water in the central part of Ekiti-State, Southwestern Nigeria. *American Journal of Water Resources,* **1:** 56-65.

WWC, 2003. Third World Water Forum and Ministorial Conference. World Water Council and Government of Japan. 16-23 March, Kyoto, Osaka and Shiaga, Japan. *Forum Bulletin,* **30:** 35-37.

Williams, J.W., Silver, S. 1984. Bacterial resistance and detoxification of heavy metals. *Enzyme and Microbiology Technology,* **6:** 530-537.

WHO, 2011. *Guidelines for Drinking Water Quality,* 4th edition, World Health Organization (WHO), Geneva, Switzerland.

WHO, 1984. *Guidelines for Drinking Water Quality,* pp. 99-102, World Health Organization (WHO), Geneva, Switzerland.

Pak. j. sci. ind. res. Ser. A: phys. sci. 2016 **59** (1) 52-55

The Comfort of Knitted Fabric as Affected by its Structure

Muhammad Qamar Tusief [a]*, Nabeel Amin[b], Mudassar Abbas[a] and Zahid Hussain[c]

[a]Department of Fibre and Textile Technology, University of Agriculture, Faisalabad, Pakistan
[b]School of Textile and Design, University of Management and Technology, Lahore, Pakistan
[c]Interloop Private Limited, Khurrianwala-Jaranwala Road, Khurrianwala, Faisalabad, Pakistan

(received September 2, 2014; revised February 16, 2015; accepted February 17, 2015)

Abstract. The present study was carried to investigate the effect of various knitted fabric structure on its comfort related properties. It was observed that, all comfort properties of knitted fabric have direct relation to its structure. The plain knitted fabric was found best for optimum comfort.

Keywords: air permeability, absorbency, drying time, fabric structure

Introduction

Developments in science and technology have brought about radical changes in the textile industry. The textile industry being the backbone of Pakistan's economy needs improvement due to the introduction of various factors like increasing competition in the global marketplace, introduction of state of the art technology in textile field, high raw material prices and quality of raw material etc. The above mentioned factors invite both, our industrialists and planners to place greater emphasis on quality as well as productivity to compete in global market.

Knitting is one of the most important sectors of textile. Knitted fabrics are commonly used because of their excellent meachanical and comfort properties. Because of their integral qualities like softness, coolness, sweat absorbance and durability, such garments are very popular all over the world, particularly in the developed countries. In addition, the comfort knitted fabric give light weight, warmness, resistance to wrinkle and easy care due to stretch imparted by the looped yarn structure (Ogulata and Mavruz, 2010).

From the last few years, living standards of people have changed that increased the demand of fabrics having some special features. Now a days clothing is not only for aesthetic and ethical reasons; but its comfort parameters are also included like elasticity, softness, air permeability, thermal insulation and water vapour permeability are expected from garments. Comfort is mainly affected by type of fibre, yarn properties and structure of fabric. During the previous decades the knitting technology has been developed in respect of knitted structure, modified yarn and various kinds of knitting instruments. The fabric properties are not only affected by the yarn properties but also by the parameters of the fabric construction. Wetting and wicking are the properties producing major issues in the processing and application of fibre materials. Wicking and wetting both are the significant characteristics related to the comfort properties of knitted fabric that occur during wearing. The nature, volume, arrangement and division of fibres, fabric structure, yarn kind and different types of chemicals affect on the wetting performance of the fabrics (Yanilmaz *et al.,* 2012).

Knitting is the procedure of forming a fabric that involves the inter-looping of thread in a sequence of connected loops through needles. Knitted fabrics have famous outstanding comfort characteristics. Knitted fabrics are commonly used because of their excellent mechanical and comfort properties. They possess high extensibility under low loads, allowing comfortable fit on any part pulled. The advantages of using knitted fabrics, as opposed to conventional fabrics, lie in their low cost, improved barrier properties, adequate strength, and comfort properties. They are also lightweight and flexible.

They not only allow stretching and light movement, but also have good handling characteristics and facilitate a smooth transition of moisture from the body. These characters make knitted fabric the commonly favourite choice for casual wear, fire fighters' socks, gloves, helmet liner, sportswear and underwear. Comfort is one of the most important characteristic of clothing. For the selection of knitted fabric comfort plays very important role. Several factors effect on comfort provided by clothing like thermal comfort, flexibility, moisture flow and softness, etc. Comfort

*Author for correspondence; E-mail: qamartosief@yahoo.com

properties like drying time, air permeability, wicking and absorbency are influenced by fabric properties like knitted structure, fabric, thickness, fabric porosity, density, type of weave and yarn properties like yarn count, yarn twist, yarn hairiness etc. The interest in knitted fabric have been increased for the last few years because of their simple production methods, low cost, high level of comfort ability and wide product range (Chidambaram *et al.,* 2011; Ibrahim *et al.,* 2011, 2010). The research projects upon studying the effects of various yarn and fabric variables on the comfort of knitted fabrics were made in past but an integrated work to check the effect of knitted structure on the comfort properties of knitted fabric was not reported especially in Pakistan. Hence, this research study was planned to check the manipulation of knitting structure of fabric on its comfort in order to optimize the quality of the fabric to make it best for wearing near to skin as well as a guide path for the manufacturers and users to make a right choice for their product.

Materials and Methods

Circular knitting machine of the following specification was engaged for the preparation of plain, terry and rib knitted grey fabrics.

Brand	= Lonati
Gauge	= 14"
Stitch length	= 0.30
No. of needles	= 144
Voltage	= 380V
Machine speed	= 22 rpm

The fabric samples so made were subjected to test for their comfort related properties. Therefore, methods applied to test the comfort properties like air permeability, absorbency, vertical wicking, drying time of fabric are given as under:

Air permeability. The air permeability of the fabric samples were tested according to the standard test method as suggested by ASTM Committee D-737-04 (ASTM, 2008).

Absorbency. The absorbency characteristics of a fabric can influence the uniformity and completeness of bleaching and dyeing by the ability to take in water into the fibre, yarn, or fabric construction. The suitability of a fabric for a particular use as in the case of gauze or toweling is also dependent upon the fabrics ability and propensity to take up water. The absorbency of the fabric samples were tested according to AATCC absorbency test method D-79 (AATCC, 2010).

Vertical wicking. Vertical wicking of the knitted fabric samples were tested according to AATCC method (AATCC, D-197., 2013).

Drying time. The drying time of the fabric samples was calculated using the apparatus and procedure as recommended by AATCC (AATCC, D-199., 2013).

Results and Discussion

Air permeability. The individual comparison of means for knitting structures (S) have been presented in Table 1. It shows that the mean value of air permeability for different knitting structures plain, terry and rib are 35.417, 32.334 and 34.00 (cm^3/ cm^2/ sec), respec-tively. These values differ significantly from each other. The present findings are also disclosed in Fig.1. The results reveal that plain knitted structure gives the maximum value while the minimum value is recorded for terry knitted structure. These results are well supported from the research study of Ogulata (2006) who stated that the air permeability was mainly dependent upon the fabric's weight and construction (thickness and porosity). He also stated that the air permeability of fabrics was influenced by several factors: the type of fabric structure, the number of warp and weft yarns per centimeter (or inch), the amount of twist in yarn structure. Similarly, Raj and Sreenivasan (2009) also discussed that the increase in more open structure of the fabric and the fineness of the yarn improved air permeability of the fabric. Therefore, it can be explained that structural parameters of fabric influence on air permeability.

Absorbency. The comparison of mean values of fabric absorbency for various knitting structures, plain, terry and rib as given in Table 1, are 11.167, 16.917 and 14.083 (sec), respectively. These values differ significantly from

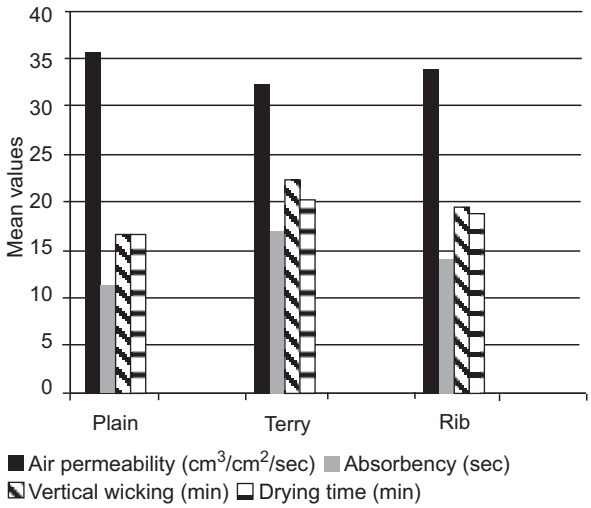

Fig. 1. Comfort properties of knitted fabric for its various structures.

Table 1. Mean values of various fabric comfort related properties for various knitted fabric

Knitting structure	Fabric properties			
	Air permeability ($cm^3/cm^2/sec$)	Absorbency (sec)	Vertical wicking (min)	Drying time (min)
Plain	35.417	11.167	16.750	16.667
Terry	32.334	16.917	22.500	20.250
Rib	34.000	14.083	19.500	18.917

each other. These findings are also explained in Fig.1. The results reveal that terry knitted structure gives the maximum value while, the minimum value is recorded for plain knitted structure. These results show that in terry structure there exists less space within the fabric structure as compared to that of other structures. These results are well supported from the research study of Ogulata (2006) who in study reported that the water absorbency of the fabric mainly depended on the moisture regain of component fibre and open spaces within the fabric structure.

Vertical wicking. The comparison of mean values of vertical wicking for different knitting structures of the fabric i.e. plain, terry and rib are 16.750, 22.500 and 19.500 (min), respectively (Table 1). These values differ significantly from each other. The range of vertical wicking for different knitting structures is recorded from 16.750 to 22.500 (min). These findings are also interpreted in Fig. 1. The results reveal that terry knitted fabric gives the maximum value while the minimum value is recorded for plain knitted structure. These results are well supported from the research study of Onofrei *et al.*(2011) who accomplished that the knitted structure influenced on wicking ability and the drying ability was mostly determined by raw material and knitted structure parameters. Single jersey fabric having highest water up-take capacity and very high initial wicking rate. This behaviour is most probably due to the structures' ability to behave like a capillary system, removing and transporting water through the structure. Knitting structures having high thickness showed the worse wicking ability.

Drying time. The mean values of drying time of fabric for knitting structures, plain, terry and rib as presented in Table 1, are 16.667, 20.250 and 18.917 (min), respectively. These values differ significantly from each other. These results are also elaborated in Fig.1. The results reveal that terry knitted structure gives the maximum value while the minimum value is recorded for plain knitted structure. These results are well supported from the research study of Onoferi *et al.* (2011) who stated that knitted structure parameters affect drying ability. Single jersey fabrics have the highest drying rate and also the largest water diffusion area. This is probably due to fabric characteristics, namely, low thickness and mass per unit area and knitted structure. In the same line Laing *et al.* (2007) depicted that the fabrics which dried most rapidly on the line were typically thinnest and lightest, whereas those taking the longest time to dry were typically the non-woven, wool, and among the heaviest but not always the thickest.

Conclusion

From the above research study it is concluded that plain knit structure showed better results in sense of the comfort related properties of the knitted fabric as compared to that of terry and rib knitted structure.

References

AATCC, 2013. Test method for vertical wicking and drying time of textiles. D-197, 199, USA: American Association of Textile Chemists and Colorists, USA.

AATCC, 2010. Test method for absorbency of textile. D-79. USA: American Association of Textile Chemists and Colorists, USA.

ASTM, 2008. Standard test method for measurement of fabric properties. ASTM Designation: D-737-04. American Society for Testing and Material, Philadelphia, USA.

Chidambaram, P., Govind, R., Venkataraman, K.C. 2011. The effect of loop length and yarn linear density on the thermal properties of bamboo knitted fabric. *AUTEX Research Journal,* **11:** 102-105.

Ibrahim, N.A., Khalifa, T.F., El-Hossamy, M.B.,Twafik, T. M. 2011. Factors affecting the functional and comfort-related properties of reactive dyed cotton knits, *Journal of Industrial Textiles,* **41:** 41-56.

Ibrahim, N.A., Khalifa, T.F., El-Hossamy, M.B.,Twafik, T. M. 2010. Effect of knit structure and finishing treatments on functional and comfort properties of cotton knitted fabrics. *Journal of Industrial Textiles,* **40:** 49-64.

Laing, R.M., Wilson, C.A., Gore, S.E., Carr, D.J., Niven, B.E. 2007. Determining the drying time of apparel fabrics. *Textile Research Journal,* **77:** 583-590.

Oglakcioglu, N., Marmarali, A. 2007. Thermal comfort properties of some knitted structures. *Fibres & Textiles in Eastern Europe,* **15:** 94-96.

Ogulata, R.T., Mavruz, S. 2010. Investigation of porosity and air permeability values of plain knitted fabrics.

Fibre and Textile in Eastern Europe, **5:** 71-75.

Ogulata, R.T. 2006. Air permeabillity of woven fabrics. *Journal of Textile and Apparel,Technology and Management,* **5:** 1-10.

Onofrei, E., Rocha, A., Catarino, A. 2011. The influence of knitted fabrics' structure on the thermal and moisture management properties. *Journal of Engineered Fibres and Fabrics,* **6:** 10-22.

Raj, S., Sreenivasan, S. 2009. Total wear comfort index as an objective parameter for characterization of overall wearability of cotton fabrics. *Journal of Engineered Fibres and Fabrics,* **4:** 29-41.

Yanilmaz, M., Plev, B.F., Kalaoglu, F. 2012. A study on the influence of knit structure on comfort properties of acrylic knitted fabrics. *Smartex Research Journal,* **1:** 88-92.

Pak. j. sci. ind. res. Ser. A: phys. sci. 2016 **59** (1) 56-59

Short Communication

An Investigation into the *In situ* Preparation of Hetero Bifunctional Monochlorotriazinyl-Vinyl Sulphone Reactive Dyes for Cotton

Khalid Pasha[a]* and John Anthony Taylor[b]

[a]Textile Engineering Department, NED University of Engineering and Technology, Karachi, Pakistan
[b]Colour Synthesis Solution Ltd., Hexagon Tower, Manchester M9 8ZS, UK

(received June 3, 2014; revised March 3, 2015; accepted April 1, 2015)

Abstract. An attempt has been made in *in-situ* preparation and application of two isomers (para and meta) of aminophenyl-β-sulphatoethyl sulphone reagents (PABSES and MABSES) with three dichlorotriazinyl dyes i.e. CI Reactive Orange 86, CI Reactive Red 11 and CI Reactive Blue 168 to generate mixed hetero bifunctional dyes in dye bath. Dyeing results when compared with similar targeted type of commercially available Sumifix Supra dyes were found not up to the mark. Build up properties of all *in situ* prepared dyes were lower except for few light depth of shades as compared to preformed commercial Sumifix Supra dyes. This could be because of inefficient condensation of dichlorotriazinyl dyes with the aminophenyl-β-sulphatoethyl sulphone. However, meta isomer of aminophenyl-β-sulphatoethyl sulphone appeared to be more effective than the para isomer.

Keywords: colouration, reactive dyes, cotton, hetero bifunctional dyes, fixation

Sumifix Supra dyes developed by Sumitomo showed minimal sensitivity to changes in electrolyte, alkali, liquor and exhibit high fixation over a range of processing conditions as compared with homobifunctional dyes (Aspland, 1993; Abeta *et al*., 1984; Fujioka and Abeta, 1982). These hetero bifunctional reactive dyes are also robust to changes in processing conditions such as application temperature (Hunter and Renfrew, 1999). Earlier it was assumed that under strict neutral conditions and at constant temperature the major reaction would be the condensation reaction of dichlorotriazinyl dyes with aminophenyl-β-sulphatoethyl sulphone not the hydrolysis of dichlorotriazinyl dyes or of vinyl sulphone group with water (Lewis and Loan, 2007; Weber and Vicki, 1993). An attempt was made in this research work to condense dichlorotriazine dyes with aminophenyl-β-sulphatoethyl sulphone in the dye bath under neutral conditions prior to addition of salt and alkali required for the (neutral) exhaustion and (alkaline) fixation stages.

Dichlorotriazinyl dyes CI Reactive Orange 86, CI Reactive Red 11, CI Reactive Blue 168 and dyes of Sumifix Supra type CI Reactive Yellow 145, CI Reactive Red 195, CI Reactive Blue 221 were available commercially. All other chemicals used in this study were of general laboratory grade purchased from Aldrich or Merck. Samples of para and meta aminophenyl-β-sulphatoethyl sulphone were generously provided by BASF. The strength of dyestuff samples were estimated from the ratio of its actual molecular weight (MW) to its effective molecular weight (Mole In) estimated by titanous chloride titration method (Murtagh, 2004) and is given in Table 1.

Table 1. Effective dye strength

Dyes	Moles In
CI Reactive Orange 86	1792
CI Reactive Red 11	1482
CI Reactive Blue 168	2919
CI Reactive Yellow 145	1472
CI Reactive Red 195	1705
CI Reactive Blue 221	3310

Experimental results suggested that for *in situ* application of dichlorotriazine dye and sulphatoethyl sulphones agents, temperature of dye bath should be at 70 °C, and pH should be 6.0–6.5 using phosphate buffer with reaction time of 1 h, however, reaction period of 2 and 4 h were also measured. Each dye was applied to bleach unmercerised woven cotton at five depths, *viz*. 1, 2, 4, 6 and 9% dye o.m.f. at 60 °C and liquor ratio 10:1, using the quantities of Glauber's salt (exhaustion for 30 min) and soda ash (fixation for 60 min) as shown in

*Author for correspondence; E-mail: drkpasha@hotmail.com

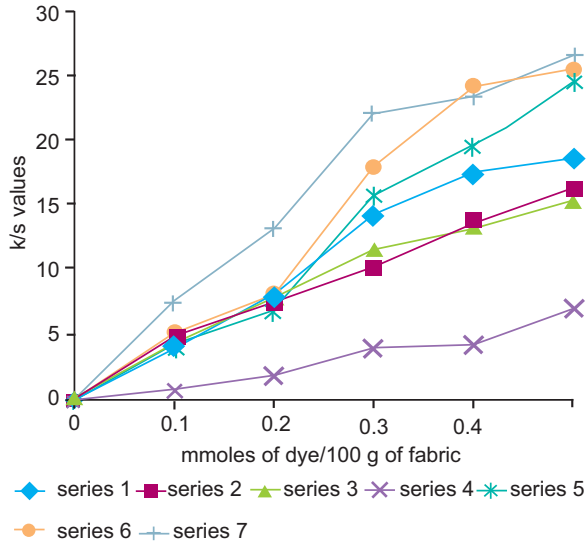

Legends: Series 1: CI Reactive Orange 86 with para aminophenyl-β-sulphatoethyl sulphone (PABSES), reaction time one hour at 70 °C before dyeing, **Series 2:** CI Reactive Orange 86 with PABSES, reaction time two hour at 70 °C before dyeing, **Series 3:** CI Reactive Orange 86 with PABSES, reaction time four hour at 70 °C before dyeing, **Series 4:** CI Reactive Orange 86 kept in dye bath under same conditions as for series 1, 2 and 3 but without PABSES before dyeing, **Series 5:** CI Reactive Orange 86 dyed to cotton without any modification at standard Sumifix Supra dyeing conditions, **Series 6:** CI Reactive Orange 86 dyed to cotton without any modification at standard MX dyeing conditions, **Series 7:** Commercial CI Reactive Yellow 145 dyed to cotton without any modification at standard Sumifix Supra dyeing conditions.

Fig. 1. CI Reactive Orange 86 with PABSES.

Table 2. After dyeing, the fabric was rinsed with cold and hot water before soaping at boil for 10 min and finally rinsed with cold water and air dried at room temperature. Colorimetric properties of dyeing were determined using a Spectraflash 600 spectrophotometre (D65 illumination, 10° observer). To facilitate the comparison of the build-up properties of these dyes, k/s values versus dye concentrations in millimoles per 100 g of fabric were plotted.

Table 2. Amount of salt and alkali used

Shades	Sodium sulphate (g/L)		Sodium carbonate(g/L)	
% dye (o.m.f)	Procion MX	Sumifix supra	Procion MX	Sumifix supra
1 & 2	35	35	10	20
4	45	50	15	20
6 & 9	55	50	20	20

Dyeing results of CI Reactive Orange 86 with PABSES (Fig. 1) showed that the depths of shade under these conditions are far inferior to when PABSES is present, supporting the premise that a Sumifix Supra type of heterobifunctional dye is indeed formed in the dye bath. Dyeing results appeared to indicate partial conversions of dichlorotriazine to a monochlorotriazine-vinyl sulphone mixed reactive system. Results for meta isomer (MABSES) are given in Fig. 2 and shows that significant conversion to mixed bifunctional dye had occurred within two hours but again build up was inferior on an equimolar basis to CI Reactive Yellow 11.

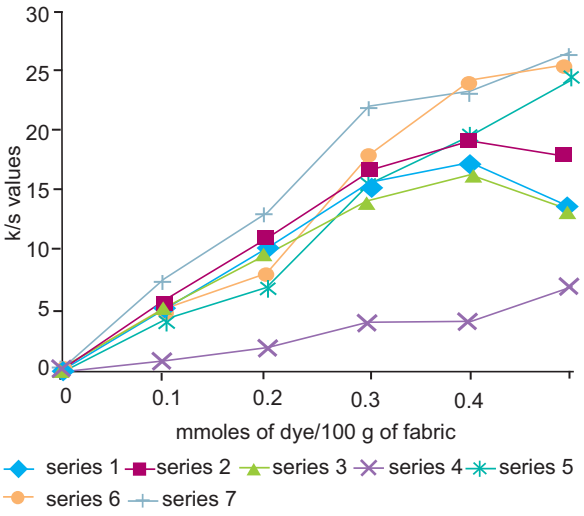

Legends: Series 1: CI Reactive Orange 86 with meta amino-phenyl-β-sulphatoethyl sulphone (MABSES), reaction time one hour at 70 °C before dyeing, **Series 2:** CI Reactive Orange 86 with MABSES, reaction time two hour at 70 °C before dyeing, **Series 3:** CI Reactive Orange 86 with MABSES, reaction time four hour at 70 °C before dyeing, **Series 4:** CI Reactive Orange 86 kept in dye bath under same conditions as for series 1, 2 and 3 but without MABSES before dyeing, **Series 5:** CI Reactive Orange 86 dyed to cotton without any modification at standard Sumifix Supra dyeing conditions, **Series 6:** CI Reactive Orange 86 dyed to cotton without any modification at standard MX dyeing conditions, **Series 7:** Commercial CI Reactive Yellow 145 dyed to cotton without any modification at standard Sumifix Supra dyeing conditions.

Fig. 2. CI Reactive Orange 86 with MABSES.

Results for both isomers (PABSES and MABSES) with CI Reactive Red 11 are depicted in Fig. 3-4 and shows that the best build up was obtained when dichlorotriazine and amine were reacted at 70 °C for 2 h prior to addition of salt and alkali. Interestingly, with CI Reactive Red 11, the para isomer performed significantly better than the meta isomer.

CI Reactive Blue 168 showed mixed results which are shown in Fig. 5-6. In some cases build-up was almost comparable to CI Reactive Blue 168 (commercial counterpart). However, in all cases build-up tailed off above 4% depth of dye shade.

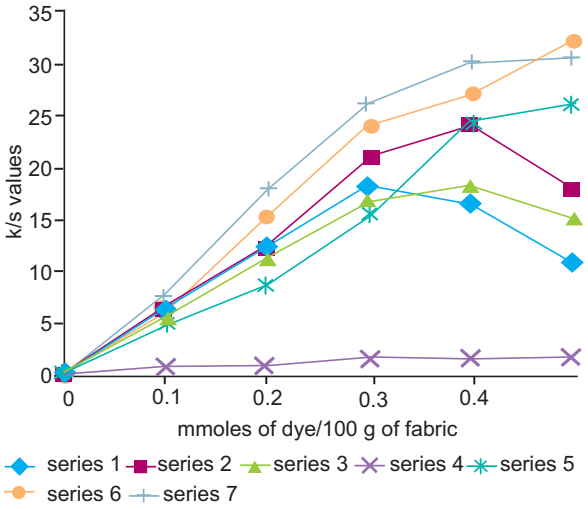

Legends: Series 1: CI Reactive Red 11 with para aminophenyl-β-sulphatoethyl sulphone (PABSES), reaction time one hour at 70 °C before dyeing, **Series 2:** CI Reactive Red 11 with PABSES, reaction time two hour at 70 °C before dyeing, **Series 3:** CI Reactive Red 11 with PABSES, reaction time four hour at 70 °C before dyeing, **Series 4:** CI Reactive Red 11 kept in dye bath under same conditions as for series 1, 2 and 3 but without PABSES before dyeing, **Series 5:** CI Reactive Red 11 dyed to cotton without any modification at standard Sumifix Supra dyeing conditions, **Series 6:** CI Reactive Red 11 dyed to cotton without any modification at standard MX dyeing conditions, **Series 7:** Commercial CI Reactive Red 195 dyed to cotton without any modification at standard Sumifix Supra dyeing conditions.

Fig. 3. CI Reactive Red 11 with PABSES.

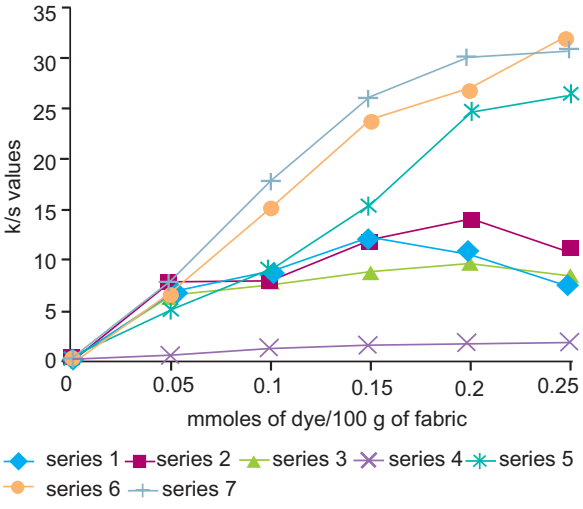

Legends: Series 1: CI Reactive Red 11 with meta amino-phenyl-β-sulphatoethyl sulphone (MABSES), reaction time one hour at 70 °C before dyeing, **Series 2:** CI Reactive Red 11 with MABSES, reaction time two hour at 70 °C before dyeing, **Series 3:** CI Reactive Red 11 with MABSES, reaction time four hour at 70 °C before dyeing, **Series 4:** CI Reactive Red 11 kept in dye bath under same conditions as for series 1, 2 and 3 but without MABSES before dyeing, **Series 5:** CI Reactive Red 11 dyed to cotton without any modification at standard Sumifix Supra dyeing conditions, **Series 6:** CI Reactive Red 11 dyed to cotton without any modification at standard MX dyeing conditions, **Series 7:** Commercial CI Reactive Red 195 dyed to cotton without any modification at standard Sumifix Supra dyeing conditions.

Fig. 4. CI Reactive Red 11 with MABSES.

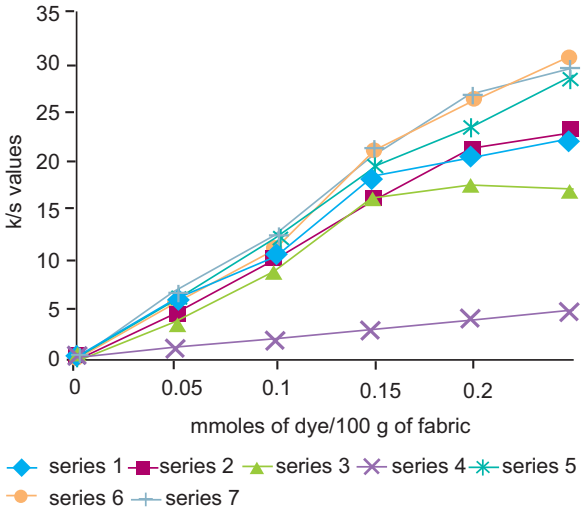

Legends: Series 1: CI Reactive Blue 168 with para amino-phenyl-β-sulphatoethyl sulphone (PABSES), reaction time one hour at 70 °C before dyeing, **Series 2:** CI Reactive Blue 168 with PABSES, reaction time two hour at 70 °C before dyeing, **Series 3:** CI Reactive Blue 168 with PABSES, reaction time four hour at 70 °C before dyeing, **Series 4:** CI Reactive Blue 168 kept in dye bath under same conditions as for series 1, 2 and 3 but without PABSES before dyeing, **Series 5:** CI Reactive Blue 168 dyed to cotton without any modification at standard Sumifix Supra dyeing conditions, **Series 6:** CI Reactive Blue 168 dyed to cotton without any modification at standard MX dyeing conditions, **Series 7:** Commercial CI Reactive Blue 221 dyed to cotton without any modification at stand. Sumifix Supra dyeing conditions.

Fig. 5. CI Reactive Blue 168 with PABSES.

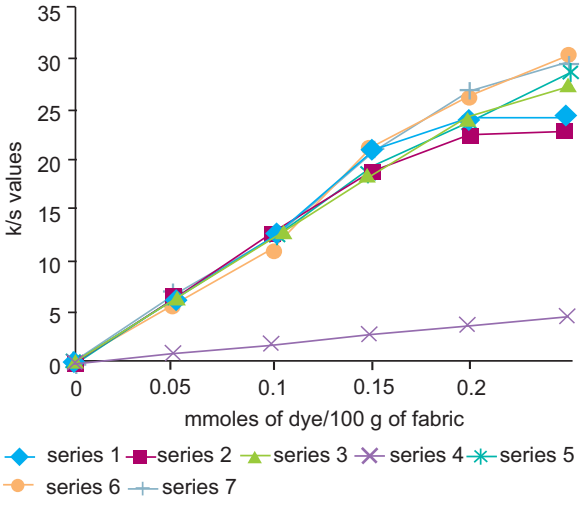

Legends: Series 1: CI Reactive Blue 168 with meta amino-phenyl-β-sulphatoethyl sulphone (MABSES), reaction time one hour at 70 °C before dyeing, **Series 2:** CI Reactive Blue 168 with MABSES, reaction time two hour at 70 °C before dyeing, **Series 3:** CI Reactive Blue 168 with meta MABSES, reaction time four hour at 70 °C before dyeing, **Series 4:** CI Reactive Blue 168 kept in dye bath under same conditions as for series 1, 2 and 3 but without MABSES before dyeing, **Series 5:** CI Reactive Blue 168 dyed to cotton without any modification at standard Sumifix Supra dyeing conditions, **Series 6:** Procion Blue MX-4GD dyed to cotton without any modification at standard MX dyeing conditions, **Series 7:** Commercial CI Reactive Blue 221 dyed to cotton without any modification at standard Sumifix Supra dyeing conditions.

Fig. 6. CI Reactive Blue 168 with MABSES.

Dyeing results when compared with commercial Sumifix Supra dyes of similar shades were inferior in performance. Meta isomer of aminophenyl-β-sulphatoethyl sulphone appeared to be more effective than the para isomer. This probably reflects more nucleophilic character of the former isomer (Sheng, 1998). The falling-off of the build-up properties of some of the dyes at darker shades may be due to blocking effect.

References

Abeta, S., Yoshida, T., Imada, K. 1984. Problems and progress in reactive dyes. *American Dyestuff Reporter*, **73:** 26-49.

Aspland, J.R. 1993. *A Series on dyeing*, Chapter 15, Colour, colour measurement and control. *Journal of the American Association of Textile Chemists and Colourists*, **25:** 34-42.

Fujioka, S., Abeta, S. 1982. Development of novel reactive dyes with a mixed bifunctional reactive system. *Dyes and Pigments*, **3:** 281-294.

Renfrew, A.H.M. 1999. *Reactive Dyes for Textile Fibres*. 224 pp., Society of Dyers and Colourists, Bradford, UK.

Lewis, D.M., Loan, T.T.V. 2007. Dyeing cotton with reactive dyes under neutral conditions. *Coloration Technology*, **123:** 306-311.

Sheng, Y., Zhenghua, Z. 1998. Kinetic study of reaction of vinylsulfonyl aniline and dichlorotriazinyl group. *Dyes and Pigments*, **38:** 137-146.

Taylor, J.A., Murtagh, V. 2004. A simple titrimetric method for the estimation of reactive dye fixation on cellulosic fabrics. *Dyes and Pigments*, **63:** 17-22.

Weber, E.J., Stickney, V.C. 1993. Hydrolysis kinetics of reactive blue 19-vinyl sulfone. *Water Research*, **27:** 63-67.

Pak. j. sci. ind. res. Ser. A: phys. sci. 2015 **59** (1) 60-62

Short Communication

Activated Sludge Process and its Suitability for Treatment of Tannery Waste Water

Niaz Ahmed Memon[a]*, Nisar Ahmed[b], Nusrat Jalbani[a], Tahira Ayaz[b], Razia Bagum[a] and Alia Bano Munshi[a]

[a]PCSIR Laboratories Complex, Shahrah-e-Dr. Salimuzzaman Siddiqui, Karachi-75280, Pakistan
[b]Leather Research Centre, PCSIR, D-102, S.I.T.E., South Avenue, Karachi-75700, Pakistan

(receivd April 30, 2014; revised January 1, 2015; accepted January 14, 2015)

Abstract. This study was conducted for the treatment of tannery wastewater and to develop simple design criteria under local conditions. BOD_5, COD, total Cr, SO_4^{2-}, S^{2-}, SS, TDS and TS of the influent and effluent were measured to find process efficiency at various mixed liquor volatile suspended solids (MLVSS), dissolved oxygen (DO) and hydraulic detention time. Results of the study demonstrated that an efficiency of above parameters 93.0%, 92.5%, 94.9%, 62.6%, 98.2%, 87.9%, 82.1% and 82.4%, respectively, could be obtained if the activated sludge process (ASP) is operated at the MLVSS concentration of 3500-4500 mg/L, (DO) concentration of 4.1-5.5 mg/L keeping an aeration time of 12 h.

Keywords: activated sludge, biological treatment, tannery wastewater

Treatment of tannery effluent through the use of activated sludge process has been reported by many researchers (Ahmed *et al*., 2014; Al-Hussieny *et al*., 2014; Deepika *et al*., 2014; Pal *et al*., 2014; Shyam *et al*., 2014; Ambreen *et al*., 2013; Mouna *et al*., 2013; Niaz *et al*., 2012; Durai *et al*., 2011). All these studies indicate a BOD removal of 90-97% and COD 60-80% when combined with physicochemical pretreatment for the tannery effluent. The characteristics of tannery effluent vary considerably from tannery to tannery (Ilou *et al*., 2014). A survey was conducted in Pakistan for quality characteristics range of effluent from tanneries processing as given in Table 1 (Iqbal *et al*., 1998). Various parameters of importance relating to growth of microorganisms and substrate utilization on which the operation of the reactor is based has been studied by Bestawy *et al*. (2014); Khairnar *et al*. (2014) and Marco *et al*. (2014).

The present work was carried out that activated sludge process (ASP) for the treatment of settled tannery effluent and to develop general guidelines for the process design under local conditions. A bench scale continuous flow activated sludge reactor was used in this study. It consisted of an aeration tank of 300 L capacity and a settling portion of 200 L capacity.

The influent was subjected to settling in an underground tank. A peristaltic pump used to fill the settled influent to the aeration tank and pure oxygen cylinder was used to inject the oxygen to the aeration tank; a portion of gas was wasted from the tank to reduce the concentration of carbon dioxide. Pure oxygen was supplied by a fine bubble diffuser; flow was regulated at 4 mg/L/min by a flow meter. The reactor had to operate at different MLVSS and DO concentrations. Due to unavailability of mechanical return sludge facility, 100% of the settled sludge was daily removed from the final clarifier tank and manually returned to the aeration tank. In order to maintain the desired MLVSS and DO concentration in the reactor the calculated fraction of the volume of the aeration tank (ranging from one third to one tenth) was removed manually on daily basis and the tank was filled to the original volume by the treated effluent. No external nutrients were added to the influent (Vaiano *et al*., 2014; Pradyut *et al*., 2013).

Pure oxygen was supplied through diffuser stones to maintain a DO level of more than 3 mg/L. Temperature and pH values for settled influent and effluent were measured on daily basis while, MLVSS in the reactor, COD, BOD, total Cr, SO_4^{2-}, S^{2-}, SS, TDS and TS of influent and effluent were measured twice a week.

The three chosen operating parameters i.e. MLVSS concentration, detention time (è) and DO were varied during the course of the study keeping into consideration the generally applied range in activated sludge process for industrial effluent treatment (Pooja, 2014; Zahrim *et al*., 2009). The reactor was operated for an MLVSS concentration range of 1500-4500 mg/L, DO concentration 1.9-5.5 mg/L and è value of 4-12 h, respectively.

*Author for correspondence; E-mail: niazmemon2000@yahoo.com

During the course of study, pH of the reactor was varied between 7.8 and 8.23 which is a suitable range for biological treatment. DO of the reactor was maintained above 4 mg/L which is required for satisfactory biological treatment. A large amount of sludge is generated along with high energy consumption in the process (Table 1).

Table 1. Range of tannery effluent quality parameters

Parameters	Range
pH (unsettled effluent)	7.3-10
BOD_5, mg/L (30 min settling)	840-18,620
COD, mg/L (30 min settling)	1320-54,000
Suspended solids, mg/L (30 min settling)	220-1610
Settleable solids, mg/L (30 min settling)	11-40
Sulphate, mg/L (unsettled effluent)	800-6480
Sulphide, mg/L (at 0 time settling)	800-6480
Chromium, mg/L (unsettled effluent)	41-133

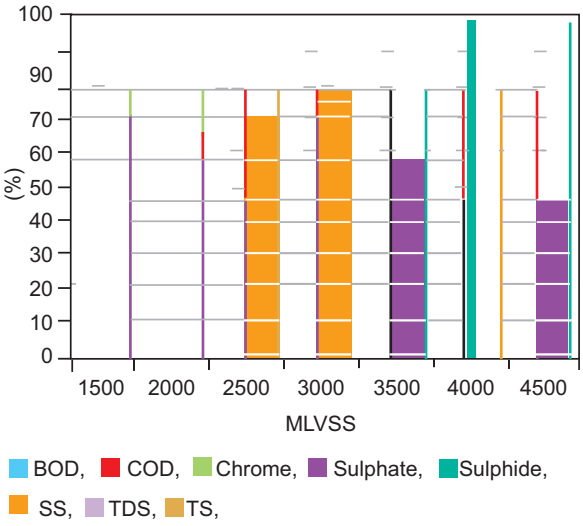

Fig. 1. Removal of pollutants.

Experimental work was performed for a period of 190 days. The treatment efficiency of the reactor in terms of BOD, COD, total Cr, SO_4^{2-}, S^{2-}, SS, TDS and TS removals was studied for MLVSS concentrations of 1500, 2000, 2500, 3000, 3500 and 4500 mg/L, DO 1.9, 1.8, 3.2, 3.1, 4.1 and 4.3 mg/L and retention time 2, 4, 6, 8 and 12 h. It was noted that the process efficiency improved with increase in MLVSS, DO concentrations and è. Under optimum conditions thus the results are showed, ASP should be operated at MLVSS concentration of 3500-4500 mg/L, DO concentration 4.5 mg/L and è value of 12 h. It is thus proposed to carry out bench scale studies for obtaining optimal values of the above said parameters for a specific tannery before designing a biological treatment system.

As shown in Fig. 1, maximum removal efficiency of 93.0%, 92.5%, 94.9%, 62.6%, 98.2%, 87.5%, 82.1% and 82.4% was achieved at MLVSS concentration of 3500-4500 mg/L and è of 12 h for BOD_5, COD, total Cr, SO_4^{2-}, S^{2-}, SS, TDS and TS, respectively, as summarized in Table 2. Furthermore, residual values of BOD_5 and COD at this MLVSS and è are 65 mg/L and 140 mg/L, respectively. It shows that BOD_5 and COD meet National Environmental Quality Standards (NEQS) limits, which are 80 and 150 mg/L. As indicated in Table 3, an average COD/BOD_5 ratio of 1.93 and 2.01, respectively. In the light of these results, it was concluded that a reasonably good approximation of BOD_5 can be obtained from a COD measurement once a relationship has been established between the two parameters from the available data.

Table 2. Removal efficiency at 3500-4500 MLVSS mg/L, 12 h time, 5.5 mg/L DO and pH 7.93

Parameters	Mean influent	Mean effluent	Removal efficiency (%)
BOD_5 (mg/L)	982	69	93.0
COD (mg/L)	1876	140	92.5
Total chrome (mg/L)	917	47	94.9
Sulphate (mg/L)	5378	2010	62.6
Sulphide (mg/L)	285	05	98.2
SS (mg/L)	1260	152	87.9
TDS (mg/L)	8536	1530	82.1
TS (mg/L)	9517	1668	82.4

Table 3. Influent and effluent COD and BOD_5 ratio

Average COD (mg/L)		Average BOD_5 (mg/L)		Average COD/BOD_5
Range	Mean	Range	Mean	
Influent				
1700-2023	1861	901-1025	963	1.93
Effluent				
140-1018	579	511-65	288	2.01

ASP is a feasible treatment technology for tannery wastewater especially where limited space restricts the use of other biological methods. ASP for Leather Research Centre may be operated with MLVSS concentration of 3500-4500 mg/L, DO concentration of 4.1-4.3 mg/L and è value of 10-12 h in order to obtain optimal removal

efficiencies with respect to BOD_5, COD, total Cr, SO_4^{2-}, S^{2-}, SS, TDS and TS. However, for a specific tannery, bench scale studies to find out the optimal values of these parameters are needed prior to the design of biological unit. The effluent meets NEQS for BOD_5, COD, S^{2-} and SS at the above stated MLVSS, DO concentration and è value (Fig. 1). However, total Cr, SO_4^{2-}, TDS and TS limit for NEQS could not be qualified. In addition, it must be required with physicochemical pretreatment for the tannery effluent and it is suggested that Pakistan Environmental Protection Agency may consider modifying the NEQS limits. In addition, effect of different MLVSS, DO concentration and detention time on the efficiency of settling tank may be investigated.

References

Ahmed, M., Abou, E., Mahmoud, M.S. 2014. Tannery wastewater treatment using activated sludge process system (Lab scale modeling). *International Journal of Engineering and Technical Research (IJETR)*, **2:** 21-28.

Al-Hussieny, A.A., Lamyia, A., Thijar, A.F., Elaf, S.M. 2014. Study of sludge and comparison for various wastewater treatment. *International Journal of Advanced Research*, **2:** 292-304.

Ambreen, L., Muhammad, N.C., Shazia, I. 2013. Biological treatment of dairy wastewater using activated sludge. *Science Asia*, **39:** 179-185.

Bestawy, E., Al-Hejin, A., Amer, R., Kashmeri, R.A. 2014. Decontamination of domestic wastewater using suspended individual and mixed bacteria in batch system. *Journal of Bioremediation Biodegradation*, **5:** 231.

Deepika, J., Gengadevi, R., Saravanan, K. 2014. Effluent treatment of tannery industries: Optimization of experimental data using RSM. *Journal of Chemical Engineering and Research*, **2:** 1-9.

Durai, G., Rajasimman, M. 2011. Biological treatment of tannery wastewater, A review. *Journal of Environmental Science and Technology*, **4:** 1-17.

Ilou, I., Souabi, S., Digua, K. 2014. Quantification of pollution discharges from tannery wastewater and pollution reduction by pre-treatment station. *International Journal of Science and Research (IJSR)*, **3:** 1706-1715.

Iqbal, M., Haque, I., Berns, J.A.S. 1998. *The Leather Sector, Environmental Report*, Environmental Technology Programme for Industry (ETPI), Federation of Pakistan Chambers of Commerce and Industry, (FPCCI), Federation House, Karachi, Pakistan.

Khairnar, K., Pal, P., Chandekar, R.H., Paunikar, W.N. 2014. Isolation and characterization of bacteriophages infecting nocardioforms in wastewater treatment plant. *Biotechnology Research International*, DOI:10.1155/2014/151952.

Marco, S., Javier, M., Ochando, P., Luca, D.P. 2014. On the relationship between suspended solids of different size, the observed boundary flux and rejection values for membranes treating a civil wastewater stream. *Membranes*, **4:** 414-423.

Mouna, F., Mohammed, M., Mohamed, B. 2013. Contribution to optimize the biological treatment of synthetic tannery effluent by the sequencing batch reactor. *Journal of Materials and Environmental Science*, **4:** 532-541.

Niaz, A., Saeed, M., Ayaz, T., Khan, M.A. 2012. Removal of pollutants from the liming effluent in course of leather processing. *Pakistan Journal of Scientific and Industrial Research*, **55:** 155-162.

Pal, P., Khairnar, K., Paunikar, W.N. 2014. Causes and remedies for filamentous foaming in activated sludge treatment plant. *Global NEST Journal*, **16:** 762-772.

Pooja, R.N. 2014. Removal of organic matter from wastewater by activated sludge process – Review. *International Journal of Science, Engineering and Technology Research*, **3:** 1260-1263.

Pradyut, K., Anupam, D., Somnath, M. 2013. Treatment of slaughter house wastewater in a sequencing batch reactor: Performance evaluation and biodegradation kinetics. *BioMed Research International*, DOI: 10.1155/2013/134872.

Shyam, K., Pradyumna, S., Sapkal, V.S., Sapkal, R.S. 2014. Performance enhancement of recirculated membrane bioreactor (RMBR) with dual effect of cross flow velocity and operating temperature for wastewater treatment. *International Journal of Emerging Technology and Advanced Engineering*, **4:** 134-140.

Vaiano, V., Sannino, D., Caracciolo, D., Naviglio, B., Calvanese, G., Ciambelli, P. 2014. Catalytic combustion of tannery sludge in a rotating reactor. *Journal of Advanced Chemical Engineering*, **4:** 1-5.

Zahrim, A.Y., Rachel, F.M., Menaka, S., Su, S.Y., Melvin, F., Chan, E.S. 2009. Decolourisation of anaerobic palm oil mill effluent via activated sludge granular activated carbon. *World Applied Sciences Journal*, **5:** 126-129.

Pakistan Journal of Scientific and Industrial Research

PCSIR - Scientific Information Centre

PCSIR Laboratories Campus, Shahrah-e-Dr. Salimuzzman Siddiqui, Karachi - 75280, Pakistan

Ph: 92-21-34651739-42, Fax: 92-21-34651738, E-mail: info@pjsir.org Website: www.pjsir.org

EXCHANGE FORM

We wish to receive Pakistan Journal of Scientific and Industrial Research Ser. A: Phys. Sci: and/or Ser. B: Biol. Sci. in exchange of :

Name of Journal: _____
Frequency: _____
Subjects Covered: _____
Institution: _____
Address: _____
_____
_____

Signature: _____
Name: _____
Designation: _____
Date: _____
E-mail: _____
Fax: _____
Phone: _____

Pakistan Journal of Scientific and Industrial Research

PCSIR - Scientific Information Centre

PCSIR Laboratories Campus, Shahrah-e-Dr. Salimuzzman Siddiqui, Karachi - 75280, Pakistan

Ph: 92-21-34651739-42, Fax: 92-21-34651738, E-mail: info@pjsir.org Website: www.pjsir.org

SUBSCRIPTION FORM

I / we wish to subscribe to 'Pakistan Journal of Scientific and Industrial Research' Ser. A: Phys. Sci: and/or Ser. B: Biol. Sci. The filled in proforma is being returned for compliance.

Subscriber's data:
Name: _____
Address: _____
_____
_____
E-mail: _____
Fax: _____
Phone: _____

Signature: _____
Order Membership No. (if any): _____

Tick the relevant box: ☐ Send invoice ☐ Bill later on ☐ Cheque for .....enclosed

RevisedSubscription Rates:
Local: Rs. 2500/ = per volume; Rs. 425/ = per copy
Foreign: US$ 450/ = per volume; US$ 75/ = per copy

Payment should be made through cross cheque in favour of Pakistan Journal of Scientific and Industrial Research and mailed to the Director PCSIR - Scientific Information Centre, PCSIR Laboratories Campus, Shahrah-e-Dr. Salimuzzaman Siddiqui, Karachi-75280, Pakistan.